

การเกิดนิวเคลียสผลึกแบบปีตาคอมพอสิตพอลิโพรพิลีน/แร่ดินเหนียว



นายยงยุทธ ประจำ

ศูนย์วิทยทรัพยากร

วิทยานิพนธ์นี้เป็นส่วนหนึ่งของการศึกษาตามหลักสูตรปริญญาวิทยาศาสตรมหาบัณฑิต

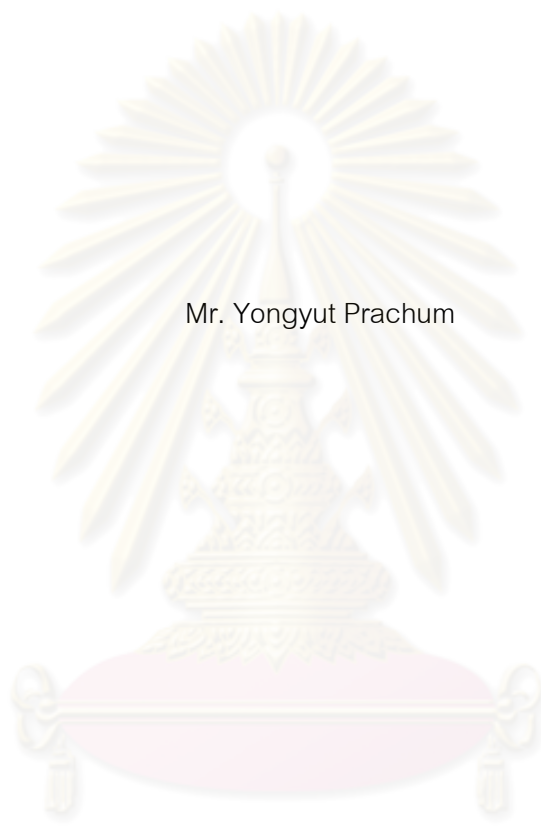
สาขาวิชาปิโตรเคมีและวิทยาศาสตร์พอลิเมอร์

คณะวิทยาศาสตร์ จุฬาลงกรณ์มหาวิทยาลัย

ปีการศึกษา 2551

ลิขสิทธิ์ของจุฬาลงกรณ์มหาวิทยาลัย

BETA-NUCLEATION OF POLYPROPYLENE/MONTMORILLONITE COMPOSITES



Mr. Yongyut Prachum

ศูนย์วิทยทรัพยากร
จุฬาลงกรณ์มหาวิทยาลัย

A Thesis Submitted in Partial Fulfillment of the Requirements
for the Degree of Master of Science Program in Petrochemistry and Polymer Science

Faculty of Science


Chulalongkorn University

Academic Year 2008


Copyright of Chulalongkorn University


Thesis Title BETA-NUCLEATION OF POLYPROPYLENE/MONTMORILLONITE
COMPOSITES
By Mr. Yongyut Prachum
Field of Study Petrochemistry and Polymer Science
Thesis Principal Advisor Professor Suda Kiatkamjornwong, Ph.D.
Thesis Co-advisor Roman Helmuth Adam Strauss, Ph.D.


Accepted by the Faculty of Science, Chulalongkorn University in Partial Fulfillment of the
Requirements for the Master's Degree


.....Dean of the Faculty of Science
(Professor Supot Hannongbua, Dr. rer. nat.)


THESIS COMMITTEE


.....Chairman
(Professor Pattarapan Prasassarakich, Ph.D.)


.....Thesis Principal Advisor
(Professor Suda Kiatkamjornwong, Ph.D.)


.....Thesis Co-advisor
(Roman Helmuth Adam Strauss, Ph. D.)


.....Member
(Assistant Professor Warinthorn Chavasiri, Ph.D.)


.....External Member
(Thevarak Rochanapruk, Ph.D.)

ยงยุทธ ประจำ: การเกิดนิวเคลียสผลึกแบบบีตาของคอมพอสิตพอลิโพรพิลีน/แร่ดินเหนียว
(BETA-NUCLEATION OF POLYPROPYLENE/MONTMORILLONITE COMPOSITES)

อ. ที่ปรึกษาวิทยานิพนธ์หลัก: ศ.ดร. สุดา เกียรติกำจรวงศ์, อ. ที่ปรึกษาร่วม: ดร. Roman Helmuth Adam Strauss, 88 หน้า.

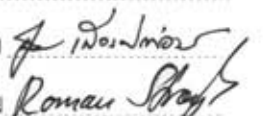
งานวิจัยนี้เป็นการศึกษาการเกิดนิวเคลียสผลึกแบบบีตาของคอมพอสิตของพอลิโพรพิลีน/แร่ดินเหนียว โดยกระบวนการผสมหลอมเหลวผ่านเครื่องอัดรีดสกรูคู่ พบว่าการเติมสารก่อผลึกแอริลแอไมด์ในปริมาณร้อยละโดยน้ำหนักระหว่าง 0.05-0.30 สามารถก่อให้เกิดผลึกบีตาของพอลิโพรพิลีนและพอลิโพรพิลีน/พอลิโพรพิลีนกราฟต์มาเลอิกแอนไฮไดรด์/แร่ดินเหนียวได้ ได้ศึกษาพฤติกรรมของการเกิดผลึกของคอมพอสิตด้วยเทคนิค differential scanning calorimeter (DSC) ได้ศึกษาผลของปริมาณการเติมสารก่อผลึกแอริลแอไมด์ต่อโครงสร้างและสมบัติของพอลิโพรพิลีนคอมพอสิต และได้อภิปรายถึงความสัมพันธ์ระหว่างสัณฐาน โครงสร้างผลึกของพอลิเมอร์คอมพอสิตซึ่งได้จากการวิเคราะห์ด้วยเทคนิค scanning electron microscopy (SEM), transmission electron microscopy (TEM) และ X-ray diffraction (XRD) กับสมบัติเชิงกล การไหล และความร้อนของพอลิเมอร์คอมพอสิต นอกจากนี้ ได้ศึกษาอันตรกิริยาระหว่างพอลิโพรพิลีน พอลิโพรพิลีนกราฟต์มาเลอิกแอนไฮไดรด์และแร่ดินเหนียว ด้วยเทคนิค Fourier transform infrared spectroscopy (FTIR) ผลการศึกษานี้ พบว่าการเติมสารก่อผลึกแอริลแอไมด์ในปริมาณร้อยละโดยน้ำหนักระหว่าง 0.05-0.30 ก่อให้เกิดผลึกบีตาของพอลิโพรพิลีน/แร่ดินเหนียว และให้ค่า k_p คือ 0.50, 0.92, 0.92 ตามลำดับ การเกิดผลึกบีตาสามารถพัฒนาสมบัติทางความร้อน และเชิงกลของพอลิโพรพิลีนและพอลิโพรพิลีน/แร่ดินเหนียวคอมพอสิตได้ การเติมแร่ดินเหนียวปรับแต่งนั้นสามารถเพิ่มสมบัติเชิงกลด้านความแข็งแรงเหนียว และการทนแรงกระแทกของพอลิโพรพิลีนคอมพอสิตได้อย่างชัดเจน แต่สมบัติด้านการยืดจนขาดจะลดลง ขณะที่ความหนาแน่นของคอมพอสิตจะเพิ่มขึ้น การเติมสารก่อผลึกแอริลแอไมด์สามารถชดเชยการสูญเสียสมบัติเชิงกลด้านการยืดจนขาด และลดความหนาแน่นของพอลิโพรพิลีนคอมพอสิตได้ และที่สำคัญที่สุดงานวิจัยนี้พบว่าการเติมสารก่อผลึกแอริลแอไมด์ในคอมพอสิตของพอลิโพรพิลีน/พอลิโพรพิลีนกราฟต์มาเลอิกแอนไฮไดรด์/แร่ดินเหนียว สามารถเพิ่มอุณหภูมิการตกผลึกของพอลิโพรพิลีน/พอลิโพรพิลีนกราฟต์มาเลอิกแอนไฮไดรด์/แร่ดินเหนียว/แอริลแอไมด์ ได้อย่างชัดเจน ถึง 12 องศาเซลเซียส

สาขาวิชา ปิโตรเคมีและวิทยาศาสตร์พอลิเมอร์.....ลายมือชื่อนิสิต

ปีการศึกษา.....2551.....

ลายมือชื่อ อ.ที่ปรึกษาวิทยานิพนธ์หลัก

ลายมือชื่อ อ.ที่ปรึกษาวิทยานิพนธ์ร่วม

4973410623 : MAJOR PETROCHEMISTRY AND POLYMER SCIENCE

KEY WORD: ISOTACTIC POLYPROPYLENE/BETA-NUCLEATOR/POLYPROPYLENE/POLYPROPYLENE COMPOSITES

YONGYUT PRACHUM: BETA-NUCLEATION OF POLYPROPYLENE/MONTMORILLONITE COMPOSITES. THESIS PRINCIPAL ADVISOR: PROF. SUDA KIATKAMJORNWONG, Ph.D., THESIS CO-ADVISOR: ROMAN HELMUTH ADAM STRAUSS, Ph.D., 88 pp.

This research investigated the beta nucleation of polypropylene (PP)/montmorillonite composites via melt compounding in a co-rotating twin-screw extruder. Polypropylene (PP) and polypropylene/polypropylene-*g*-maleic anhydride/montmorillonite clay (PP/PP-*g*-MA/montmorillonite clay) composites were modified with 0.05, 0.10 and 0.30 wt% aryl amide nucleator (beta-nucleator) to promote the formation of the hexagonal (beta) crystal modification during melt crystallization. The non-isothermal crystallization behavior of PP, PP/PP-*g*-MA/montmorillonite composites and beta-nucleated PP/PP-*g*-MA/montmorillonite composites was studied by means of differential scanning calorimetry (DSC). The structure-property relationships of PP-composites prepared by melt processing have been investigated with the main focus on the quantity of aryl amide. The morphological and crystal structure observations obtained from scanning electron microscopy (SEM), transmission electron microscopy (TEM) and X-ray diffraction (XRD) were discussed in conjunction with the mechanical, rheological and thermal properties of these composites. The chemical interaction in composites was observed by FTIR. The PP/PP-*g*-MA/montmorillonite clay composites modified with 0.05, 0.10 and 0.30 wt% aryl amide nucleator promoted growth of the hexagonal (beta) crystal with the k_{β} values of 0.50, 0.92 and 0.92, respectively. The beta-crystal modification was found to increase thermal and mechanical properties of the PP and PP-composites, whereas the nanoclay dramatically increased stiffness and impact of the composites, the loss of tensile elongation was found to be partially compensated by aryl amide. The effect on increasing density by the clay compound was reduced via the beta-nucleation of aryl amide. The most important finding of aryl amide nucleation of PP/PP-*g*-MA/montmorillonite clay composites was the dramatic increase in crystallization temperature of the PP/PP-*g*-MA/organoclay/aryl amide by 12 °C.

Field of Study ..Petrochemistry and Polymer Science... Student's signature.....

Academic year.....2008..... Principal Advisor's signature.....

Co advisor's signature.....

ACKNOWLEDGEMENTS

The author is grateful to Professor Dr. Suda Kiatkamjornwong, the thesis principal advisor and Dr. Roman Helmuth Adam Strauss, the thesis co-advisor for their guidance, suggestions, reviewing the experimental work, thesis writing and manuscript preparation for journal and conference publications, for their continual encouragement during the study.

The author thanks Professor Dr. Pattarapan Prasassarakich, Assistant Professor Dr. Warinthorn Chavasiri, and Dr. Thevarak Rochanapruk for serving as chairperson and on member of thesis committees, respectively.

In addition, the author would like to acknowledge the Research and Development Department and Quality control 1, IRPC (Public) Co., Ltd., for analysis and permission to use the equipment and instruments and others support during the courses of research. Acknowledgements also go to Graduate School, Chulalongkorn University and the Department of Imaging Science and Printing Technology for support.

Finally, the author is grateful to his family for their love, understanding, encouragement, and support. Many thanks go to his friends, who contribute suggestions and support during the course of research.

ศูนย์วิทยทรัพยากร
จุฬาลงกรณ์มหาวิทยาลัย

CONTENTS

	PAGE
Abstract in Thai	iv
Abstract in English.....	v
Acknowledgements.....	vi
Content.....	vii
List of Tables.....	x
List of Figures.....	xi
List of Abbreviations.....	xiv
CHAPTER I Introduction.....	1
1.1 Statement of problems.....	1
1.2 Research objective.....	2
1.3 Scope of the research.....	2
CHAPTER II Theory and literature review	3
2.1 Polypropylene growth and use	3
2.2 Isotactic polypropylene (<i>i</i> PP).....	5
2.2.1 Structure and morphology.....	5
2.2.2 Alpha modifications.....	8
2.2.3 Beta modifications	8
2.2.4 Gamma modification	13
2.2.5 Smectic	15
2.3 Additives in PP.....	16
2.4 Crystallization behavior.....	17
2.5 Polymer/layered silicate (PLS) nanocomposites.....	18
2.5.1 Structure and properties of layered silicates.....	18
2.5.2 Structure and properties of organically modified layered silicate.....	19

2.5.3	Types of nanocomposites.....	20
2.6	Techniques used for the characterization of nanocomposites.....	22
2.7	Composite preparation (melt compounding).....	23
2.8	Literature review.....	24
CHAPTER III Experimental.....		30
3.1	Materials.....	30
3.2	Instruments.....	30
3.3	Experimentals.....	31
3.3.1	The effects of the compatibilizers (PP- <i>g</i> -MA) on physical properties of PP/organomontmorillonite (OMMT: organoclay) composites.....	31
3.3.2	The effects of the screw configuration on physical properties of PP/compatibilizer/OMMT (organoclay) composites.....	32
3.3.3	The effect of beta-nucleating agent on physical properties of PP/OMMT (organoclay) composites.....	35
3.3.4	Morphology characterization.....	36
3.3.4.1	X-ray diffraction (XRD).....	36
3.3.4.2	Transmission electron microscopy (TEM).....	36
3.3.4.3	Scanning electronic microscopy (SEM).....	36
3.3.5	Rheological properties.....	37
3.3.5.1	Small amplitude oscillatory shear analysis (Cone and Plate Rheometer).....	37
3.3.5.2	Capillary Rheometer.....	38
3.3.5.3	Melt flow Index.....	38
3.3.6	Thermal analysis.....	39
3.3.7	Fourier transforms infrared spectroscopy (FT-IR) analysis.....	40
3.3.8	Mechanical properties.....	40
3.3.8.1	Izod impact strength.....	40
3.3.8.2	Flexural modulus and strength.....	41
3.3.8.3	Tensile property measurement.....	42

3.3.8.4 Heat deflection temperature.....	42
3.3.9 Density.....	42
CHAPTER IV Results and discussion.....	43
4.1 Preliminary study of the effects of compatibilizers on the performance of PP/compatibilizer(PB3200:PP-g-MA)/organomontmorillonite (OMMT: organoclay, Nanofil [®] SE3000) composites.....	43
4.2 Preliminary studies of the effects of screw configuration on physical Properties of PP/compatibilizer/OMMT(organoclay) composites.....	44
4.3 Effects of compatibilizer on the performance of PP/ compatibilizer/OMMT (organoclay) composites (Invention I screw configuration).....	45
4.3.1 Morphology characterization.....	45
4.3.2 Adhesion and chemical interaction.....	52
4.3.3 Rheological properties.....	55
4.3.4 Microscopic observations.....	59
4.4 Effects of beta-nucleating agent (aryl amide) on the performance of PP/compatibilizer/OMMT(organoclay) composites.....	61
4.4.1 Morphology and density.....	61
4.4.2 Thermal properties.....	67
4.4.3 Chemical interaction.....	71
4.4.4 Rheological properties.....	73
4.4.5 Microscopic observations.....	76
CHAPTER V Conclusion and suggestions for further work.....	79
5.1 Conclusions.....	79
5.2 Suggestions for further work.....	79
REFERENCES.....	80
APPENDIX.....	84
VITA.....	88

LIST OF TABLES

TABLE		PAGE
2.1	Nucleator types and their crystal forms.....	10
2.2	Characteristic parameters of organophilic clay, PP-MA and PPCNs.....	26
2.3	Mechanical properties and the k_{β} value of iPP/EPR blend filled with bi-component nucleating agent of calcium stearate and pimelic acid (Ca-Pim) at various filler loadings.....	28
3.1	The formulations of PP/PP-g-MA/OMMT (organoclay) melt compounding.....	31
3.2	The Screw configuration for normal polyolefin of Twin Screw Co-rotation extruder.....	33
3.3	The Screw configuration (Invention I configuration) of Twin Screw Co-rotation extruder.....	34
3.4	The formulations of PP/PP-g-MA/organoclay/beta-nucleating agent melt compounding.....	35
4.1	The mechanical properties of controls and PP/PP-g-MA/OMMT (Nanofil® SE3000) composites with various amounts of PP-g-MA compatibilizer processed in a normal polyolefin screw configuration.....	44
4.2	XRD-derived interlayer spacing for composite materials, calculated according to Figure 4.2.....	47
4.3	XRD information and density of neat PP and PP/PP-g-MA/OMMT (organoclay) composites with various amounts of aryl amide nucleator.....	62
4.4	Thermal properties of PP and PP/PP-g-MA/OMMT composites with various amounts of aryl amide nucleator at various heating and cooling rates based on DSC curves recorded at the cooling and heating rates from 2.5-20 °C/min).....	70
4.5	Mechanical properties of PP/PP-g-MA/OMMT composites with various amount of beta-nucleating and the control of the neat PP.....	78

LIST OF FIGURES

FIGURE	PAGE
2.1 Supply of polypropylene monomer.....	5
2.2 Representation of the spatial dispersion of CH ₃ (R) in (a) isotactic, (b) syndiotactic, (c) atactic polypropylene chain segment	6
2.3 Wide angle X-ray patterns of isotactic, syndiotactic and atactic PP.....	8
2.4 X-ray diffraction diagrams showing mixed alpha and beta crystalline.....	12
2.5 X-ray diffractogram of pure beta- <i>i</i> PP.....	12
2.6 Optical micrograph of pure beta- <i>i</i> PP crystallized at T _c = 398 K.....	13
2.7 X-ray diffraction diagrams of <i>i</i> PP crystalline forms.....	14
2.8 Comparison of the WAXD pattern of the aPP (amorphous), <i>i</i> PP in the mesomorphic form, and <i>i</i> PP in the alpha-form.....	15
2.9 Schematically illustration of three different types of thermodynamically achievable polymer/layered silicate composites.....	21
2.10 Illustration for dispersed clay structure and the inter-fibrillar structure for: a) PPCN2 and b) PPCN7.5.....	26
3.1 Melt flow Indexer.....	39
3.2 Izod impact strength apparatus and test specimen	41
3.3 Flexural modulus and flexural strength testing	41
3.4 Tensile testing apparatus and test specimen	42
4.1 Effects of screw configuration on physical properties of PP/compatibilizer/ OMMT composites (90/5/5).....	45
4.2 XRD patterns of organoclay and PP/PP- <i>g</i> -MA/OMMT composites filled and unfilled composites with various amount of PP- <i>g</i> -MA with Invention I screw configuration.....	47
4.3 Transmission electron micrographs of PP/PP- <i>g</i> -MA/OMMT composites (95/0/5/0) showing (a) agglomeration clay and (b-d) intercalated- and-flocculated of clay layers.....	48
4.4 Transmission electron micrographs of PP/PP- <i>g</i> -MA/OMMT composites (90/5/5/0) showing (a) intercalated-and-flocculation clay	

	and (c-d) intercalated clay layers.....	49
4.5	Transmission electron micrographs of PP/PP- <i>g</i> -MA/OMMT composites (75/20/5/0) showing (a) uniform distribution of clay and (b-d) intercalated and partially exfoliated clay layers.....	50
4.6	TEMs of PP/PP- <i>g</i> -MA/OMMT composites, show agglomerated intercalated and partially exfoliated clay layers of 95/0/5/0, 95/5/5/0, 75/20/5/0, (a-c) at 6,000x and (d-f) at 100,000x, respectively.....	51
4.7	SEM micrographs of the fractured surfaces of the neat PP (upper left), the PP/PP- <i>g</i> -MA/OMMT composites of 95/0/5/0 (upper right), 90/5/5/0 (lower left) and 75/20/5/0 (lower right).....	53
4.8	Fourier Transform infrared spectra of the neat PP, PP- <i>g</i> -MA, PP/PP- <i>g</i> -MA/OMMT composites (90/5/5/0) and the organoclay.....	54
4.9	Fourier transform infrared spectra of neat PP and PP/PP- <i>g</i> -MA/OMMT with various amount of PP- <i>g</i> -MA in the range from 0-20 wt%.....	54
4.10	The rheological properties, (a) G' , Storage modulus, (b) η^* , Complex viscosity of PP/PP- <i>g</i> -MA/OMMT composites and blanks with various amount of PP- <i>g</i> -MA and determined by Cone and Plate rheometer.....	56
4.11	Shear viscosity of PP/PP- <i>g</i> -MA/OMMT composites and the control (neat PP) with various amounts of PP- <i>g</i> -MA determined by Capillary Rheometer at 220 °C.....	58
4.12	Optical micrographs of PP/PP- <i>g</i> -MA/OMMT composite and blank and isothermally crystallized at 135 °C.....	59
4.13	Mechanical properties of PP/PP- <i>g</i> -MA/OMMT composites with various amounts of PP- <i>g</i> -MA and the neat PP as a control.....	60
4.14	XRD patterns of PP and PP/PP- <i>g</i> -MA/OMMT composites with various amounts of aryl amide nucleator, 1 : 99.9/0/0/0.1, 2 : Neat PP, 3 : 89.7/5/5/0.3, 4 : 89.9/5/5/0.1, 5 : 89.95/5/5/0.05, 6 : 89.95/5/5/0.05 (repeat) and 7 : 90/5/5/0.....	62
4.15	Transmission electron micrographs of PP/PP- <i>g</i> -MA/OMMT composites (a-b) 90/5/5/0.1, (c-d) 95/0/5/0 and (e-f) 70/25/5/0.....	64
4.16	TEM micrographs of PP/PP- <i>g</i> -MA/OMMT composites showing flocculated, intercalated and exfoliated clay layers of (a-b) : 89.9/5/5/0.1 and (c-d) : 90/5/5/0 at 6,000x and 100,000x, respectively.....	65

4.17	Scanning electron micrographs showing etched impact fractured surface PP and PP/PP- <i>g</i> -MA/OMMT composites (a-b): with and (c-d) without aryl amide nucleator.....	66
4.18	Scanning electron micrographs showing unetched and etched impact fractured surfaces of PP and PP/PP- <i>g</i> -MA/OMMT composites with 0.30 wt% of aryl amide nucleator.....	67
4.19	DSC thermograms (a) melting temperature, (b) crystallization temperature of PP and PP/PP- <i>g</i> -MA/OMMT composites with various amount of aryl amide nucleator (The results based on DSC curves recorded at the cooling and heating rate of 10 °C/min from 25-200 °C by Mettler Toledo instrument).....	70
4.20	Crystallization temperatures of PP and PP/PP- <i>g</i> -MA/OMMT composites with various amounts of aryl amide nucleator at cooling rates of 2.5 °C/min, 5.0 °C/min, 10.0 °C/min and 20.0 °C/min.....	71
4.21	Fourier transform infrared spectroscopy spectra of a) OMMT, PP, PP- <i>g</i> -MA, PP/PP- <i>g</i> -MA/OMMT composites, b) PP/PP- <i>g</i> -MA/OMMT composites without and with 0.3 wt% of aryl amide nucleator.....	72
4.22	Rheological properties,(a) storage modulus, (b) complex viscosity and (c) loss modulus of PP, PP/PP- <i>g</i> -MA and PP/PP- <i>g</i> -MA/organoclay composites with various loading of aryl amide nucleator determined by cone and plate Rheometer.....	75
4.23	Optical micrographs of the neat PP, PP/PP- <i>g</i> -MA/OMMT with and without the beta-nucleating agent under isothermal condition at 135 °C: (a) Neat PP (>95% alpha-form) after 20 min, spherulite size, 70-100 µm; (b) 99.9/0/0/0.1 (92% beta-form), 20 min, 10 µm and 100 µm; (c) 90/5/5/0, 20 min, 50-80 µm; (d) 89.9/5/5/0.1, 10 min, 10-25 µm.....	77

ABBREVIATIONS

CEC	cation exchange capacity
DSC	differential scanning calorimetry
FTIR	fourier-transform infrared spectrophotometer
HDT	heat deflection temperature
ΔH_c	heat evolved during crystallization
$\Delta H-\alpha$	heat fusion of alpha crystal
$\Delta H-\beta$	heat fusion of beta crystal
Φ_β	beta crystal fraction
L/D	extruder length per diameter ratio
MFI	melt flow index
OMMT	organomontmorillonite
PLS	polymer/layered silicate
PP	polypropylene
PP-g-MA	polypropylene graft maleic anhydride
SEM	scanning electron microscopy
TEM	transmission electron microscopy
T_c	crystallization temperature
T_{co}	crystallization onset temperature
T_{cp}	crystallization peak temperature
T_m	melting temperature
wt%	weight percentage
XRD	X-ray diffraction
X_α	crystallinity of alpha crystal
X_β	crystallinity of beta crystal

CHAPTER I

INTRODUCTION

1.1 Statement of problems

Polypropylene (PP) is a commodity polymer used in the wide ranging from automotive applications such as automotive bumpers and interior parts of automobiles to packaging applications such as pouches for ready-to-eat meals and other food containers. Enhancement of mechanical and thermal properties of PP can be obtained by making PP composites, by adding micro-fillers (conventional fillers) in PP matrix. Conventional fillers such as talc, mica and glass fiber are used at a rather high loading of 20 to 40 wt% to improve mechanical properties and dimensional stability while also increasing part weight because of its low surface area and aspect ratio. Montmorillonite or clay (silicate nanolayers) is a nano-filler which has much larger aspect ratio and surface area and can enhance stiffness, thermal properties and scratch resistance significantly at a much lower loading (2-7 wt%) when they are well dispersed and oriented. However, the mechanical properties in the case of toughness or impact strength of PP composite was also decreased which led to reduced impact-stiffness balance of PP composite. Isotactic polypropylene is known to exhibit four different crystalline forms; alpha-form, beta-form, delta-form and smectic form. Under normal processing conditions, alpha-PP is the principle constituent which may be accompanied by the relative low amount of β -modification. The formation of β -PP can be promoted in PP by adding various beta-nucleators such as quinacridone dye, calcium carbonate or wallastonite. The most beneficial selectivity and activity were found for calcium salts of pimelic (Ca-pim) and aryl amide compounds. The beta-form PP exhibits a higher impact energy but lower yield strength and elastic modulus than alpha-PP.

In this work, it is our interest to prepare PP composites by adding organoclay to improve stiffness and thermal properties and simultaneously adding a beta-nucleating agent for improving impact strength so as to generate a better impact-stiffness balance of PP composites.

1.2 Research objective

The main purpose of this study is focused on studying the effect of filler (organoclay) and the beta-nucleating agent (aryl amide compounds) on crystalline structure, thermal properties and mechanical properties of PP homopolymer.

1.3 Scope of the research

The scope of this research work includes

1. Literature review
2. Preparation of PP nanocomposites by melt compounding of the Homo-PP, organoclay (OMMT), compatibilizer (PP-*g*-MA: PB3200) and beta-nucleating agent via a twin screw co-rotating extruder and study factors as follows;
 - 2.1 Composition ratio of the composites;
Homo-PP/PP-*g*-MA/organoclay: 100/0/0, 95/5/0, 95/0/5, 92.5/2.5/5, 90/5/5, 88/7/5, 85/10/5, 80/15/5, and 75/20/5.
 - 2.2 Amount of beta-nucleating agent adding to the composites, in the range from 0.05-0.30 wt%.
3. Characterization of thermal properties of the composites using DSC.
4. Determine physical properties of the nanocomposites according to ASTM D-256 (impact strength) and ASTM D-790 (flexural modulus).
5. Characterization of crystal forms in the PP composite using DSC and XRD.
6. Characterization of the morphology of composites using SEM, TEM and XRD.
7. Characterization of the rheology of composites using Rheometer.
8. Summarizing the results and discussions.
9. Writing a publicable article for an international journal and writing a thesis.

CHAPTER II

THEORY AND LITERATURE REVIEW

2.1 Polypropylene growth and use

Polypropylene was initially produced commercially about 50 years ago after the successful development of a suitable stereo-specific catalyst, which enabled the polymer to have a kind of structural characteristics useful for rigid items. The continuous growth of polypropylene is expected to continue into the next millennium as raw materials in an expanding number of end-use products for the automotive and film industries [1]. Earlier, the performance of polypropylene was considered intermediate to polyethylene and polystyrene (PS). But, a late, there is significant inter-material competition to replace engineering polymers as materials of construction by polypropylene base resin.

The significant growth of PP use is attributed to combination of any factors besides a good balance in physical and chemical properties. Because of the appropriate melt rheology and thermal behavior, PP-based materials are widely process able on variety of different equipment ranging from injection molding to some designed for the use in order industries , like calendaring and air-quenched blow film equipment. Additionally, by the having the lowest density among commodity plastics at approximately 0.90 g/cm^3 , continued market penetration of at the current rate of growth is almost ensured on the basis of good mechanical properties at reduced cost per volume. Finally, because many major companies are designing their products, polypropylene stands out as the main product with the widest design flexibility and simplicity of recycling. its excellent thermal stability, low density (assisting in separating from other materials), chemical and environmental inertness, even its caloric in the case of incineration all add to its attractiveness as materials of construction.

The global supply from several producers located throughout the world ensures good supply at competitive prices. From the mid-1990s end of the 20th century, significant capacity increases will occur. The supply and demand balance

works favorably to the consumers is benefit. This keeps prices in check and ensures that suitable supply will be available. Additionally, in the next 10 years, significant amounts of polypropylene from recycled materials vary widely in cleanliness but are though to be suitable for a variety of applications, including operation, and this will continue. Additionally, post consumer waste primarily from packaging is becoming more available but often of lower quality (e.g., sometimes limited to black pigmented products)

Polypropylene homopolymer consists of molecular chains with repeating unit of propylene monomer generated in the reactor. It is derived from three major sources today. Globally, most propylene monomer comes from the steam cracking processing naphtha, a valuable fraction of crude oil. Usually, naphtha crackers target products are ethylene monomer. Propylene is a by product of the cracking process produced at various ratios depending on the crude oil feedstock. Many cracking processes have a propylene plant intimately connected effectively use the propylene that comes from naphtha cracking. The second largest production of propylene comes from the gasoline refining process.

Finally, and most recently, a new process by which propane is dehydrogenated to propylene monomer has been used to produce propylene. Despite certain economical short coming, when propane is readily available and transportation to market is less favorable, this process is now starting to be applied. Propylene purity requirement for the production of polymers is very high. Trace impurities in the polymerization process cause poisoning of the catalyst during production. The industrial routes to produce propylene monomer and the region capacities with expected growth are outlined in Figure 2.1 [1].

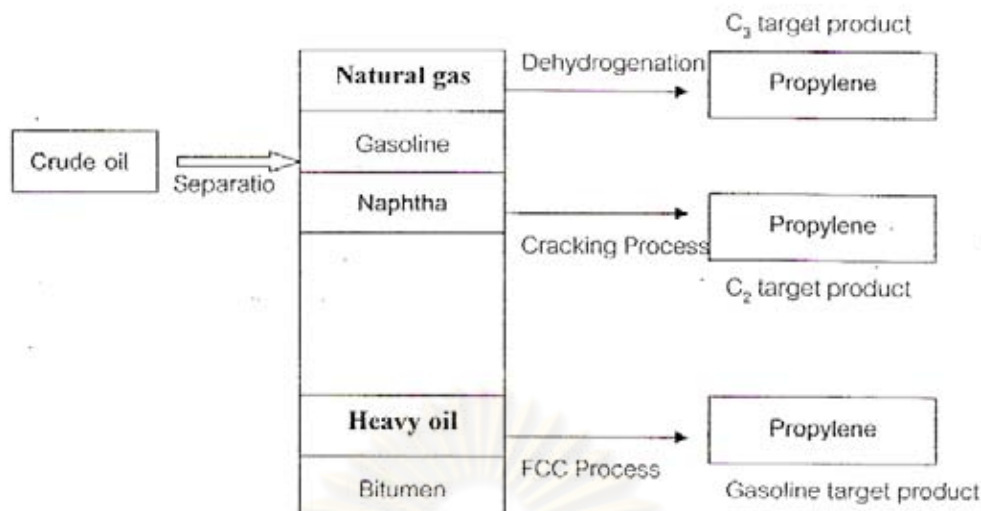


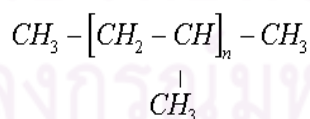
Figure 2.1 Supply of polypropylene monomer [1].

2.2 Isotactic polypropylene (*i*PP)

2.2.1 Structure and morphology

Propylene is one of the most important of hydrocarbon polymers and is the first synthetic stereoregular polymer to achieve considerable commercial and industrial importance.

Stereoregular polypropylene was first obtained by Natta and co-workers in the 1950s that the chain conformation of *i*PP is a threefold helix, which can be either right or left-hand, with a periodicity of 6.5 Å as shown in Structure I.



Structure I

The molecular structure of polypropylene is formally derived from polyethylene by the substitution of one of the H atoms on alternate C atom of the chain by CH₃ group. Stereoregular configuration can be described as Figure 2.2. Figure 2.2a is isotactic, in which all pendent CH₃ groups are attached on the same side of the chain, that is, all units have a spatially identical arrangement of atom; Figure

2.2b is syndiotactic, in which the configuration of the C atom carrying the side group shows a regular alternation along the chain; Figure 2.2c is atactic, which there is a random arrangement of pendent CH_3 groups [2].

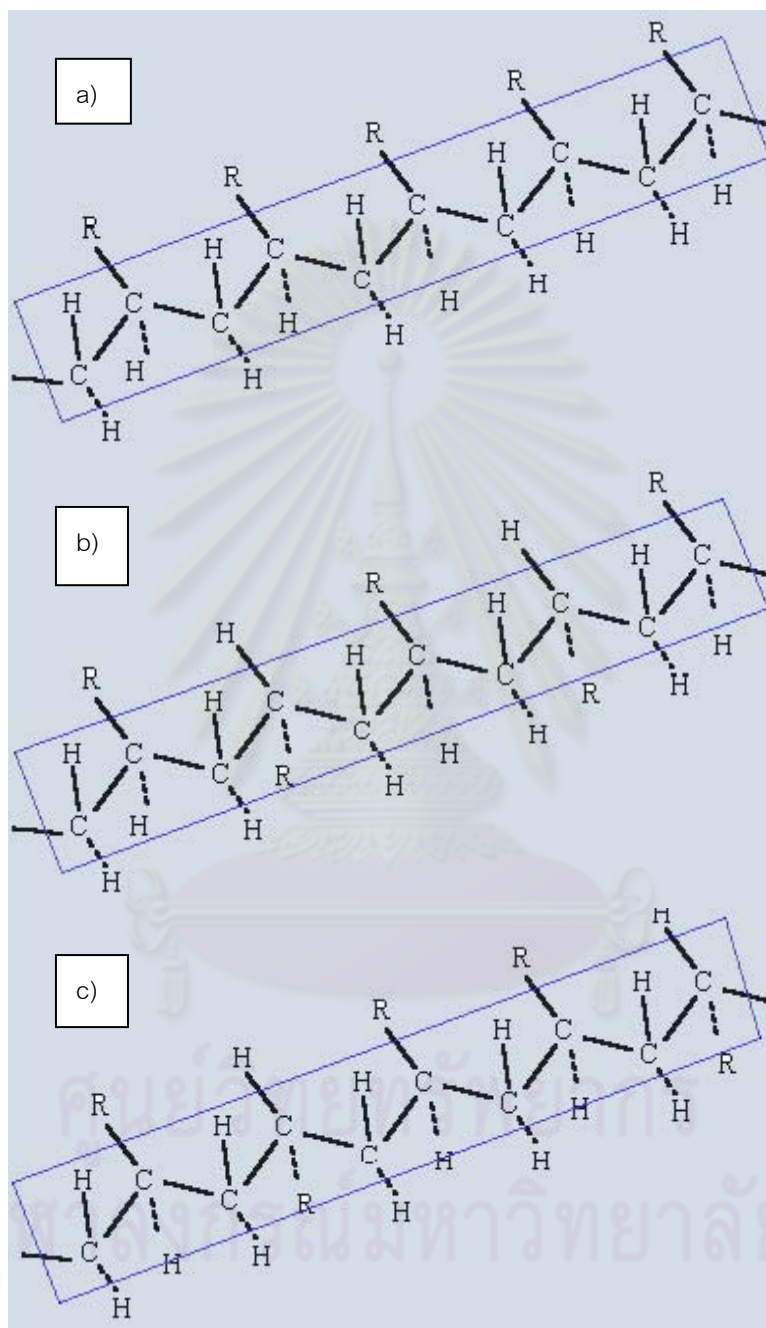


Figure 2.2 Representation of the spatial dispersion of CH_3 (R) in (a) isotactic, (b) syndiotactic, (c) atactic polypropylene chain segment [2].

The stereoregularity of polymer molecules is of high importance for the properties of materials. It determines the possibility for adjacent molecules to fit together and therefore to crystallize. It also controls the strength of forces between molecules, on which the mechanical properties of the materials depends.

Commercial polypropylene generally has about 0.95 or higher is tactic indices. High isotactic index contributes to higher crystallization of the polymer and much improved mechanical properties of the products. It increases, for example, the yield stress, elastic modulus, hardness, and brittle point of the polymer.

The crystallizability of the chain is a critical factor governing the resultant morphology. The degree of crystallinity of PP homopolymers is governed primarily by the tacticity of the chain. Isomeric chains result from the head-to-tail addition of polypropylene monomer units, where the methyl groups always have the same configuration with respect to the polymer backbone. Syndiotactic chains result from the same head-to-tail addition of monomer units, but the methyl groups have the alternating configuration with respect to polymer backbone. The stereospecificity (isospecific or syndiospecific) refers to the consistent placement of the methyl groups.

The stereochemistry of the PP chain strongly influences the crystallinity this is shown in Figure 2.3, which shows wide angle X-ray patterns of isotactic, syndiotactic and atactic PP. Figure 2.3 shows pronounced crystalline reflections when the PP chain contains either regular isotactic or syndiotactic sequences. Those patterns are related to the specific crystal unit cell symmetries for the isotactic and syndiotactic PP. Atactic PP shows no strong reflections, exhibiting only a very broad and diffuse characteristic of a non-crystalline material.

On the crystal lattice level, isotactic PP shows well-known crystalline forms, namely monoclinic alpha-form, beta-form, triclinic gamma form and smectic: delta-form (partial order of micro crystal of the hexagonal and/or monoclinic). The alpha-form dominates in the crystallization of the PP grades used in mostly industrial applications. Among these four crystalline structures the beta-form demonstrates higher performance such as higher tensile elongation and higher impact resistance.

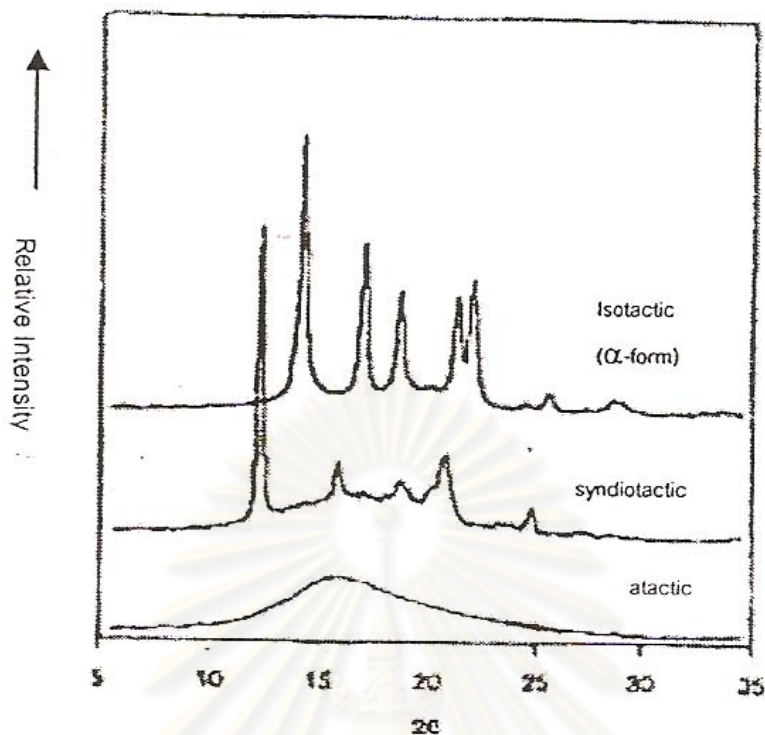


Figure 2.3 Wide angle X-ray patterns of isotactic, syndiotactic and atactic PP [2, 3]

2.2.2 Alpha modification

The principal isotactic form (the alpha form) was first observed by Natta in melt crystallized material. It is normally observed also in solution-grown crystals. The structure determinations carried out on alpha phase isotactic polypropylene showed that the crystal structure is monoclinic and the chains assume a helical conformation. From the x-ray data it follows that the identity in the main direction of the chain comprise three monomer units. The symmetry of the helix is characterized by a threefold screw axis. Consequently right- and left-handed helices are possible. They are arranged in regular pattern, a left-handed helix always facing a right-handed one.

2.2.3 Beta modification

Commercial grades of *i*PP, when processed in laboratory or industrial scale, crystallize essentially into alpha-modification. At first Padden and colleagues [4] demonstrated by X-ray diffract metric and optical microscopic studies that, at the high

super cooling, the formation of the alpha-modification was accompanied by appearance of the beta-modification.

Turner-Jones and coworkers [5] were the first to report the formation of polymers highly rich in beta-modification. They crystallized a particular (unspecified) *i*PP sample in the range of 393-403 K into a nearly pure beta- *i*PP. They introduced a k_{β} value for characterizing the proportion of beta-modification by X-ray diffractometric data, as shown in Equation 2.1 [5].

$$k_{\beta} = \frac{H_{\beta 1}}{H_{\beta 1} + (H_{\alpha 1} + H_{\alpha 2} + H_{\alpha 3})} \quad (2.1)$$

Where $H_{\alpha 1}$, $H_{\alpha 2}$ and $H_{\alpha 3}$ are the intensities of alpha-diffraction peaks corresponding to angle $\theta_s = 7.1^\circ$, 8.5° and 9.4° , respectively, and $H_{\beta 1}$ is the intensity of beta-diffraction peaks corresponding to angle $\theta_s = 8.1^\circ$. The k_{β} value is a relative measure for characterizing the polymorphic composition but it does not express the absolute value of beta-content numerically, although its value is 0 for alpha- *i*PP and 1 for beta- *i*PP, as is apparent.

Several attempts were subsequently made to prepare the beta-modification in pure form. Two methods have been used successful to prepare samples rich in beta modification; the temperature gradient method and introduction of beta nucleating agents. Furthermore, it is known that shear stress also promotes the formation of beta-modification.

The use of nucleating agent can affect the physical and/or optical properties of PP products. Regardless of which effect is desired, it is brought about by the same mechanism; increased nucleation of the crystallizing PP. In general, PP cans crystalline form, depending on the nucleating agent type which is used. Typical nucleating agents are shown in following Table 2.1.

Table 2.1 Nucleator types and their crystal forms [6]

Nucleator types	Crystal form provided
1) lithium,sodium, potassium benzoate	Alpha-crystalline form
2) sodium salts or organophosphates	
3) talcum, finely divided (<40 nm) clays	
4) milled, bis-(3,4-dimethylbenzylidene sorbitol diacetal)	
5) quinacridone dye	Beta-crystalline form
6) triphenol ditrazine	
7) aluminium quinizarin sulfonic acid	
8) disodium, calcium phthalate	
9) aryl amide nucleator [7]	

The beta-form PP is easily identified by X-ray diffraction, polarized optical microscopy, and scanning electron microscopy due to its high birefringence. The beta-form has been obtained by crystallization at higher temperature ($t_3 = 120-140\text{ }^\circ\text{C}$) and can only be studied if the sample temperature is maintained above $110\text{ }^\circ\text{C}$. Moreover, beta crystallization is reduced in copolymers of propylene with ethylene [7].

Numerous investigations have been carried out involving the subject of the beta *i*PP crystal structure but most previous studies were only concentrated on the techniques are used to promote the beta-form are following.

1. Addition of beta-nucleators.
2. Crystallization in a temperature gradient/thermal gradient.
3. Shear-induced technique.

Crystallization in the presence of beta-nucleating agents promises to be the most reliable method for industrial applications. The most well know and beta nucleating agents is a gamma-quinacridone red pigment (Permanent Rot E3B) as an effective nucleating agent. Their k_β value is around 0.8 as calculated from X-ray

diffractometric data but, when crystallized under given thermal conditions, k_{β} value may reach about 0.9 [8]. Even though gamma-quinacridone is one of the most effective beta-nucleating agents, pure beta-*i*PP could not be prepared in its presence. In other words, its alpha nucleating effect is not negligible. It was also observed that beta nucleating activity is reduced during processing. This indicates a modification in the physical or chemical structure of this red pigment due to the high pressure and temperature of processing. A drawback of gamma-quinacridone is its intense red color, which may restrict its practical application.

The internal microstructure of the beta form spherulites is thought to be composed of radial arrays of parallel stacked lamellae. In this regard, the lamellar microstructure of the beta-form exhibits much greater similarity to the conventional microstructure of semi crystalline photopolymers than does the alpha form with its unique tendency for cross-hatch formation. Various studies have suggested that the crystallographic a-axis direction, assuming a hexagonal unit cell [9]. Table 2.1 gives the types and crystal forms of nucleator used for polymer modifications.

Various mechanisms have been postulated for beta-form melting and the beta-to alpha-form recrystallization process. Many of the associated effects bear close resemblance to general reorganization phenomena in semi-crystalline polymers. Varga and co-workers have extensively investigated and reviewed the transition of beta-form to alpha-form crystallinity in optical microscopy and DSC experiments. Using preferentially nucleated materials, these studies suggested that the optimum isothermal crystallization temperature for formation of beta-crystallinity is between 100 °C and 141°C. It was proposed that recrystallization of the beta-form to alpha-form is promoted if the temperature is lowered, following crystallization, below critical temperature. This critical temperature, TR^* , was in the range of 100 °C to 110 °C [3]. The proposed mechanism was thought to occur by formation of alpha-form nuclei act as sites for alpha-form recrystallization following melting of metastable beta-form crystallites on heating. Figures 2.4 and 2.5 show the typical X-ray diffraction diagrams. Figure 2.6 shows optical micrograph of pure beta-*i*PP crystallized [8].

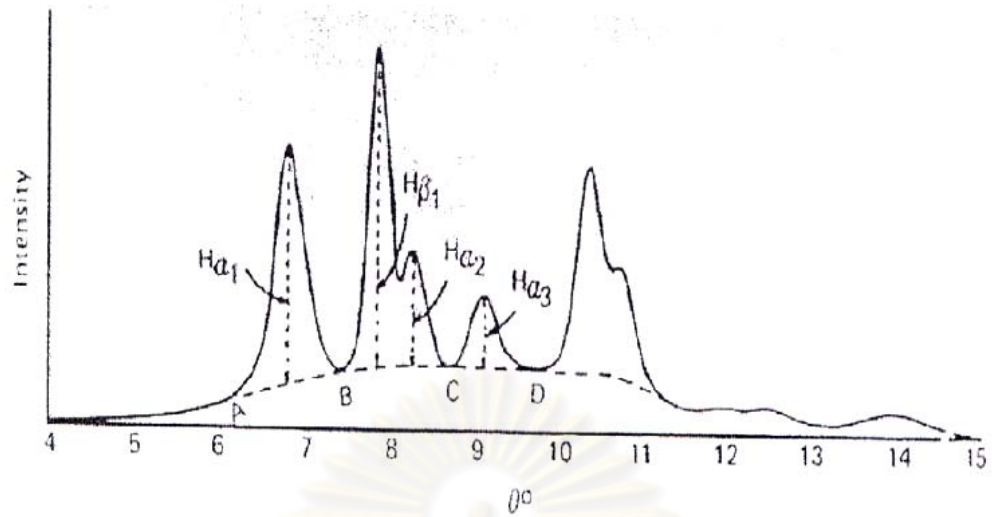


Figure 2.4 X-ray diffraction diagrams showing mixed alpha and beta crystalline [10].

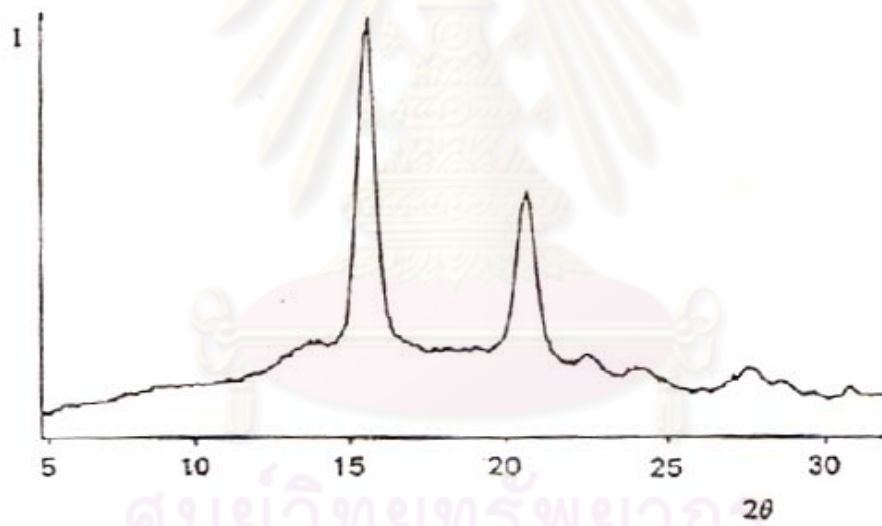


Figure 2.5 X-ray diffractogram of pure beta-*i*PP [10].

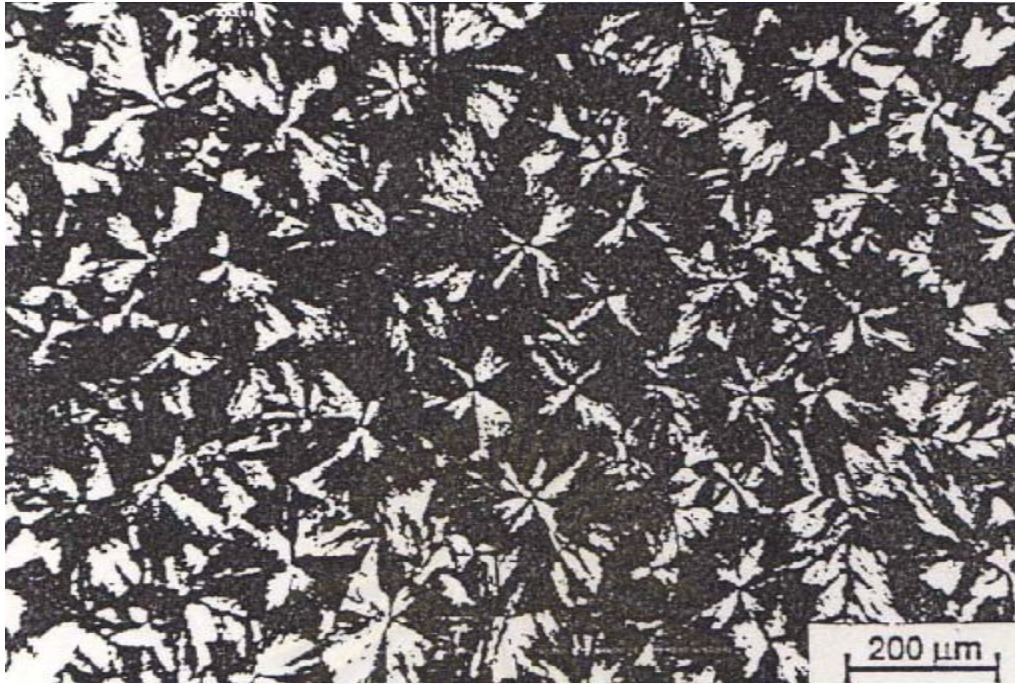


Figure 2.6 Optical micrograph of pure beta- *i*PP crystallized at $T_c = 398$ K [8, 10].

2.2.4 Gamma Modification

The third crystalline modification of *i*PP is gamma-form. It was first described [4] as observed only in polypropylene with low molecular weight having a degree of isotacticity not too low. It was later obtained from solvent fractionation [2]. A fraction of isotactic polypropylene precipitated from petrol ether or xylene is the temperature range 35-70 °C, melted and slowly cooled from 190 °C, under vacuum, at 6 °C/h to room temperature, shows gamma-form crystallinity. It is therefore not necessarily associated with low molecular weight polymer crystallinity.

This crystalline modification has been obtained, free of alpha form, by melt crystallization under conditions of elevated pressure. In this case a difference in behavior was found between specimens prepared at a large degree of supercooling ($\Delta < 40$ °C). In the first case the samples; examined by long-angle X-ray diffraction, show long spacings, which are characteristic of chain-folded lamellar crystals. For the second one, no long spacings are obtained. These data suggest that for the samples

prepared at elevated pressure with low supercooling the amount of chain folding is minimal. It is suggested that in this case the gamma-phase is composed by extended chain crystallization.

The most likely unit cell for the gamma form is triclinic. The method of crystallization and the molecular weight of the sample play an important role in determining the phases present in the sample. Figure 2.7 presents the X-ray diffraction diagrams of three crystalline form of isotactic polypropylene. The gamma phase polypropylene crystallized at elevated hydrostatic is metastable in character. The DSC thermogram a sample crystallized under pressure at the large degree of supercooling shows that material transforms entirely to the alpha phase prior to melting. On the contrary, when the gamma phase is prepared with low degree of super cooling it is stable, showing no transformation to the alpha phase up to 173 °C, temperature at which the X-ray scan obtained showed only the presence of gamma phase as shown in Figure 2.7.

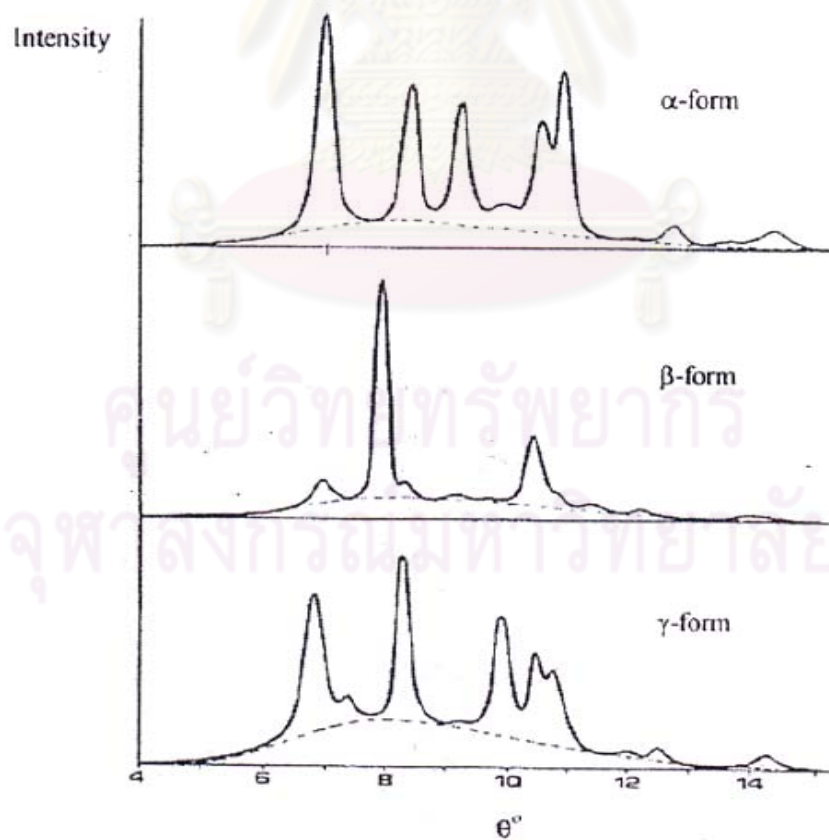


Figure 2.7 X-ray diffraction diagrams of *i*PP crystalline forms [3].

2.2.5 Smectic

Many commercial fabrication processes utilize rapid cooling conditions. Under these conditions, it is common to observe the crystallization of *i*PP in the mesomorphic form, also commonly referred to as the smectic form. The mesomorphic phase represents a state. Figure 2.8 shows a comparison of the wide angle X-ray pattern of the mesomorphic form compared to the patterns of the atactic PP (amorphous) and the alpha-form of *i*PP.

Early work suggested a hexagonal crystallographic symmetry in the mesomorphic form [3, 11]. This assignment of the hexagonal structure was based on the observation that the primary diffraction intensity maxima of the mesomorphic form more closely corresponded to the two most intense reflections of the beta-form, which was classified as a hexagonal unit cell. The mesomorphic form could be induced by compressive deformation of *i*PP in the alpha-form, provided that the deformation temperature was below the upper stability of the mesomorphic form. Similarly, some experiments have suggested that an oriented mesomorphic form results from drawing samples with beta-form crystallinity at low temperature.

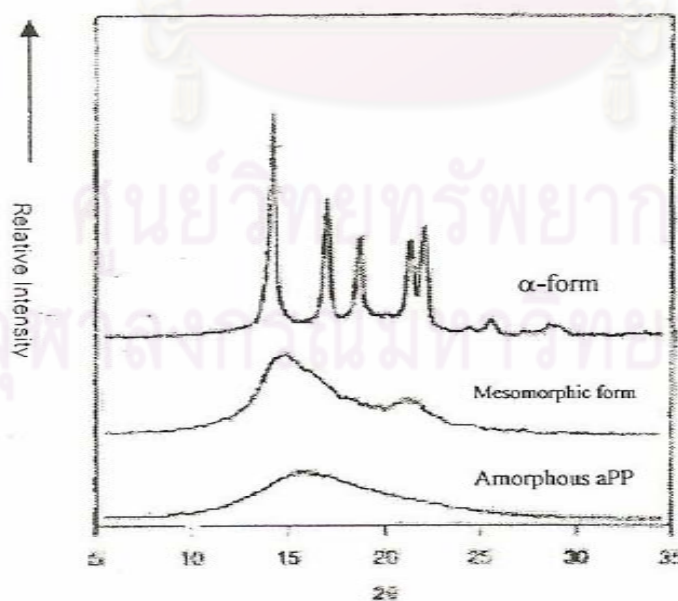


Figure 2.8 Comparison of the WAXD pattern of the *a*PP (amorphous), *i*PP in the mesomorphic form, and *i*PP in the alpha-form [3].

2.3 Additives in PP

Virgin PP directly from a commercial process is very susceptible to air oxidation. If stored unstabilized at ambient temperature, the physical properties of the product deteriorate rapidly over a period of weeks or months depending on the physical form, temperature, available oxygen, and other considerations. This exothermic reaction can be prevented by the addition of a few parts per million of an antioxidant to the reactor to the product before drying and storage. This is often referred to as an in-process stabilizer [3].

Beyond the need for stabilization, additives are used in PP for the following reasons:

Adjust color: Polypropylene is whitish in color. Pigments are used to add color to the manufactured articles. Pigments may also have an impact on stability and physical properties.

Alter stiffness: Polypropylene homopolymers and copolymers are typically semi-crystalline materials which are manufactured to obtain various degrees of stiffness. The stiffness can be further adjusted through the addition of plasticizers, nucleators, or fillers.

Control transparency: Polypropylene is translucent. Its transparency is dramatically improved with clarifying additives. It can also be rendered opaque with pigments and fillers.

Lower molecular weight and molecular weight distribution: Additives can be used to reduce the molecular weight and narrow the molecular weight distribution. This alters processing characteristics and physical properties.

Decrease static buildup: Polypropylene is a natural insulator and can build static charge. Several types of additives are used as antistats.

Control surface properties: various additives can be used to modify the frictional and adhesion properties of PPs.

Neutralize catalyst residues: Acid scavengers are routinely incorporated to neutralize catalyst residues and prevent equipment corrosion.

Suppress transition metal catalyzed: The oxidation of PP is accelerated by certain metals. Several types of metal chelators successfully suppress this phenomenon.

Enhance whiteness: Fluorescent or brilliancy of pigmented and unpigmented articles.

Prevent biological growth: Biocides are used to prevent biological growth on the surface of PP articles.

2.4 Crystallization behavior

Polypropylene is a semi-crystalline polymer. Its properties are determined by its crystalline structure and the relative amount of amorphous and crystalline phases, crystal structure, size and perfection of crystallites, dimensions of spherulites and the number of tie molecule. The crystalline phase of polymers consists of thin plates or ribbons with chains oriented along the thin dimension. The amorphous region consists of chain-end cilia, totally occluded chains, and chains which are incorporated into two or more crystals (tie chains). The tie chains determine the mechanical continuity of the system and thereby control the elastic modulus as well as yield strength.

The higher crystallinity of the PP with coarse spherulitic structure to a larger volume contraction and thus to formation of voids and micro cracks. Consequently, the crack path tends to follow the weak spherulite boundaries, resulting in a very low fracture toughness value.

In general, it is believed that the spherulitic nucleation takes place at heterogeneities in the melt such as catalyst residues, dust particle low-molecular weight fractions, branch points, stereo-irregular molecules, fillers or specific nucleating agents. The spherulite size is primarily dictated by the volumetric nucleation rate, which depends on thermal history, nature of the surface and degree of under cooling. The amount of crystallinity and spherulite size influences the modulus and strength of PP. Spherulite size and spherulite boundaries significantly influences the yield and the failure behavior of polymers. These effects are manifested in the macroscopic nature the fracture path.

The fine spherulite microstructure produced by adding nucleating agents gives rise to greatly enhanced ductility, yield strength, and impact strength. In general, refinement of the spherulite size by either homogeneous or heterogeneous nucleation, or by reducing the crystallization temperature results in improved ductility and strength. It is clear that the large spherulite exhibits cracks at spherulite boundaries, whereas systems with smaller spherulite draw smoothly.

2.5 Polymer/layered silicate (PLS) nanocomposites

Polymer/layered silicate (PLS) nanocomposites have attracted great interest, both in industry and in academia, because they often exhibit remarkable improvement in materials properties when compared with virgin polymer or conventional micro and macro-composites. These improvements can include high moduli, increased strength and heat resistance, decreased gas permeability and flammability, and increased biodegradability of biodegradable polymers. [12]

2.5.1 Structure and properties of layered silicates

The commonly used layered silicates for the preparation of PLS nanocomposites belong to the same general family of 2:1 layered or phyllosilicates. Their crystal structure consists of layers made up of two tetrahedrally coordinated silicon atoms fused to an edge-shared octahedral sheet of either aluminum or magnesium hydroxide. The layer thickness is around 1 nm, and the lateral dimensions

of these layers may vary from 30 nm to several microns or larger, depending on the particular layered silicate. Stacking of the layers leads to a regular Van der Waals gap between the layers called the interlayer or gallery. Isomorphic substitution within the layers (for example, Al^{3+} replaced by Mg^{2+} or Fe^{2+} , or Mg^{2+} replaced by Li^{1+}) generates negative charges that are counter balanced by alkali and alkaline earth cations situated inside the galleries. This type of layered silicate is characterized by a moderate surface charge known as the cation exchange capacity (CEC), and generally expressed as mequiv/100 gm. This charge is not locally constant, but varies from layer to layer, and must be considered as an average value over the whole crystal. MMT, hectorite, and saponite are the most commonly used layered silicates. Layered silicates have two types of structure: tetrahedral-substituted and octahedral substituted. In the case of tetrahedrally substituted layered silicates the negative charge is located on the surface of silicate layers, and hence, the polymer matrices can react interact more readily with these than with octahedrally-substituted material.

Two particular characteristics of layered silicates are generally considered for PLS nanocomposites. The first is the ability of the silicate particles to disperse into individual layers. The second characteristic is the ability to fine-tune their surface chemistry through ion exchange reactions with organic and inorganic cations. These two characteristics are, of course, interrelated since the degree of dispersion of layered silicate in a particular polymer matrix depends on the interlayer cation [12].

2.5.2 Structure and properties of organically modified layered silicate

The physical mixture of a polymer and layered silicate may not form a nanocomposite. This situation is analogous to polymer blends, and in most cases separation into discrete phases takes place. In immiscible systems, which typically correspond to the more conventionally filled polymers, the poor physical interaction between the organic and the inorganic components leads to poor mechanical and thermal properties. In contrast, strong interactions between the polymer and the layered silicate in PLS nanocomposites lead to the organic and inorganic phases being dispersed at the nanometer level. As a result, nanocomposites exhibit unique properties not shared by their micro counterparts or conventionally filled polymers.

Pristine layered silicates usually contain hydrated Na^+ or K^{2+} ions. Obviously, in this pristine state, layered silicates are only miscible with hydrophilic polymers, such as poly(ethylene oxide) (PEO), or poly(vinyl alcohol) (PVA). To render layered silicates miscible with other polymer matrices, one must convert the normally hydrophilic silicate surface to an organophilic one, making the intercalation of many engineering polymers possible. Generally, this can be done by ion-exchange reactions with cationic surfactants including primary, secondary, tertiary, and quaternary alkylammonium or alkylphosphonium cations. Alkylammonium or alkylphosphonium cations in the organosilicates lower the surface energy of the inorganic host and improve the wetting characteristics of the polymer matrix, and result in a larger interlayer spacing. Additionally, the alkylammonium or alkylphosphonium cations can provide functional groups that can react with the polymer matrix, or in some cases initiate the polymerization of monomers to improve the strength of the interface between the inorganic and the polymer matrix. Traditional structural characterization to determine the orientation and arrangement of the alkyl chain was performed using wide angle X-ray diffraction (WAXD). Depending on the packing density, temperature and alkyl chain length, the chains were thought to lie either parallel to the silicate layers forming mono or bi-layers, or radiate away from the silicate layers forming mono or bimolecular arrangements. However, these idealized structures have been shown to be unrealistic by using FTIR experiments [12].

2.5.3 Types of nanocomposites

Layered silicates have layer thickness on the order of 1 nm and a very high aspect ratio (e.g. 10–1000). A few weight percent of layered silicates that are properly dispersed throughout the polymer matrix thus create much higher surface area for polymer/filler interaction as compared to conventional composites. Depending on the strength of interfacial interactions between the polymer matrix and layered silicate (modified or not), three different types of PLS nanocomposites are thermodynamically achievable (see Figure 2.9) [12]:

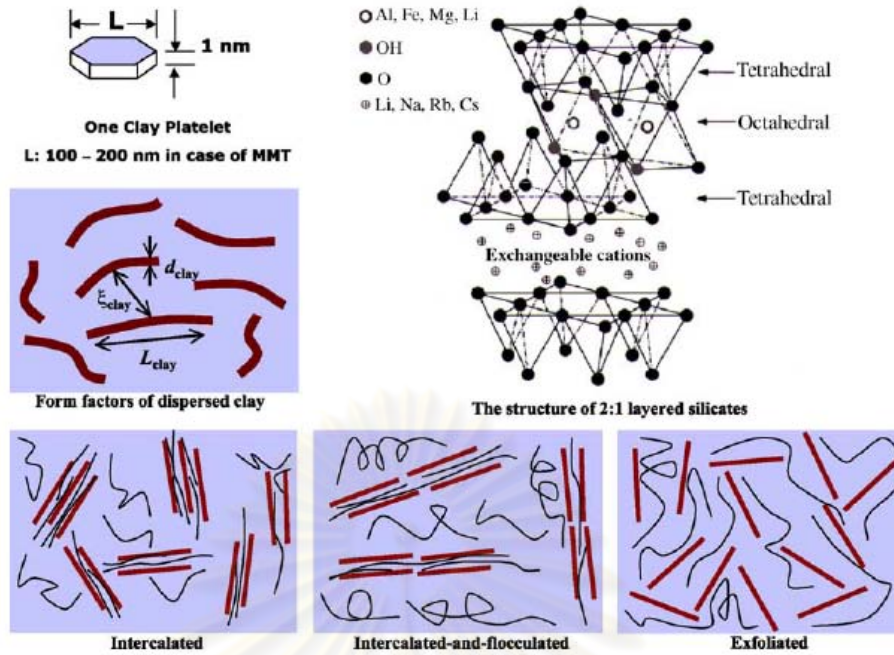


Figure 2.9 Schematic illustration of three different types of thermodynamically achievable polymer/layered silicate nanocomposites [12].

a. Intercalated nanocomposites: in intercalated nanocomposites, the insertion of a polymer matrix into the layered silicate structure occurs in a crystallographically regular fashion, regardless of the clay to polymer ratio. Intercalated nanocomposites are normally interlayer by a few molecular layers of polymer. Properties of the composites typically resemble those of ceramic materials.

b. Flocculated nanocomposites: conceptually this is same as intercalated nanocomposites. However, silicate layers are some times flocculated due to hydroxylated edge-edge interaction of the silicate layers.

c. Exfoliated nanocomposites: in an exfoliated nanocomposite, the individual clay layers are separated in a continuous polymer matrix by an average distances that depends on clay loading. Usually, the clay content of an exfoliated nanocomposite is much lower than that of an intercalated nanocomposite.

2.6 Techniques used for the characterization of nanocomposites

The structure of nanocomposites has typically been established using WAXD analysis and transmission electron micrographic (TEM) observation. Due to its easiness and availability WAXD is most commonly used to probe the nanocomposite structure and occasionally to study the kinetics of the polymer melt intercalation. By monitoring the position, shape, and intensity of the basal reflections from the distributed silicate layers, the nanocomposite structure (intercalated or exfoliated) may be identified. For example, in an exfoliated nanocomposite, the extensive layer separation associated with the delamination of the original silicate layers in the polymer matrix results in the eventual disappearance of any coherent X-ray diffraction from the distributed silicate layers. On the other hand, for intercalated nanocomposites, the finite layer expansion associated with the polymer intercalation results in the appearance of a new basal reflection corresponding to the larger gallery height. Although WAXD offers a convenient method to determine the interlayer spacing of the silicate layers in the original layered silicates and in the intercalated nanocomposites (within 1–4 nm), little can be said about the spatial distribution of the silicate layers or any structural non-homogeneities in nanocomposites. Additionally, some layered silicates initially do not exhibit well-defined basal reflections. Thus, peak broadening and intensity decreases are very difficult to study systematically. Therefore, conclusions concerning the mechanism of nanocomposites formation and their structure based solely on WAXD patterns are only tentative. On the other hand, TEM allows a qualitative understanding of the internal structure, spatial distribution of the various phases, and views of the defect structure through direct visualization. However, special care must be exercised to guarantee a representative cross-section of the sample. Both TEM and WAXD are essential tools for evaluating nanocomposite structure. However, TEM is time-intensive, and only gives qualitative information on the sample as a whole, while low-angle peaks in WAXD allow quantification of changes in layer spacing. Typically, when layer spacing exceed 6–7 nm in intercalated nanocomposites or when the layers become relatively disordered in exfoliated nanocomposites, associated WAXD features weaken to the point of not being useful. However, recent simultaneous small angle X-ray scattering (SAXS) and WAXD studies yielded quantitative characterization of nanostructure and crystallite structure in N6 based nanocomposites [12].

2.7 Composites preparation (Melt compounding)

PP composites can be prepared by using a melt compounding process through a twin screw extruder. Because PP is a low polarity polymer, it is extremely challenging to make a well-dispersed PP composite. Numerous parameters can influence nanocomposite formation in a melt compounding process [13, 14] as follows:

a. Effect of base resin

The characteristic properties of a base resin (mainly molecular weight and molecular weight distribution) play an important role in making PP nanocomposites. At a low melt flow range (high molecular weight), good improvement in mechanical properties is achieved. However, for a high melt flow PP, the improvement in mechanical properties is relatively small. The enhanced properties for the low melt flow PP are attributed to the corresponding higher melt viscosity with increased shear deformation of the ingredients during the extrusion process which enhance clay dispersion.

b. Effect of clay surface treatment

The most common method to modify clay surface is by ion-exchange reaction using alkylammonium. The molecular chain length of alkylammonium has a pronounced effect on clay surface polarity, and therefore affects the interaction between the polymer matrix and modified clay.

c. Effect of compounding conditions

Melt extrusion processing conditions are one of the most important factors to disperse layered silicate such as screw design, screw speed and processing temperature.

d. Effect of compatibilizer

The effect of reinforcement by layered silicate in PP is determined by at least two important factors: clay dispersion (intercalation or exfoliation) and interaction between the clay and polymer. When the clay surface is covered by a sufficient amount of organic surfactant, (such as alkylammonium) modified clay (organoclay) can be well dispersed in the PP matrix by using appropriate compounding techniques. However, in many case, the mechanical properties remain quite poor due to inadequate stress transfer from the polymer matrix under applied stress to load-bearing clay reinforcement. The case for this weakness is attributed to poor compatibility in the interphase region that exists between nonpolar PP molecules and polar clay layers. To overcome this problem, the most effective approach is to an adding bi-functional compatibilizer to the nanocomposite formulation to enhance adhesion at the polymer-clay interface.

2.8 Literature review

Reichert and coworkers [15] modified inorganic clay using protonated C4 to C18 alkylamine. PP nanocomposites were then compounded using different organoclay with (or without) maleic anhydride modified polypropylene (PP-g-MA) as compatibilizer. In the absence of compatibilizer, Young's modulus of the PP composites was very similar to that of neat resin. However, with the addition of PP-g-MA, there was significant improvement in Young's modulus when the chain length of alkyl groups in alkylamine were 12 carbon atoms or higher. This influence of alkyl chain length on mechanical properties was attributed to the changes of superstructures. In the absence of compatibilizer, the interaction between polymer matrix and organoclay was limited. No matter what alkyl chain length is in the organoclay, a macrocomposite formed that behaved as a conventionally filler. On the other hand, when the alkyl chain length was 12 and higher, partially exfoliated nanocomposites were formed in the presence of a compatibilizer. The exfoliated structure was detected by a broadened peak from wide-angle X-ray scattering (WAXS) and TEM. As a result, the mechanical properties of these nanocomposites are greatly improved.

Wu and coworkers [16] studied the effect of compatibilizer (PP-g-MA) on making PP nanocomposite through a melt compounding process. They concluded that

there were at least two important factors that helped the exfoliation and homogeneous dispersion of the clay layers: (1) the intercalation capability of the compatibilizers in the clay layers; and (2) the composition of the compatibilizer in the PP/clay composites. Almost complete hybrids were obtained in the case where the PP-g-MA has the intercalation capability with a PP-g-MA/clay weight ratio over 3 to 1. Rheological characterization by complex viscosity also demonstrated that PP-g-MA of low molecular weight and high MA content led to better interaction with clay. However, the addition of lower molecular weight PP-g-MA or high loading of PP-g-MA had a negative effect on mechanical and thermal properties of the PP/PP-g-MA/clay composites.

Usaki and coworkers [17] studied the dispersibility of organoclay and structure of PP composite prepared from melt extrusion process of maleic anhydride modified PP (PP-MA) and organoclay. They demonstrated the hierarchical structure of the intercalated PP composites viewed on scale from the structure of confined PP-MA chains in the space of silicate galleries (intercalating sites) of 2-3 nm width to crystalline lamellae of 7-15 nm thickness. With increasing clay content, the PP-MA chains were intercalated in the space of the intercalating sites accompanied with the stacking of the individual silicate layers. In other words, the increment of intercalating sites leads to the limitation of the exfoliation toward the individual silicate layers and obtained agglomeration of organoclay layers which effect to reduce its aspect ratio. To enhance the moduli, both the degree of intercalation of the PP-MA chains and the aspect ratio of the dispersion clay particles strongly affected the final mechanical properties of the PP composites. Table 2.2 and Figure 2.10 show characteristic parameters of organophilic clay, PP-MA and PPCNs.

Table 2.2 Characteristic parameters of organophilic clay, PP-MA and PPCNs [17].

Property	Organophilic clay	PP-MA	PPCN2	PPCN4	PPCN7.5
Clay content (vol%)	30-100 ^a	0	0.75	1.54	2.95
T_m (°C)		138.6	139.5	143.2	143.9
χ_c (%)		43.7	40.4	47.2	48.7
TEM					
d_{clay}^b (nm)			5.2±0.4	7.9±0.6	10.2±1.8
L_{clay}^c (nm)			193.3±25.0	158.9±24.8	127.3±21.4
($L_{\text{clay}}/d_{\text{clay}}$)			37.2	20.1	12.5
ξ_{clay}^d (nm)			61.7±20.0	49.5±10.8	34.6±12.4
SAXS					
d_{lamellar} (nm)		7.12	7.21	7.24	7.36
L_{lamellar} (nm)		15	14.8	15	15
Φ_c ($d_{\text{lamellar}}/L_{\text{lamellar}}$) (%)		47.5	48.7	48.3	49
Q_{SAXS}		4.9	4.5	4.85	5.35
WAXD					
$d_{(001)}$ (nm)	2.31		3.24	3.03	2.89
χ_y^e (%)		0	0	6.7	10.5

a Melt temperature rang of stearyl ammonium intercalated in silicate galleries.

b Average thickness of the dispersed clay particles.

c Average length of the dispersed clay particles.

d Correlation length of the dispersed clay particles.

e Relative percentage content of gamma phase crystallite.

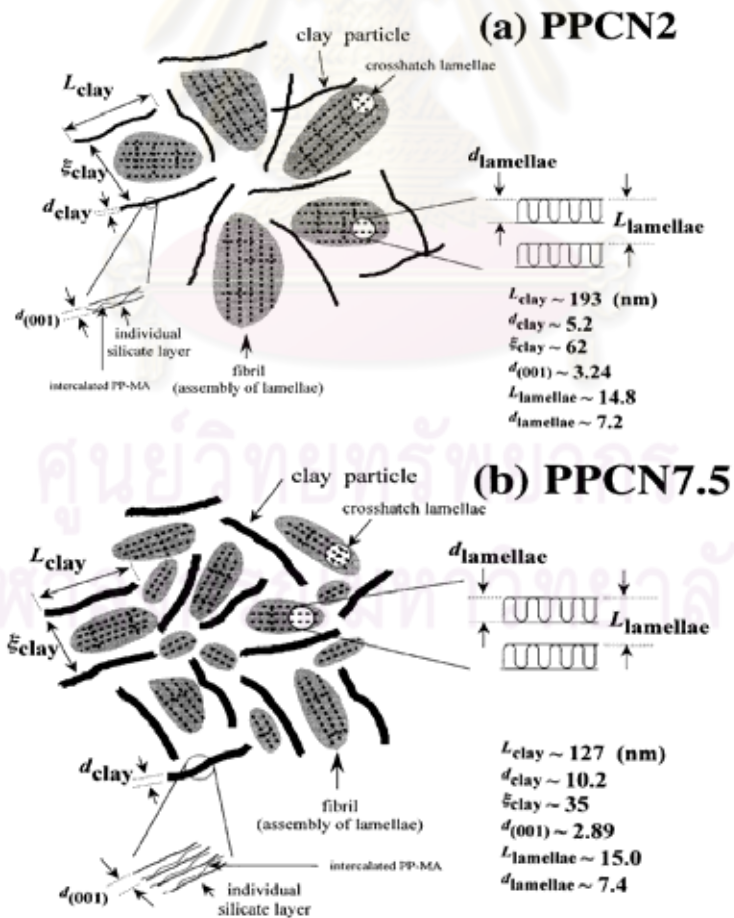


Figure 2.10 Illustration for dispersed clay structure and the inter-fibrillar structure for: a) PPCN2 and b) PPCN7.5 [17].

Turner and coworkers [5] were the first group to report the formation of polymers highly rich in beta-modification. They crystallized a particular (unspecified) *i*PP sample in the range of 393-403 K into a nearly pure beta- *i*PP. They introduced a k_β value for characterizing the proportion of β -modification by X-ray diffractometric data, as shown in Equation 2.1:

$$k_\beta = \frac{H_{\beta 1}}{H_{\beta 1} + (H_{\alpha 1} + H_{\alpha 2} + H_{\alpha 3})} \quad (2.1)$$

where $H_{\alpha 1}$, $H_{\alpha 2}$ and $H_{\alpha 3}$ are the intensities of alpha-diffraction peaks corresponding to angle $\theta_s = 7.1^\circ$, 8.5° and 9.4° , respectively, and $H_{\beta 1}$ is the intensity of beta-diffraction peaks corresponding to angle $\theta_s = 8.1^\circ$. The k_β value is a relative measure for characterizing the polymorphic composition but it does not express the absolute value of beta-content numerically, although its value is 0 for alpha-*i*PP and 1 for beta-*i*PP, as is apparent.

Tantayanon and coworkers [6] studied the effect of beta-nucleating agent on the mechanical properties of *i*PP/EPR blend. They found that the addition of a combination of calcium stearate and pimelic acid (Ca-Pim) exhibited an improvement in the notched Izod impact strength over that of the unfilled *i*PP/EPR blend. Further investigation revealed that *i*PP/EPR blend loaded with 0.001 wt% Ca-Pim showed the highest improvement in the notched Izod impact strength (an increase of ca. 3.5-fold over that of the unfilled sample) at the expense of both the tensile strength at yield and flexural modulus. All of the wide-angle X-ray diffraction, differential scanning calorimetry, and scanning electron microscopy results pointed to the presence of the beta-crystals (with the k_β value being 0.75) being responsible for the great improvement in the notched Izod impact strength of the *i*PP/EPR blend filled with 0.001 wt% Ca-Pim. However, the flexural modulus of the *i*PP/EPR blend will decrease respectively when the k_β value is higher than about 0.5 as shown in Table 2.3.

Table 2.3 Mechanical properties and the k_{β} value of *i*PP/EPR blend filled with bi-component nucleating agent of calcium stearate and pimelic acid (Ca-Pim) at various filler loadings [6].

Percentage by weight of Ca-Pim	Tensile strength at yield (MPa)	Percentage of elongation at yield (MPa)	Flexural Modulus (MPa)	Notched Izod impact strength (J/m)	k_{β} value
none	25.5±0.2	9.1±0.1	1080±6	175.4±2.5	0.21
0.1	26.4±0.1	7.7±0.1	1220±7	196.1±4.1	0.26
0.05	23.0±0.1	9.0±0.1	1116±7	320.5±5.9	0.40
0.025	21.4±0.1	9.3±0.1	994±6	557.9±3.6	0.54
0.01	21.1±0.2	9.7±0.1	973±9	582.7±4.7	0.68
0.001	21.3±0.2	10.0±0.1	897±8	627.3±3.7	0.75

Li and coworkers [18] studies the correlation between beta-crystals content on the mechanical properties of polypropylene, found that acylamino-nucleating agent is very efficient to inducing the crystallization of *i*PP into the beta-modification with a k_{β} value as 0.87 when the content of nucleating agent is 0.3%. The nucleating agent can affect the crystalline morphology of *i*PP, as well as the mechanical properties. The mechanical properties of *i*PP were changed with the increase of nucleating agent. The impact strength and elongation at break of *i*PP were significantly increased with increasing the beta-crystals. However, the tensile strength of *i*PP was decreased with increasing the beta-crystals.

Varga *et al.* [10] reported that calcium salts of pimelic and suburic acids are highly active, thermally stable beta-nucleating agents. Isotactic homopolymers and random and block copolymers of polypropylene crysyallize almost purely in beta modification, even at a low concentration. Ca-Sub proved the most effective beta-nucleating agent found *i*PP crystallize in pure beta-form up to a temperature of ~ 140 °C. These additives caused significant changes in crystallization, melting characteristics, and structure of the polymers. The degree of crystallinity of the beta-nucleated samples was markedly higher than that of the alpha-modification. similar features were found the melting behavior of alpha-and beta-*i*PP crystallized isothermally in a wide temperature range.

Todjeman *et al.* [19] studied the effect of the alpha and beta crystalline structure of polypropylene on its mechanical properties. Young modulus and yield stress reduce slowly with an increase in beta phase content and the fracture toughness of PP increases greatly with its beta phase content. They reported that the occurrence of tangential lamellae in the alpha phase makes the spherulites more rigid and causes increase in Young modulus and yield stress with the alpha phase content and these tangential lamellae restrict the elongation at break of the spherulites and make the PP more brittle.



ศูนย์วิทยทรัพยากร
จุฬาลงกรณ์มหาวิทยาลัย

CHAPTER III

EXPERIMENTAL

3.1 Materials

1. Matrix polymer: isotactic polypropylene (Homopolymer: 1100NK) supplied by IRPC Co., Ltd., Rayong, Thailand, MFI 230 °C at 2.16 kg loading = 12 g/10 min and density of 0.905 g/cm³
2. Organoclay: a natural montmorillonite clay surface modified with distearyldimethyl ammonium chloride (OMMT: Nanofil[®] SE 3000) supplied by Sud Chemie.
3. Compatibilizer: PP-g-MA; PB 3200 (Mw = 120,000, MA content of 1.0 wt% and MFI 190 °C at 2.16 kg loading = 115 g/10 min. supplied by Chemtura.
4. Beta-nucleating agent; aryl amides compounds from Xiang Yang Co., Ltd., China.

3.2 Instruments

The major instruments used in this research are as follows:

1. LTE 26-40 system twin screw co-rotating extruder (LAB TECH Engineering Co., Ltd., Thailand).
2. LZ-120/VS Pelletizing unit (LAB TECH Engineering Co., Ltd., Thailand).
3. IS100G 100MT Toshiba injection molding machine, Japan.
4. Instron 4465 universal testing machine, Instron Co., USA.
5. Pendulum impact tester, ZWICK Co., Germany.
6. DSC1, Mettler Toledo, Differential Scanning Calorimeter (DSC), Switzerland.
7. Cone and Plate Rheometer (Physica MCR 301, Anton Paar Co., Austria).
8. RH-7 Rosand Single Bore Capillary Rheometer, United Kingdom.
9. Fourier-transform infrared spectrophotometer (FTIR), Vertex 70, Bruker, Germany.
10. Microscope with polarized, Nikon and heating cell, Linkam TH 600.
11. JSM-5800LV JEOL Scanning Electron Microscope (SEM), Japan.
12. Ultramicrotome, RMC MTX Ultramicrotome with cryo mode, USA

13. JEOL-2010F Transmission electron microscopy (TEM), Japan.
14. XRD (TTRAX III, Rigaku Corp., Japan) using Ni-filtered Cu K α radiation, having a wavelength of 0.154 nm.
15. HDT, Vicat tester (YASUDA 148, Yasuda Co., Japan)
16. Density meter (AT201, Mettler Toledo Co., Switzerland)

3.3 Experimentals

3.3.1 The effects of the compatibilizers on physical properties of PP/organomontmorillonite (OMMT: organoclay) composites.

Firstly, a masterbatch of PP/PP-*g*-MA/OMMT at a weight ratio of 40/30/30 was prepared in a twin screw co-rotating extruder before letting it down with bulk PP in a twin screw co-rotating extruder. Before melt processing, all the components were dried at 80 °C for 10 h. The formulations of these melt compounding are shown in Table 3.1.

Table 3.1 The formulations of PP/PP-*g*-MA/OMMT melt compounding.

Recipe No.	PP/PP- <i>g</i> -MA/OMMT (wt%)	Weight fraction (wt%)		
		PP	PP- <i>g</i> -MA	OMMT
1	100/0/0 (Neat PP)	100	0	0
2	95/0/5	95	0	5
3	90/5/5	90	5	5
4	88/7/5	88	7	5
5	85/10/5	85	10	5
6	80/15/5	80	15	5
7	75/20/5	75	20	5

*All recipes used masterbatch for compounding

Each formulation was melt-mixed in a twin screw co-rotating extruder by screw configurations as shown in Table 3.2 at 160/160/160/160/160/160/160/160/-185/195 °C (from the hopper to the nozzle), a feed rate 45 rpm, a screw speed 250 rpm and then they were pelletized with a granulator (LZ-120/VS Pelletizing unit). These pellet samples were dried at 90 °C for 10 hours and then molded to form dumbbell shape specimens and impact specimens for mechanical testing by an injection molding machine at 210/230/230/230 °C (from the hopper to the nozzle).

3.3.2 The effects of the screw configuration on physical properties of PP/compatibilizer/OMMT (organoclay) composites.

The selected formulations which gave the higher physical properties obtained from Section 3.3.1 were prepared in a twin screw co-rotating extruder at 160/160/160/160/160/160/160/160/185/195 °C (from the hopper to the nozzle), a feed rate 45 rpm, a screw speed 250 rpm with two different screw configurations as shown in Tables 3.2 and 3.3 then they were pelletized with a granulator. These pelletized samples were prepared to form mechanical testing samples using the same procedure as Section 3.3.1.

Extruder Data	Configuration
Diameter of screw:	26mm L: D = 40: 1
Mode of operation:	Screw co-rotating
Screw operation speed:	0-800 rpm
Screw configuration:	Refer to the enclosed drawing of screw/barrel
Motor power:	11.0 KW
Heater power:	500 W per cartridge
Maximum barrel temperature:	400 °C
Minimum water pressure:	2 bars
Water flow rate:	20 liters per minute at 2 bars

3.3.3 The effect of beta-nucleating agent on physical properties of PP/organomontmorillonite (OMMT: organoclay) composites

The PP homopolymer, compatibilizer (PP-g-MA) and organoclay (OMMT) added with and without the beta-nucleating agent (aryl amide compound) were added as shown in Table 3.4, a masterbatch of PP/aryl amide nucleator at a weight ratio of 95/5 was prepared in a twin screw co-rotating extruder before letting it down with bulk PP. The masterbatch of PP/PP-g-MA/organoclay was processed in a twin screw co-rotating extruder at 160/160/160/160/160/160/160/160/185/195 °C (from the hopper to the nozzle), a feed rate 45 rpm, a screw speed 250 rpm with the invention 1 screw configurations (Table 3.3), then pelletized with a granulator (LZ-120/VS Pelletizing unit). These pelletized samples were prepared to produce mechanical testing samples using the same procedure as Section 3.3.1.

Table 3.4 The formulation of PP/PP-g-MA/OMMT/beta-nucleating agent melt compounding.

Recipe No.	PP/PP-g-MA/OMMT/beta-nucleating agent (wt%)	Weight fraction (wt %)			
		PP	PP-g-MA	OMMT	Aryl amide nucleator
1	100/0/0/0 (Neat PP)	100	0	0	0
2	99.9/0/0/0.1	99.9	0	0	0.1
3	99.7/0/0/0.3	99.7	0	0	0.3
4	90/5/5/0	90	5	5	0
5	89.95/5/5/0.05	89.95	5	5	0.05
6	89.9/5/5/0.1	89.9	5	5	0.1
7	89.7/5/5/0.3	89.7	5	5	0.3

3.3.4 Morphology characterization

3.3.4.1 X-ray diffraction (XRD)

XRD analysis was conducted with the XRD (TTRAX III, Rigaku Corp., Japan) using Ni-filtered Cu K α radiation, having a wavelength of 0.154 nm operated at 50 kV and 300 mA. The diffraction spectra were recorded over a 2θ range of 1-30° in steps of 0.02°/s. The organoclay and composite samples were compressed with a compression hot-press plate (LAB TECH Engineering Co., Ltd., Thailand) at 170 °C for 5 min to produce 2 mm thick sheets with smooth and flat surfaces. The measurements were carried out at room temperature. The basal spacing of the organoclay galleries and crystalline form was calculated from the XRD patterns.

3.3.4.2. Transmission electron microscopy (TEM)

TEM observations were carried out to examine the dispersion morphology of organoclay in the composites. Ultrathin sections (60-80 nm) for transmission electron microscopy (TEM-2010F, JFOL Corp., Japan) analysis were microtomed (RMC MTX Ultramicrotome with cryo mode, Research Manufacturing Co., Arizona, U.S.A.) from the central and skin regions of a tensile bar at -90 °C. The cuts were made perpendicular to the flow direction of the injection molded specimens from the middle of tensile bar and halfway between the top and bottom surfaces. The thin slices were placed on 300 mesh copper grids and then analyzed by TEM with LaB6 filament operating at 80 kV.

3.3.4.3 Scanning electronic microscopy (SEM)

For SEM measurement, the tensile bar specimens were fractured in the direction perpendicular to injection flow direction in liquid nitrogen, and then gold-coated and observed under an acceleration voltage of 15 kV with an SEM (JSM-5900 LV, JEOL Corp., Japan). Besides, the same fractured specimens were etched according to Olley and Basset method [20] and then gold-coated and analyzed.

3.3.5 Rheological properties

3.3.5.1 Small amplitude oscillatory shear analysis (Cone and Plate Rheometer)

The viscoelastic characteristics of the polymers in the melt-state were measured with a rotational rheometer operating in the oscillatory mode. The principle for the estimation of the storage (G') and loss modulus (G'') from such a rheometer are similar to that of DMTA. From these analyses, the flow behavior of the polymers according to its complex viscosity and shear thinning behavior were compared. Frequency sweeps were carried out to compare the shear rate dependence of the complex viscosities. Using the Cox-Merz conversion, complex viscosity versus frequency is similar to shear viscosity versus shear rate data collected by a capillary rheometer or continuous flow measurements. The G' and G'' also give an indication of the elastic and flow recovery behavior of the material [21]. For these analyses, the melt rheological behavior of PP nanocomposites was determined using an Anton Paar instrument MCR 301 rheometer. The measurements carried out under nitrogen atmosphere at 220 °C using parallel plate geometry were in a linear range therefore the results were independent on the used strain amplitude, which was within 6-10%. The disk specimens for the measurements were cut from the plate pressed from the PP nanocomposites pellet at 170 °C in the compression molded become a sheet of 2 mm in thickness. By preheating the mold for 6 minutes, it was compressed at the 1st step at 50kN for 1 minute, then the 2nd step at 100 kN hold for 1 minute and finally the 3rd at 175 kN hold for 2 minutes. The sheet was de-molded by cooling water (<40 °C), cut into a disc with a diameter of 25 mm. In these measurements, storage modulus (G'), loss modulus (G'') and complex viscosity (η^*) were obtained as a function of frequency (ω) or complex modulus (G^*). The viscosity function (η^*) versus (G^*) at low shear viscosity (η_{5kPa}) and shear thinning index were calculated. The dynamic responses of PP nanocomposites samples were tested for 3 times. The experiments were carried out at 220 °C with a frequency range of 0.01 to 100 Hz at a strain level of 5% and 1.75 mm gap.

3.3.5.2 Capillary Rheometer

An RH7 Rosand single bore capillary rheometer was used to characterize shear flow properties in terms of shear stress and shear viscosity. The tests were carried out at a wide range of shear rate (20 to 1000 s⁻¹) at a test temperature of 220 °C. Dimensions of the capillary die used were 1 mm diameter, 16 mm length and 180° entry angle with an aspect ratio (L/D) of 16:1. The material was first preheated in a barrel for 5 minutes under a pressure of approximately 0.5 MPa to get a compact mass. The excess material was then automatically purged until no bubbles were observed. The test was then carried out at a set shear rate and temperature of 220 °C in a program via a microprocessor. During the test, the pressure drop across the capillary channel and melt temperature was captured via a data acquisition system. The apparent shear stress, shear rate and shear viscosity were calculated using the derivation of the Poiseuille law for capillary flow [22]:

$$\text{Apparent wall shear stress (Pa); } \tau = \frac{R\Delta P}{2L}, \quad (3.1)$$

$$\text{Apparent wall shear rate (s}^{-1}\text{); } \dot{\gamma}_{app} = \frac{4Q}{\pi R^3}, \quad (3.2)$$

$$\text{Apparent shear viscosity (Pa s); } \eta_s = \frac{\tau}{\dot{\gamma}_{app}}, \quad (3.3)$$

where ΔP is a pressure drop across the channel (Pa), Q is volumetric flow rate (m³s⁻¹), R is the capillary radius (m), and L is the length of the capillary (m). The values of R and L used in this work were 1 mm and 16 mm, respectively.

3.3.5.3 Melt flow Index

One of the properties most quoted for both natural polymers and compound is Melt Flow Index (MFI). Melt flow index is the output rate (flow) in grams that occurs in 10 minutes through a standard die of 2.0955 ± 0.00051 mm diameter and 8 ± 0.025 mm in length when a fixed pressure is applied to the melt via a piston and a load of

total 21.6 kg at a temperature of 230 °C . Some are different weights and some even different orifice sizes. Melt flow index is an assessment of average molecular mass and is an inverse measure of the melt viscosity; In other words, the higher an MFI, the more polymer flows under test conditions. Knowing the MFI of compound is vital to anticipating and controlling its processing. Generally, higher MFI compounds are easy for extrusion processes but low molecular weights also affect physical properties of PP nanocomposites.

For this study, melt flow indices of PP composites were measured by using MPX 62.92 Gottfert (DIN ISO1133). The plunger with its rod carries two circular reference markings at a distance of 30 mm from each other.

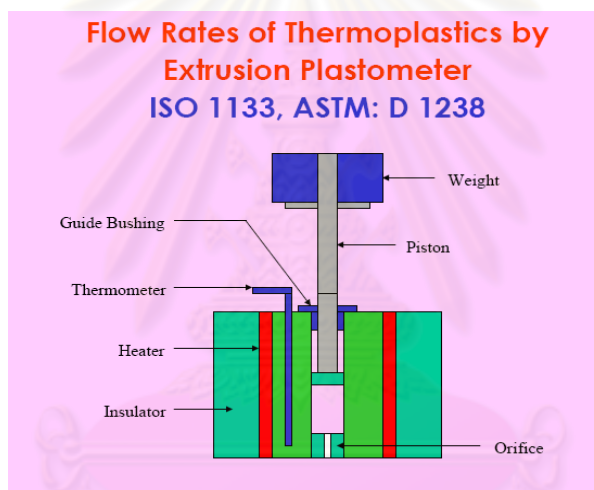


Figure 3.1 Melt flow Indexer

3.3.6 Thermal analysis

DSC measurements were made on a Perkin-Elmer, DSC-7 and Mettler Toledo thermal systems under nitrogen atmosphere with 10 °C/min heating and cooling rate. Calibration was performed using pure indium at the same heating rate. Each sample weighed about 10–15 mg. The samples were heated from 30 to 200 °C, melted at 200 °C for 5 min, and then cooled to 30 °C, followed by reheating to 200 °C for the second heating run. The crystallization and melting parameters were recorded from

the cooling and reheating scans. The percentage of beta-phase, Φ_β can be obtained from the crystallinities of the alpha-phase and beta-phase according to Ref. [23]

$$\Phi_\beta (\%) = \frac{X_\beta}{X_\alpha + X_\beta} * 100 \quad (3.4)$$

$$X_i = \frac{\Delta H_i}{\Delta H_i^\theta} * 100 \quad (3.5)$$

where X_α and X_β are the crystallinities of the alpha and beta-phases, respectively, which can be calculated separately according to Eq. (3.5), where ΔH_i is the calibrated specific fusion heat of either the alpha-form or the beta-form, ΔH_i^θ is the standard fusion heat of the alpha and the beta-crystals of iPP, being 178 J/g and 170 J/g, respectively [23, 24].

3.3.7 Fourier transforms infrared spectroscopy (FTIR) analysis

FTIR is used to investigate the interaction between PP, PP-g-MA, the organoclay, and the beta-nucleator. The PP composite was compression molded at 170 °C to obtain 50 µm film samples. FTIR scans were performed at ambient temperature in a range of 400-4000 cm⁻¹ on Bruker FTIR spectrometer (Vertex 70, Bruker Optics Co., U.S.A.)

3.3.8 Mechanical properties

3.3.8.1 Izod impact strength testing

The specimens of 64 mm x 12.7 mm x 3.2 mm dimension for the measurement of Izod impact strength were prepared by following ASTM D4101. They were tested according to the standard method of ASTM D256. A pendulum swung on its track and struck a notched, cantilevered the plastic sample. The energy lost (required to break the sample) as the pendulum continued on its path was measured from the distance of its flow through.

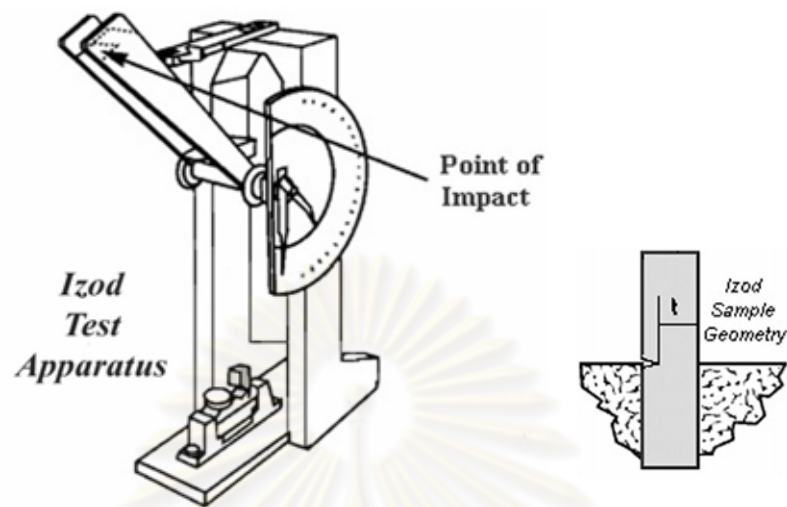


Figure 3.2 Izod impact strength apparatus and test specimen.

3.3.8.2 Flexural modulus and strength

The flexural strength measures the force required to bend a beam under 3-point loading conditions. Test specimens of 3.2 mm x 12.7 mm x 128 mm dimension for the measurement of flexural strength were prepared following ASTM D4101. They were tested according to the standard method of ASTM D790. The specimen was placed on two supports and a load was applied at the center. The load at yield measured at 1% deformation per strain of the outer surface is flexural strength. The test beam is under compressive stress at the concave surface and tensile stress at the convex surface.

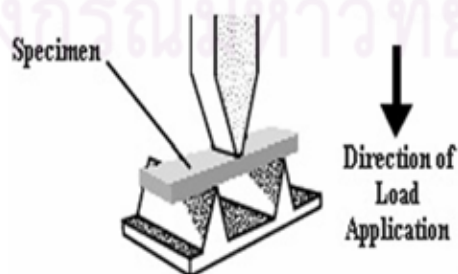


Figure 3.3 Flexural modulus and flexural strength testing.

3.3.8.3 Tensile property measurement

The dumbbell specimens for the tensile property measurement were prepared according to ASTM D4101. They were tested in accordance with ASTM D638. The sample was pulled, by the tensile testing machine, from both ends. The force required to pull the specimen apart, and how much the sample was stretched before its breaking, was measured.

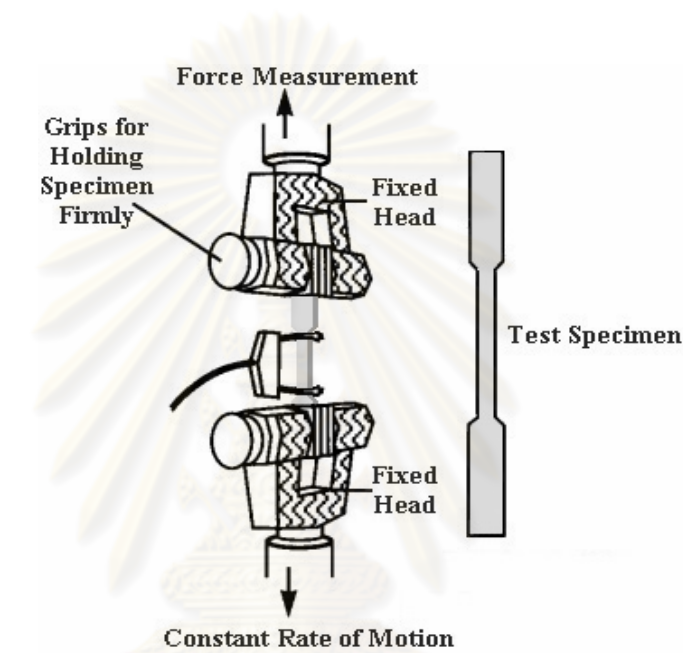


Figure 3.4 Tensile testing apparatus and test specimen.

3.3.8.4 Heat deflection temperature

For the heat deflection temperature (HDT), the specimens were also prepared (ASTM D4101) and tested by HDT, Vicat tester (YASUDA 148, Yasuda Co., Japan) according to ASTM D648 (ISO 75).

3.3.9 Density

The specimens of 12.7 x 12.7 x 3.2 mm were prepared by following ASTM D4101 and tested by Mettler Toledo AT201 SemiMicro Balance (Mettler Toledo Co., Switzerland) according to ASTM D792 method B (ISO 1183).

CHAPTER IV

RESULTS AND DISCUSSION

4.1 Preliminary study of the effects of compatibilizers on the performance of PP/compatibilizer (PB3200: PP-g-MA)/organomontmorillonite (OMMT: Organoclay: Nanofil[®]SE3000) composites.

PP composites of PP, OMMT (Nanofil[®] SE3000, 5 wt%) and PP-g-MA were prepared in the twin screw co-rotating extruder based on the condition set in Section 3.3.1 in order to seek for a suitable loading of the compatibilizer in the PP/OMMT composites. The mechanical properties of PP/PP-g-MA/OMMT composites were also examined. Table 4.1 presents the mechanical properties of PP/PP-g-MA/OMMT composites filled and unfilled with various amounts of PP-g-MA in the range from 5 to 20 wt%. The PP-g-MA of about 5 wt% gave the maximum flexural modulus and strength of about 28% higher than the neat PP, while the Izod impact strength was not significantly different. However, the tendency of improvement of the flexural modulus decreased with increasing compatibilizer greater than 7 wt%. Decreases of the MFI found in the PP composites can be associated to the good nanodispersion of organoclay. The formation of clay network is the reason for the change of MFI as the increase of compatibilizer content. It can be conceived that the orientation and flow of PP chains would be retarded if the PP chains were confined in a narrow space between the clay particles, resulting in a decrease of melt fluidity. However, when the compatibilizer contents higher than 15 wt% were added in the composites, the MFI increased due to the effects of low molecular weight and chain scission of the compatibilizer. The role of a percolated filler network is dominant in determining the macroscopic properties, resulting in low melt fluidity, retarded crystallization capability, and an enhanced thermal stability and modulus. Therefore, the tendency of heat deflection temperature (HDT) of the composites was higher than the neat PP by about 18-26%. In summary, the competition between the scission of macromolecular chains and the establishment of a filler network of percolated clay that activates and retards the motion of iPP chains, respectively, is responsible for the existence of a

turning point in the development of macroscopic properties in *i*PP/OMMT composites. [25]

Table 4.1 The mechanical properties of controls and PP/PP-*g*-MA/OMMT (Nanofil® SE3000) composites with various amounts of PP-*g*-MA compatibilizer processed in a normal polyolefin screw configuration.

Formulation	MFI (g/10 min)	*Flexural Modulus (MPa)	*Izod impact strength (J/m)	**Heat deflection temperature (°C)
100/0/0	13.2	1446±19.7	31.3±1.0	100.1±1.5
90/5/5	9.3	1842±7.6	33.4±1.4	125.6±2.5
88/7/5	11.1	1848±24.4	30±0.9	125.4±0.4
85/10/5	11.5	1680±18.0	32.6±0.2	126.3±2.7
80/15/5	15.1	1606±17.1	30.9±0.5	118.6±2.2
75/20/5	19.4	1553±71.8	29.1±0.8	117.9±3.2

* The test results are an average of 5 specimens, ** The test results are an average of 3 specimens.

4.2 Preliminary studies of the effects of screw configuration on physical properties of PP/PP-*g*-MA/OMMT composites.

The mechanical properties of PP/PP-*g*-MA/OMMT composites at the ratio of 90/5/5/0, prepared by a twin screw co-rotating extruder by different screw configurations (see Section 3.3.1) at the same temperature profile were determined. The results are presented in Figure 4.1. Izod impact strength of the composites was significantly improved when changing the screw configuration to give a higher shear and generate the better mixing. Under the Invention 1 screw configuration, the composites obtained a better impact-stiffness balance.

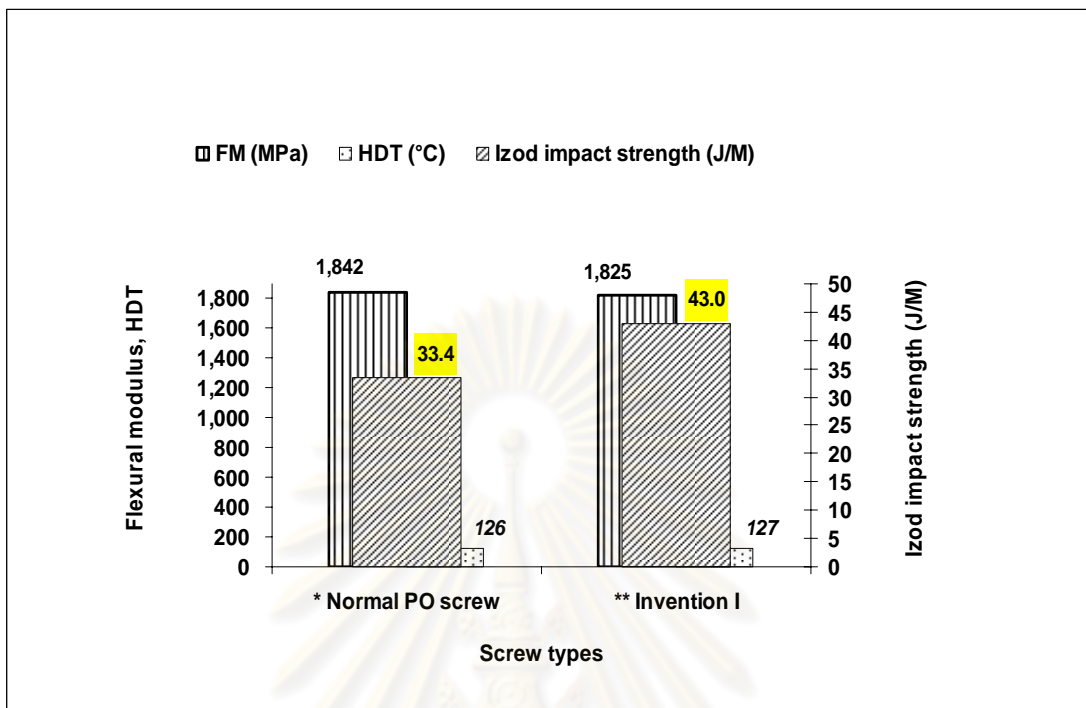


Figure 4.1 Effects of screw configuration on the physical properties of PP/PP-g-MA/OMMT composites (90/5/5). (*Screw profile with four kneading blocks without a reverse element (see detail in Table 3.2), **Screw profile with four kneading blocks with 2 reverse elements (see detail in Table 3.3)).

According to the results in Sections 4.1, and 4.2, it can be concluded that at least 2 important factors, the compatibilizer and the screw configuration, affect physical properties of the composites. In this system, the suitable formulation that should be further studied is the weight ratio of the PP/PP-g-MA/OMMT composites at about 90/5/5 and melt compounding with the invention 1 screw configuration.

4.3 The effects of compatibilizer on the performance of PP/compatibilizer (PP-g-MA)/OMMT (Nanofil[®]SE3000) composites. (Invention I screw configuration)

4.3.1 Morphology characterization

Maleic anhydride-modified PP is commonly used as a compatibilizer [16, 25-29] to promote miscibility between the organic PP resin and the inorganic layered

silicate through enhancing polarity of the PP resin and decreasing interfacial tension of the PP/layered silicate. In our composites prepared via a melt compounding, the components of basal polymer are quite different when the PP-*g*-MA loading increased from 0 to 20 wt%. The different compatibilizer contents will result in drastic differences in dispersion of organoclay among all composites, which have been identified through comparing the *d*-spacing of organoclay tactoids measured via XRD, as shown in Figure 4.2 and the dispersion degree of organoclay observed via TEM, in Figures 4.3-4.6. Figure 4.2 presents a series of X-ray diffraction spectra of the original organoclay and PP/PP-*g*-MA/OMMT composites, in which the content of PP-*g*-MA varies from 0 to 20 wt%. We recalled that the organoclay content is constant at 5 wt%. The interlayer spacing of pristine organoclay is 3.65 nm ($2\theta = 2.42$) before compounding. For the uncompatibilized system (95/0/5/0), the XRD pattern exhibits little change in interlayer spacing (3.68 nm, $2\theta = 2.40$) after the extrusion compounding. It implies that the intercalation of PP chains into the intergalleries of organoclay cannot occur at all without adding the compatibilizer. In the other words, mixing cannot take place without the compatibilizer. Moreover, the corresponding TEM images (Figure 4.3) show that the poor dispersion (agglomeration) of organoclay is in the composites and some larger organoclay blocks are surrounded by the small tactoids and individual layers are visible. Nevertheless, X-ray diffraction peaks for the compatibilized composite systems are shifted to lower angles, indicating an increase in the interlayer spacing by the intercalation of polymer. The results of interlayer spacing are summarized in Table 4.2. The interlayer spacing increases progressively, from 3.74 nm for 2.5 wt% compatibilizer and gets a maximum *d*-spacing at 3.87 nm or more for 5% compatibilizer and falls again to 3.79 nm for 20 wt% compatibilizer. Besides, XRD peaks are also investigated for both intensity and shape (broad or narrow). Above 2.5 wt% of the compatibilizer, decreasing intensity and broadening of the peaks were observed, indicating that the stacks of layered silicates become more disordered, while maintaining a periodic distance. In addition, the reduced intensity could be the result of a partial exfoliation of layered silicates [30], suggesting that the intergalleries of organoclay have been intercalated by PP chains during melt-compounding. As shown correspondingly in the TEM images (Figures 4.4-4.5), the organoclay particles are dispersed in the PP matrix as tactoids with individual layers having a high aspect ratio. The aggregation of organoclay particles are less to be detected. So it can be concluded that the dispersion

of organoclay is dominated by the compatibility between the basal polymer and organoclay.

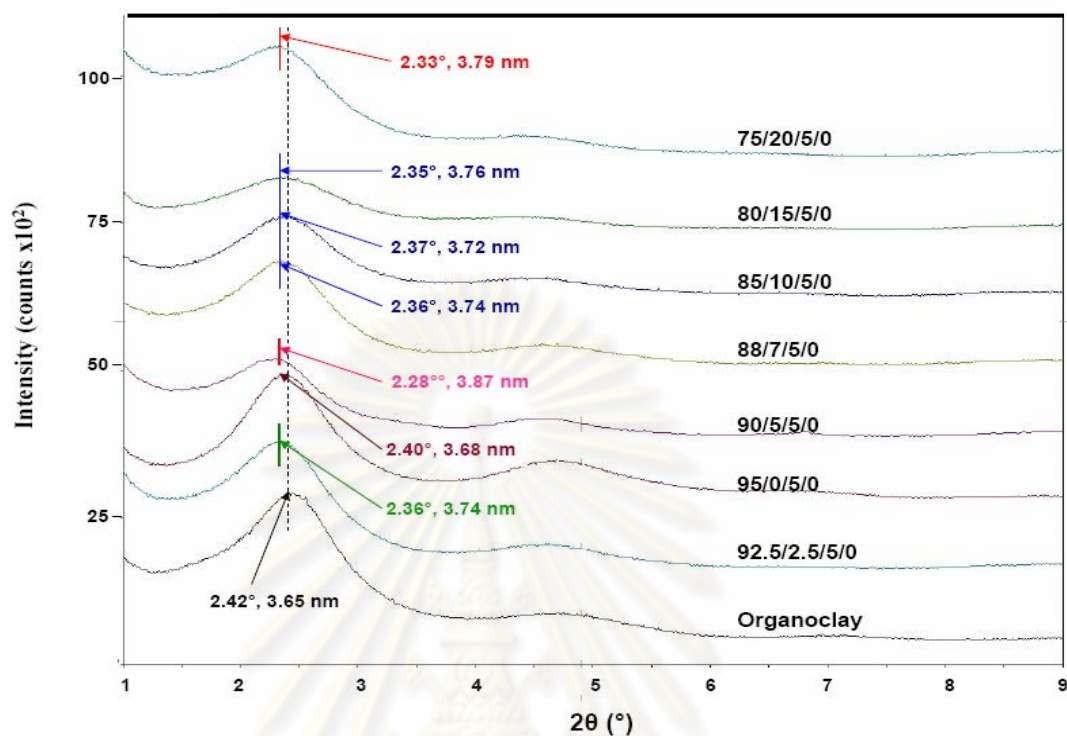


Figure 4.2 XRD patterns of organoclay and PP/PP-g-MA/OMMT composites filled and unfilled composites with various amounts of PP-g-MA with Invention I screw configuration.

Table 4.2 XRD-derived interlayer spacing for the composite materials calculated from Figure. 4.2

Formulation	2θ of (001) plane (°)	Intensity counts	d-spacing of organoclay intergallery (nm)
Organoclay	2.42	16,356	3.65
95/0/5	2.40	16,496	3.68
92.5/2.5/5	2.36	13,504	3.74
90/5/5	2.28	7,526	3.87
88/7/5	2.36	11,858	3.74
85/10/5	2.37	9,643	3.72
80/15/5	2.35	5,781	3.76
75/20/5	2.33	14,403	3.79

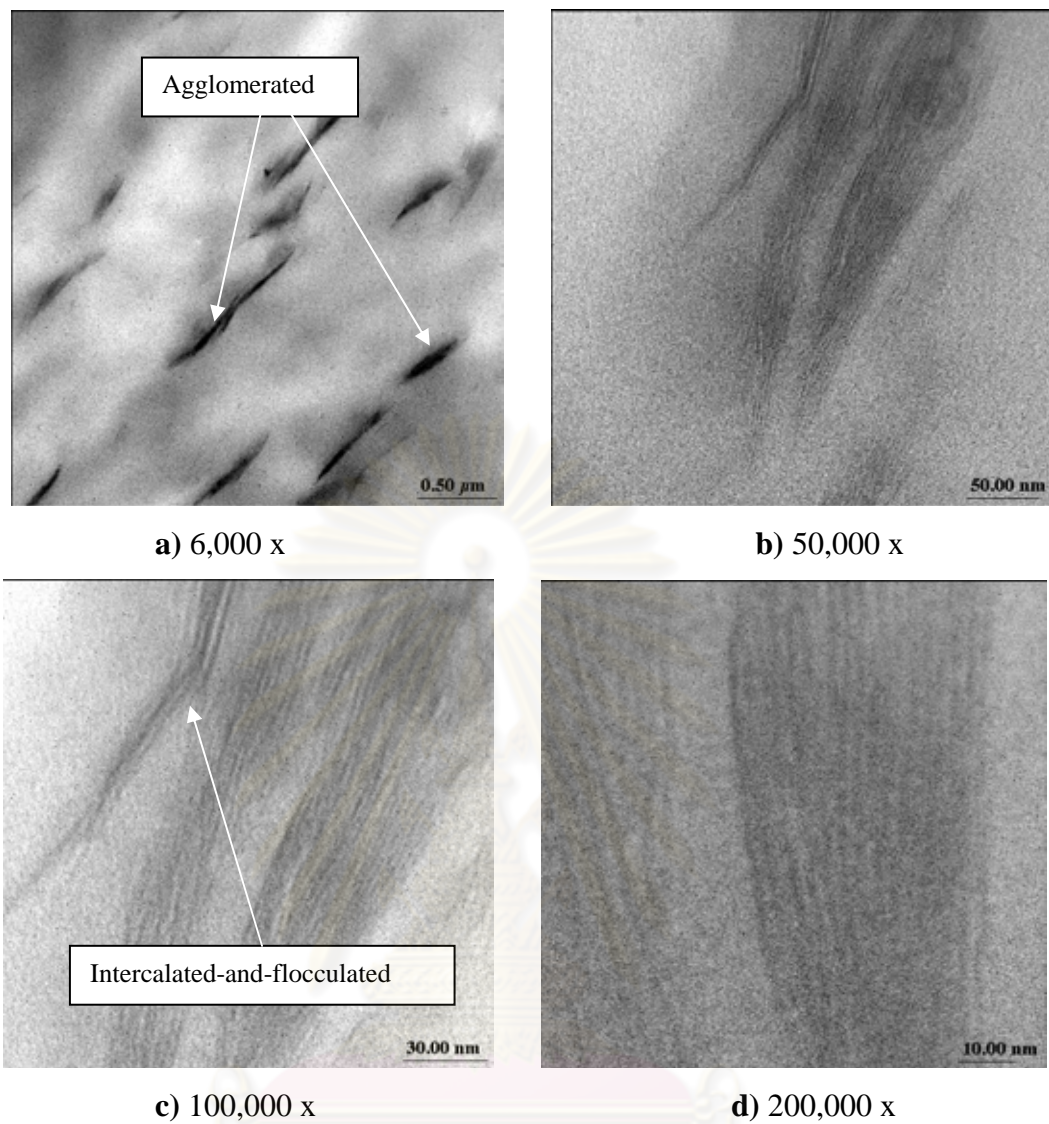


Figure 4.3 Transmission electron micrographs of PP/PP-g-MA/OMMT composites (95/0/5/0) for (a) agglomerated clay, and (b-d) Intercalated-and-flocculated clay layers.

ศูนย์วิจัยทรัพยากร
จุฬาลงกรณ์มหาวิทยาลัย

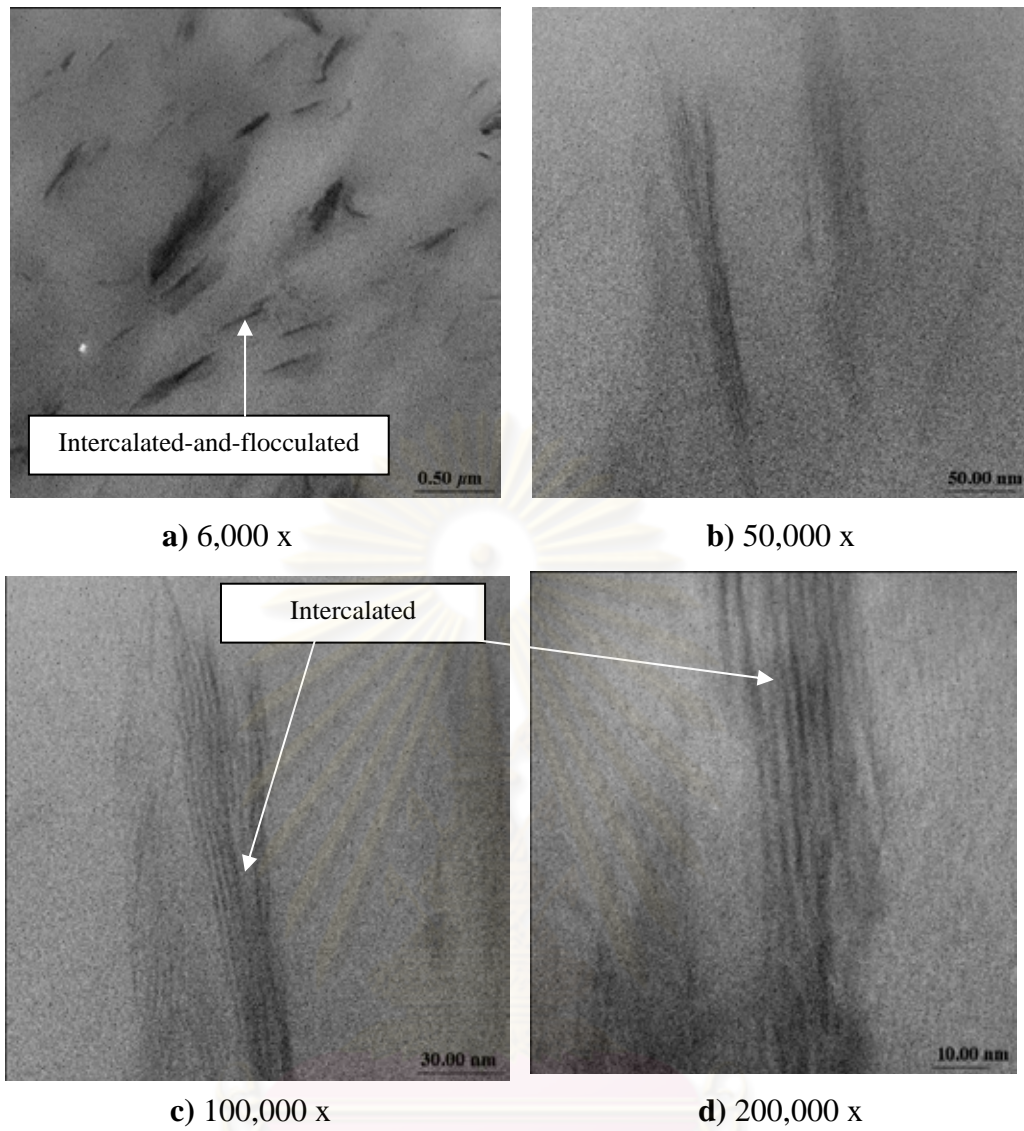


Figure 4.4 Transmission electron micrographs of PP/PP-*g*-MA/OMMT composites (90/5/5/0) for **(a)** Intercalated-and-flocculated clay, and **(b-d)** intercalated clay layers.

ศูนย์วิทยาศาสตร์
จุฬาลงกรณ์มหาวิทยาลัย

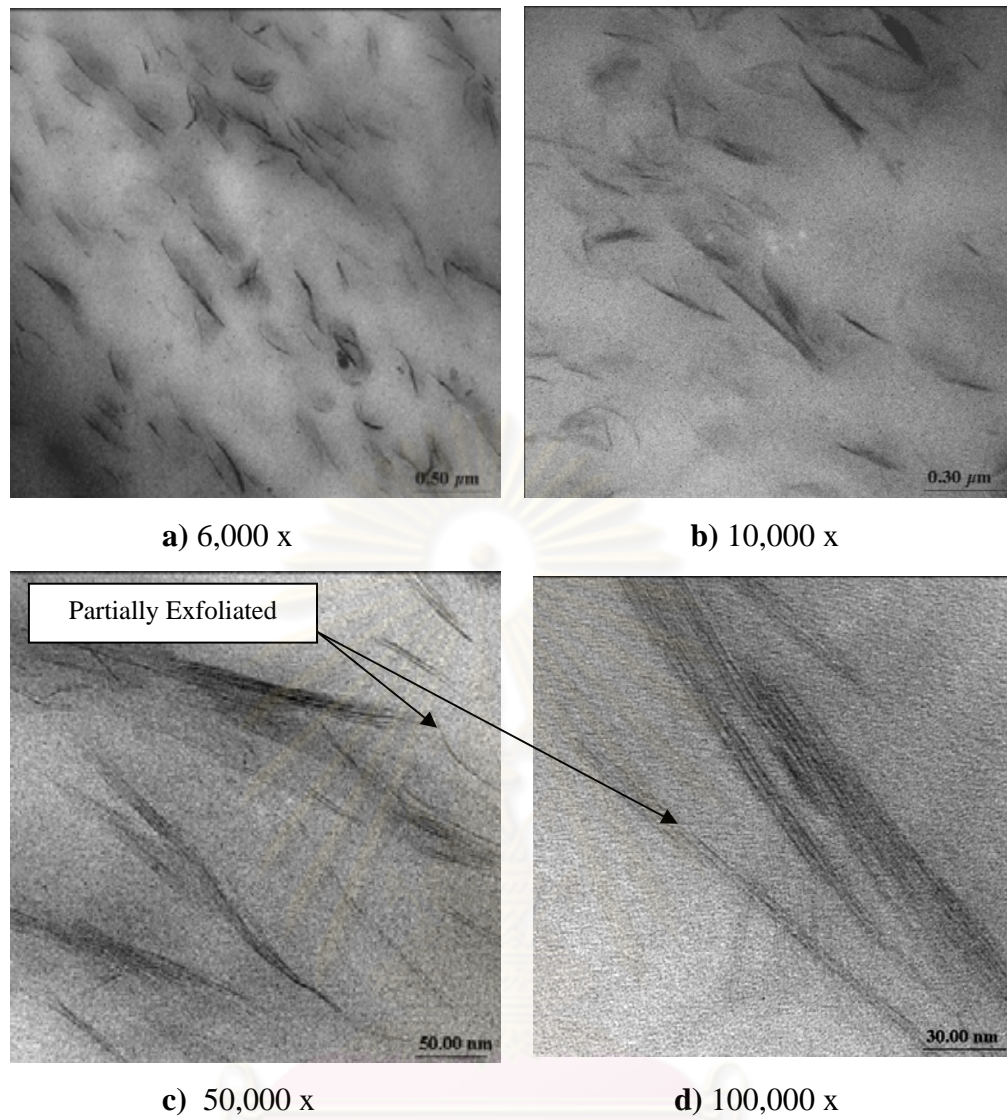


Figure 4.5 Transmission electron micrographs of PP/PP-g-MA/OMMT composites (75/20/5/0) for (a) uniform distribution of clay, and (b-d) intercalated and partially exfoliated clay layers

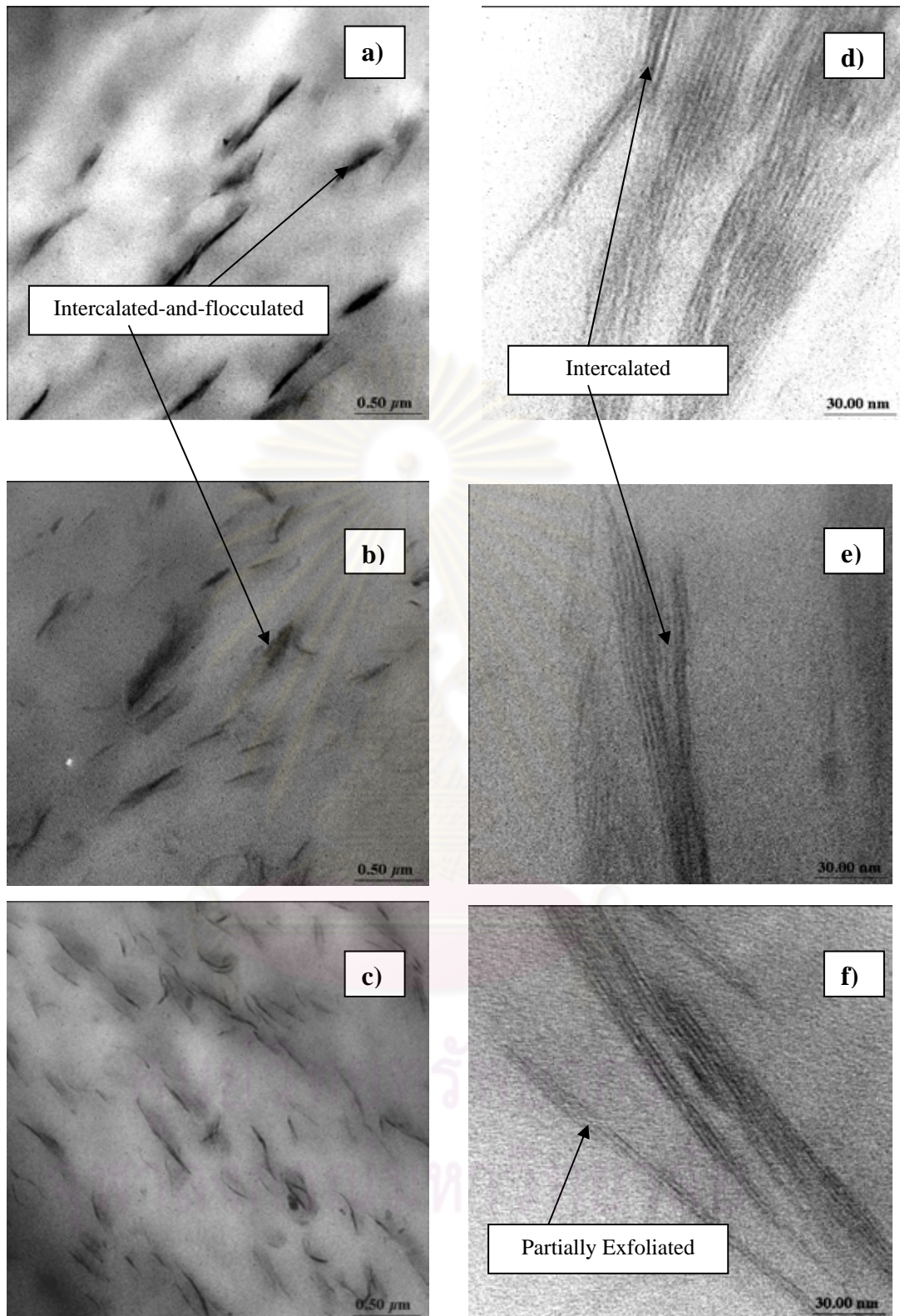


Figure 4.6 TEMs of PP/PP-g-MA/OMMT composites showing agglomerated, intercalated and partially exfoliated clay layers of 95/0/5/0, 95/5/5/0, 75/20/5/0, (a-c) at 6,000x and (d-f) at 100,000x, respectively.

4.3.2 Adhesion and chemical interaction

To estimate the adhesion and interaction between OMMT and the basal resins, interfacial morphologies of the polymer/inorganic filler are inspected through SEM images of the fractured cross-sectional surfaces of the molded bars as shown in Figure 4.7. The cracks existing at the interface between the OMMT particles and PP matrix are seen in the uncompatibilized *i*PP/OMMT composite, implying a weak interaction of the basal resin and OMMT. On the contrary, the matrix/OMMT interface is seen blurry and the adhesion between the OMMT particles and the basal resin is tight in the compatibilized composites. To further confirm the above observations, Fourier transform infrared spectroscopy (FTIR) was used to characterize the fractured surface. FTIR is an appropriate technique that enables understanding of chemical absorption and bonding of a compound. FTIR spectra for the clay, neat polymer, and PP/PP-*g*-MA/OMMT composites are presented in Figures 4.8 and 4.9. The vibration bands are summarized. For the organoclay, the sharp and strong IR peak at 1467 cm^{-1} is associated with CH_2 wagging deformation of alkyl ammonium clay surface modified, a small peak at 1116 cm^{-1} for $\nu(\text{Si-O})$ out-of-plane, a strong peak at 1050 cm^{-1} for $\nu(\text{Si-O})$ in-plane, 1033 cm^{-1} for Si-O-Si stretching, 914 cm^{-1} for $\delta(\text{Al-Al-OH})$, 797 cm^{-1} for $\delta(\text{CH})$ out-of-plane from the surface modified. Absorption peaks at 530 and 466 cm^{-1} are for Si-O, Si-O-Al stretching and Si-O, Si-O-Fe stretching, respectively. For the Neat PP, 1457 cm^{-1} for $\delta_{\text{as}}(\text{CH}_3)$; 1377 and 1358 cm^{-1} for $\delta_{\text{s}}(\text{CH}_3)$, 1327 cm^{-1} $\delta(\text{C-H})$; 1307 cm^{-1} CH_2 twisting; 1253 and 1219 cm^{-1} for CH_2 wagging; 1165 cm^{-1} for absorption perpendicular to stretch direction; 997 , 973 , 843 and 808 cm^{-1} for tertiary methyl stretch deformations. For compatibilizer, PP-*g*-MA (PB3200) shows besides the neat PP spectrum, two weak absorption peak at 1783 and 1713 cm^{-1} associated with $\nu(\text{C-OH})$ and $\nu(\text{C=O})$ stretching of maleic acid. A close examination of Figures 4.8 and 4.9 suggests that reinforcement of PP with the organoclay alters the shape and position of the infrared absorption bands of PP. The absorption bands of PP between 997 and 973 cm^{-1} corresponding to the deformation of tertiary methyl skeletal and at 1104 - 1069 cm^{-1} to the deformation of stretching of Si-O-Si bond in the tetrahedral silicate plane are highlighted by dot boxes in Figures 4.8 and 4.9. This shift in the wavenumber and deformation of the peak shape indicate a stronger interaction between PP matrix and OMMT [31].

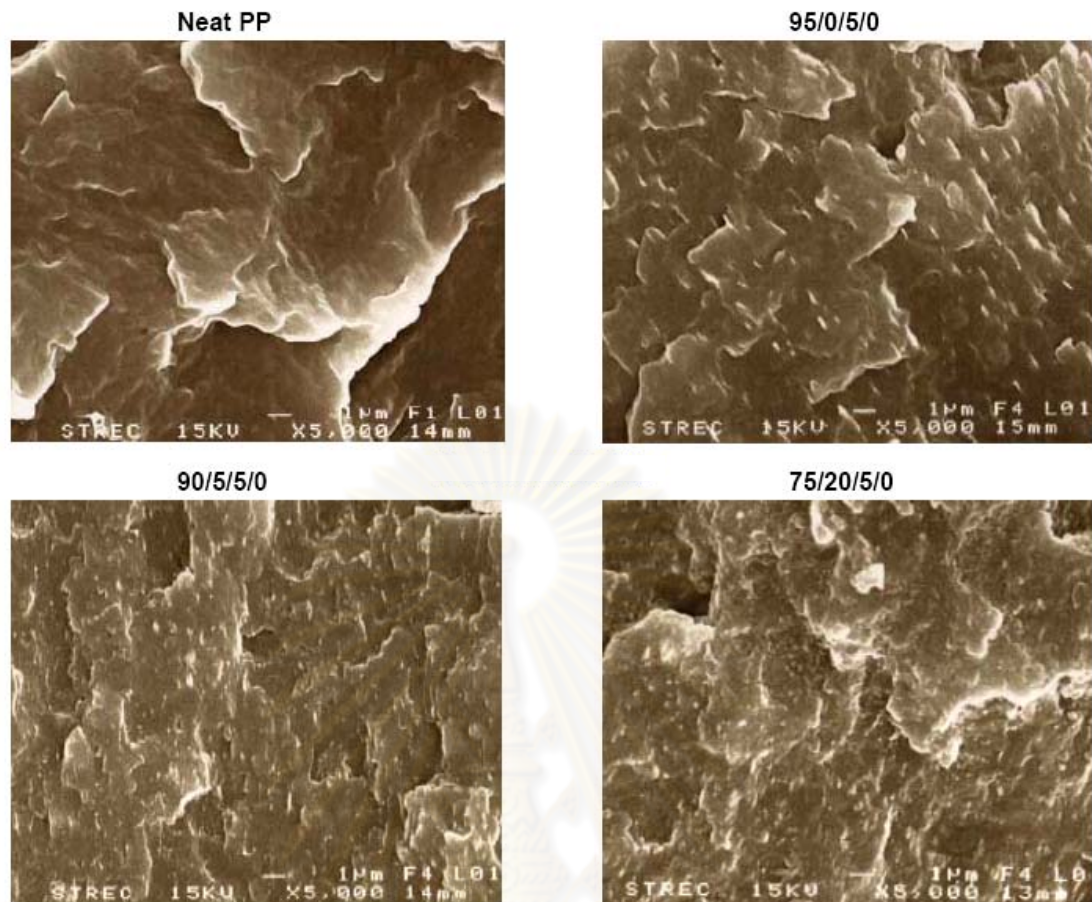


Figure 4.7 SEM micrographs of the fractured surfaces (fractured under liquid N₂) of the neat PP (upper left), the PP/PP-g-MA/OMMT composites of 95/0/5/0 (upper right), 90/5/5/0 (lower left) and 75/20/5/0 (lower right).

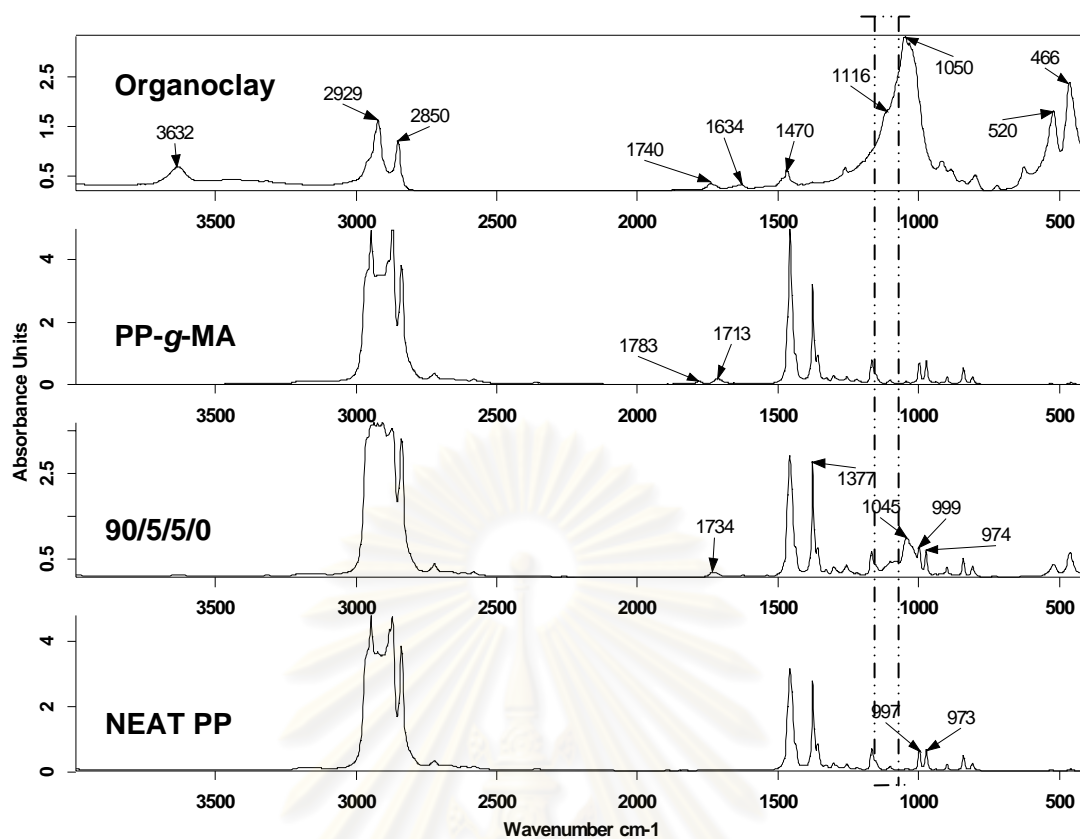


Figure 4.8 Fourier Transform infrared spectra of the neat PP, PP-g-MA, PP/PP-g-MA/OMMT composites (90/5/5/0) and the organoclay.

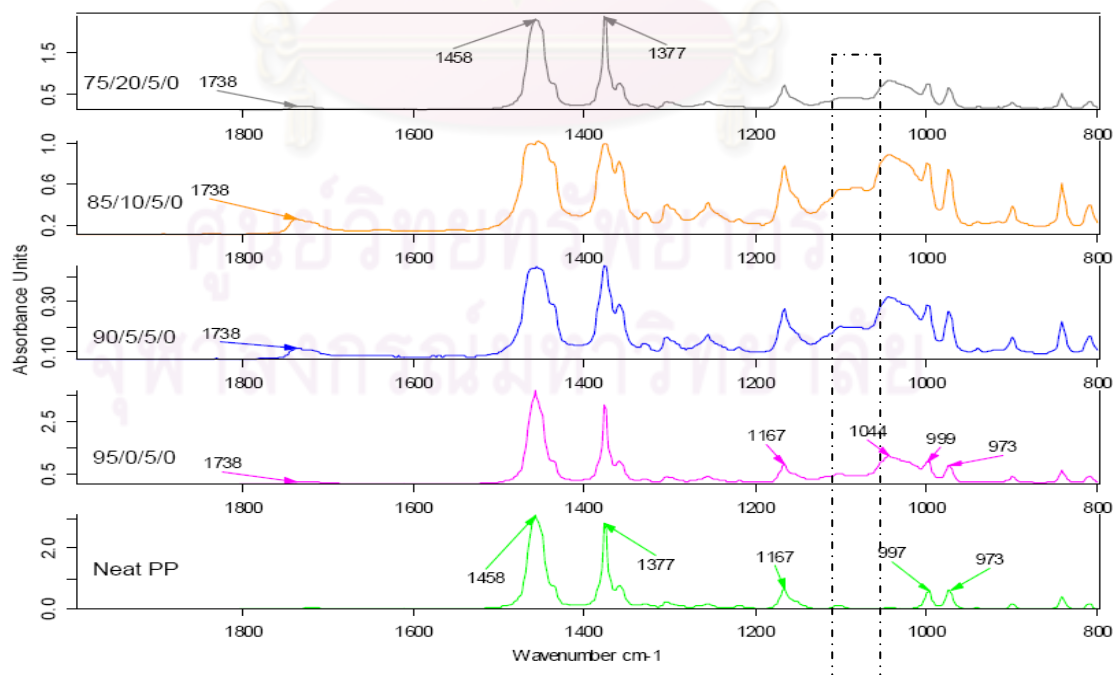


Figure 4.9 Fourier Transform infrared spectra of neat PP and PP/PP-g-MA/OMMT with various amounts of PP-g-MA in the range from 0-20 wt%.

4.3.3 Rheological properties

It is well known that the rheological properties of nanocomposites are sensitive to surface characteristics and state of dispersion of the dispersed phase. The rheological behavior of the binary mixing at various the weight ratios present in the PP/PP-*g*-MA/OMMT composites will be used as a reference matrix behavior. Therefore, rheometry can be employed as a powerful tool for characterizing the state of dispersion [16, 28, 30, 32-34]. The storage modulus, G' and the complex viscosity, η^* as a function of frequency for the PP/PP-*g*-MA melt mixing are the necessary items to be measured. Based on the MFI values of PP and PP-*g*-MA, low viscous PP-*g*-MA has an effect of 'dilution' on polypropylene viscosity [30]. Figure 4.10a shows no specific effect on the storage modulus at low frequencies (low shear rates) between the neat PP and 95/5/0/0 composite, presumably indicating a good miscibility between PP and PP-*g*-MA. Figure 4.10a also presents the storage modulus G' as a function of frequency for the composites obtained with different concentrations of PP-*g*-MA. At low frequencies (< 1 rad/s) and concentration of PP-*g*-MA at 0 wt% (95/0/5/0 composite), slight increases in the storage modulus G' , when adding only organoclay (95/0/5/0), should be associated to some partial polymer intercalation due to low dispersibility of the organoclay. According to Solomon et al. [32] and Wang et al. [25], the increase in storage modulus at low frequency, which does not exist for the corresponding matrices, could be explained by the existence of a percolated network microstructure. At higher concentrations of PP-*g*-MA, the storage modulus dramatically increases with increasing concentrations of PP-*g*-MA and reaching a maximum at 20 wt% (75/20/5/0). Therefore, it is reasonable to say that the exfoliated silicate layers increase with increases in the compatibilizer amounts in the concentration interval and these could be the state of partial exfoliation. At frequencies higher than 1 rad/s, G' decreases slightly when the concentrations of PP-*g*-MA increase because the viscosity and the molecular weight of PP-*g*-MA is lower than that of polypropylene matrix.

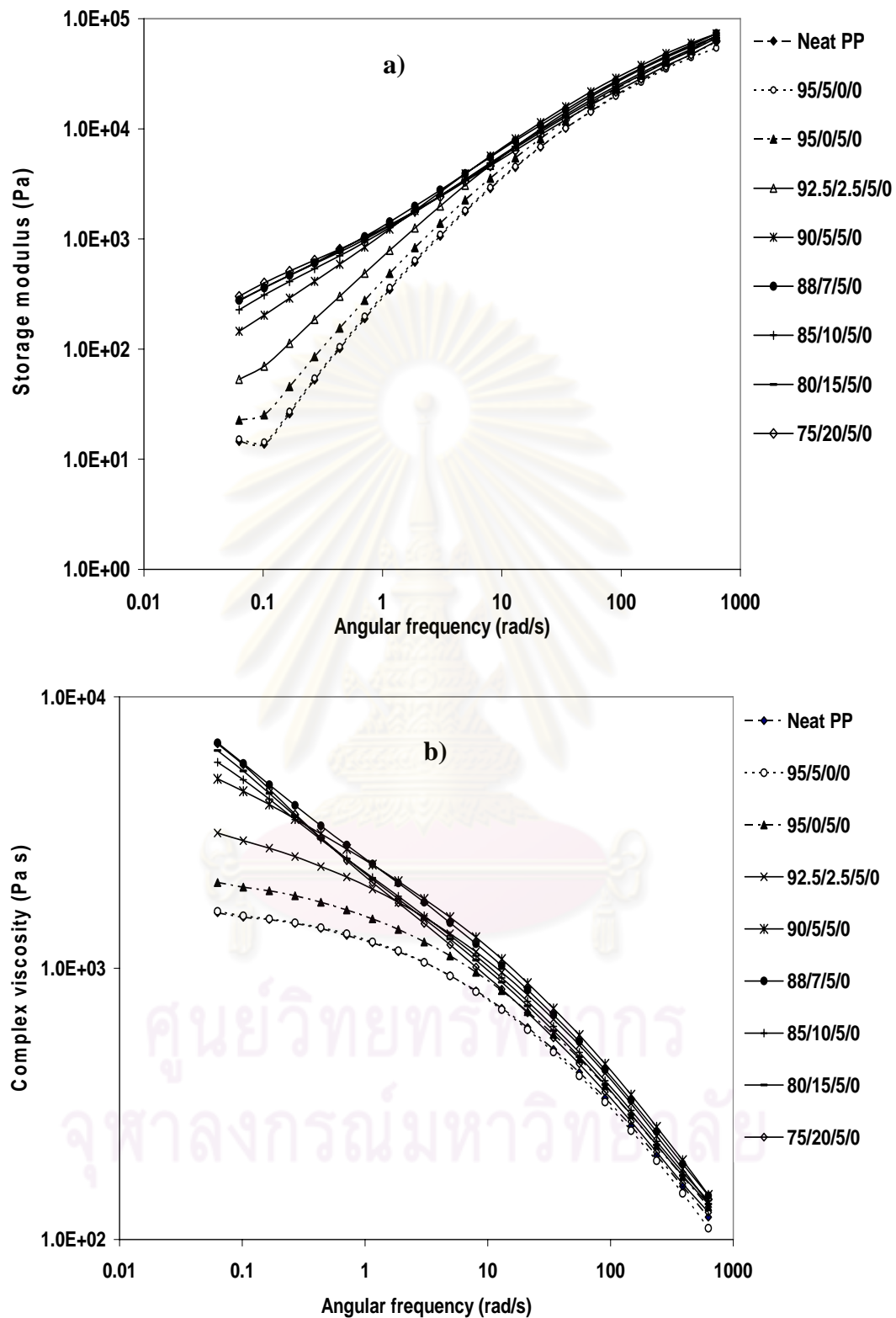


Figure 4.10 The rheological properties, **(a)** G' , Storage modulus, **(b)** η^* , Complex viscosity of PP/PP-g-MA/OMMT composites and controls with various amounts of PP-g-MA and determined by Cone and Plate rheometer

Figure 4.10b shows the complex viscosity for different amounts of PP-g-MA. Like the storage modulus, the complex viscosity increases progressively at low frequency (< 1 rad/s) with increasing amounts of PP-g-MA and reaching a maximum at 7 wt%. Above 7 wt%, the complex viscosity slightly decreases, due to the low viscosity of PP-g-MA. At frequency higher than 1 rad/s, η^* decreases with increasing concentrations of PP-g-MA due to the fact that the viscosity and the molecular weight of PP-g-MA is lower than that of polypropylene matrix.

From the rheological information above, it is essential to study further the balancing effect of the compatibility by adjusting the compatibilizer concentration. The rheological properties of the composites at high shear rates (>20 /s) are examined further by the capillary rheometer as presented in Figure 4.11. For the PP/organoclay composite without PP-g-MA (95/0/5/0), the shear viscosity of the composite is lower than the 95/5/5/0 composites containing 5 wt% PP-g-MA but higher than the composites of 85/10/5/0 with 10 wt% PP-g-MA. That indicates that the PP-g-MA compatibilizer can improve the interaction between PP and organoclay. However, the excess compatibilizer induces a negative effect in rheology. Therefore, the suitable formulation for the balance compatibility depends mainly on the compatibilizer loading; for this system the ratio of PP/PP-g-MA/OMMT (organoclay) is 90/5/5/0.

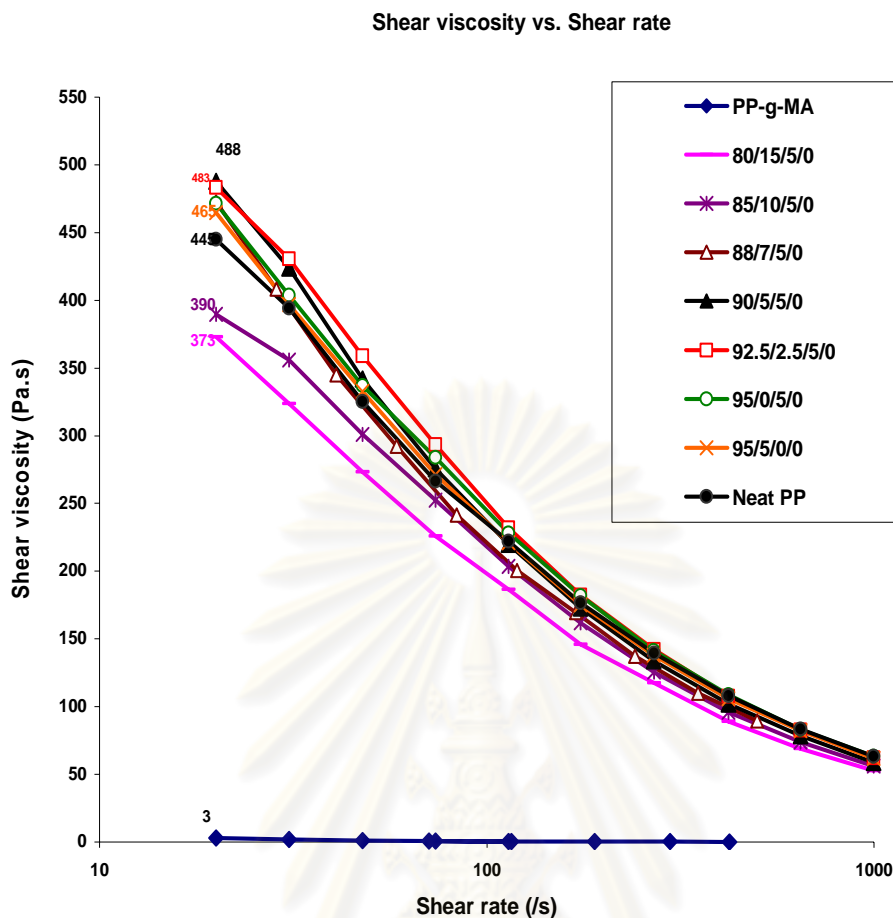


Figure 4.11 Shear viscosity of PP/PP-g-MA/OMMT composites and the control (neat PP) with various amounts of PP-g-MA determined by Capillary Rheometer at 220 °C.

One can observe from Figure 4.11 that the shear viscosity of PP/PP-g-MA/OMMT composite increases with increasing the amount of PP-g-MA. The addition of compatibilizers to polymer composite affects their flow behavior. Chemical reactions occur between the components of a composite upon compatibilization and generally increase the viscosity of the system. These are probably caused by a coupling effect of the PP-g-MA when loading the PP-g-MA into the PP/OMMT. It introduces better interfacial adhesion between PP and OMMT phases as the maleic anhydride groups and PP chains in PP-g-MA interact between OMMT and PP matrix phases, respectively. Naturally, the small molecule like PP-g-MA has a lower viscosity than the PP matrix at 200 °C. All shear rates may also induce chain scission reactions. The loading of PP-g-MA must be optimized.

4.3.4 Microscopic observations

According to the XRD pattern in Figure 4.2, the presence of a lower diffraction angle peak and intensity in PP/PP-*g*-MA/OMMT (organoclay) composites suggests a larger d-spacing and more disorder of the OMMT formed in the composite system that presumably retards the mobility of PP chains during crystallization. As a consequence, PP in the presence of OMMT and compatibilizer crystallizes at a lower temperature than does the neat PP. In inorganic particle reinforced polymers, the particle–polymer matrix interaction is, of course an important factor in determining the ultimate mechanical properties of composites. Figure 4.13 presents a significant improvement of mechanical and thermal properties of PP/PP-*g*-MA/OMMT composites in case of flexural modulus, Izod impact strength and heat deflection temperature of about 28%, 43% and 27%, respectively, for the 90/5/5/0 composition with the invention I screw configuration for compounding. However, elongation at break of the composites significantly declines.

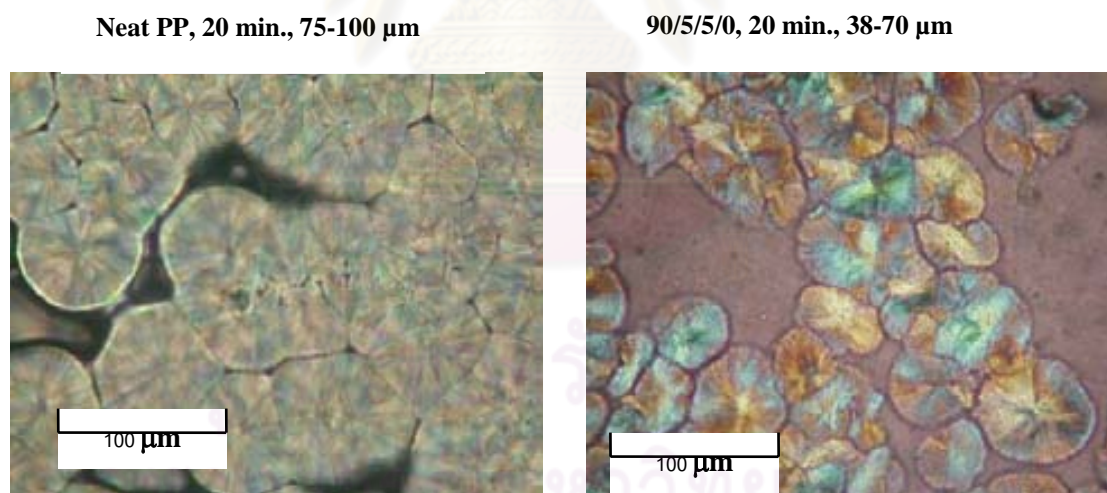


Figure 4.12 Optical micrographs of PP/PP-*g*-MA/OMMT (organoclay) composite and blank and isothermally crystallized at 135 °C.

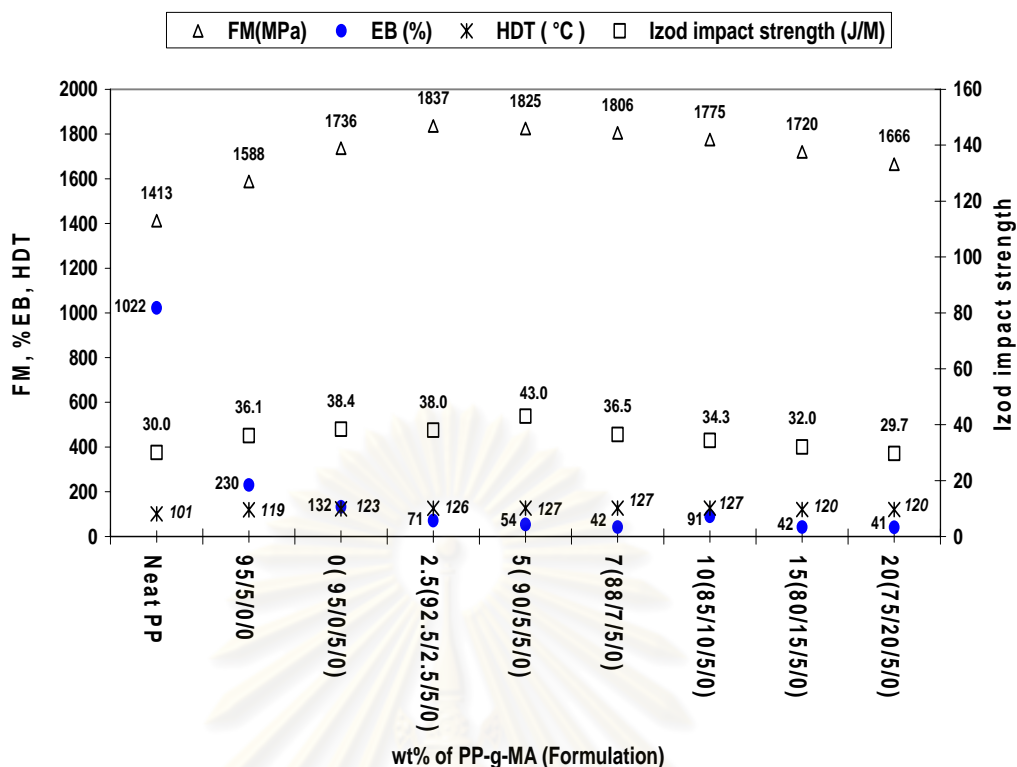


Figure 4.13 Mechanical and thermal properties of PP/PP-g-MA/OMMT composites with various amounts of PP-g-MA and the neat PP as a control.

In this PP/PP-g-MA/OMMT composites system, the crystallinity is significantly decreased, the reinforcement with the compatibilizer and OMMT decreased the crystallization temperature [29] by about 7 $^{\circ}$ C and reduced the spherulite size from 75-100 μ m of neat PP to 38-70 μ m in the 90/5/5/0 composition presented in Figure 4.12. These observations suggest that the OMMT and PP-g-MA had a strong influence on the structural and mechanical properties of PP. Figure 4.13 presents an increase in HDT and flexural modulus which is very fortunate that the flexural modulus is not accompanied by loss in impact strength. The above observations lead us to believe that the reduction in spherulite size could be at least one of the structural controlling factors responsible for the increases in toughness of the PP/PP-g-MA/OMMT composite. However, the improvement tendencies decreased with increasing the compatibilizer contents of above 7 wt%. Another important factor of concern is the PP/PP-g-MA/OMMT interaction. The decrease of the MFI found in the composites can be associated to nanodispersion of the OMMT leading to a higher melt viscosity at the low shear rates. The flexural modulus and Izod impact strength of PP/PP-g-MA/OMMT composites were significantly higher

than the neat PP corresponding to a strong interaction between the OMMT and PP matrix.

4.4 Effects of aryl amide beta-nucleating agent on the performance of PP/compatibilizer/ organoclay (OMMT) composites.

4.4.1 Morphology and density

Figure 4.14 and Table 4.3 present the morphology, XRD information and density of alpha- and beta-crystals of PP and PP composites by beta-nucleation and the neat PP as a control. The X-ray diffraction patterns of the PP alpha-modification and beta-modification in the composites in Figure 4.14 indicate that the monoclinic-phase (alpha-phase) of the neat PP and PP/PP-g-MA/OMMT composites at the (110), (040), (130), (111) and (041) crystallographic planes correspond to the diffraction angles 2θ of 14.2° , 17.0° , 18.8° , 21.2° and 22° , respectively. The neat PP and 90/5/5/0 did not show any significant formation of the hexagonal (beta-phase) form because of the lack of aryl amide. The hexagonal crystal forms in the PP and composites were only observed in the presence of aryl amide nucleator in 99.9/0/0/0.1, 89.95/5/5/0.05, 89.9/5/5/0.1 and 89.7/5/5/0.3 specimens. The two main diffraction characteristics of beta-nucleated PP and composites were clearly observed at $2\theta = 16.2^\circ$ and 21.7° , which were associated with the (300) and (301) planes, respectively. The beta-phase content in the crystalline *i*PP, the so called k_β value, was estimated using the equation proposed by Turner-Jones (Equation 2.1): [5]

$$k_\beta = \frac{H_{\beta 1}}{H_{\beta 1} + (H_{\alpha 1} + H_{\alpha 2} + H_{\alpha 3})} \quad (2.1)$$

where $H_{\alpha 1}$, $H_{\alpha 2}$ and $H_{\alpha 3}$ are the intensities of α -diffraction peaks corresponding to $\theta_s = 7.1^\circ$, 8.5° and 9.4° , respectively. $H_{\beta 1}$ is the intensity of β -diffraction peak corresponding to the angle $\theta_s = 8.1^\circ$. The fraction of the hexagonal form can be expressed by the k_β value from Equation (2.1).

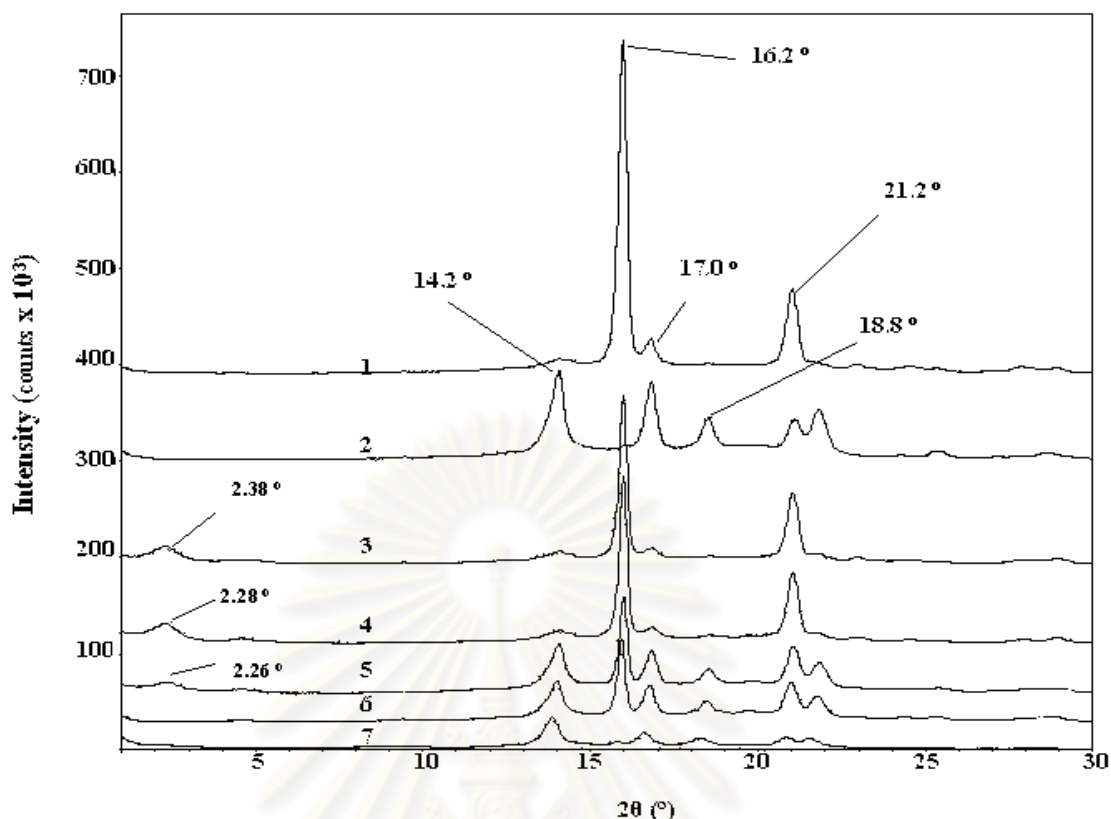


Fig. 4.14 XRD patterns of PP and PP/PP-g-MA/OMMT composites with various amounts of aryl amide nucleator, **1**: 99.9/0/0/0.1, **2**: Neat PP, **3**: 89.7/5/5/0.3, **4**: 89.9/5/5/0.1, **5**: 89.95/5/5/0.05, **6**: 89.95/5/5/0.05 (repeat) and **7**: 90/5/5/0.

Table 4.3 XRD information and density of the neat PP and PP/PP-g-MA/organoclay composites with various amounts of aryl amide nucleator.

Formulation	2θ of (001) plane (°)	d-spacing at (001) plane (nm)	Intensity at (001) plane	k_{β} value	*Density (g/cm ³)
Neat PP	none	none	none	0.01	0.904
99.9/0/0/0.1	none	none	none	0.93	0.901
90/5/5/0	none	none	none	0.02	0.921
90/5/5/0 (repeat)	2.28	3.87	7526	0.00	**nd
89.95/5/5/0.05	none	none	none	0.50	nd
89.95/5/5/0.05 (repeat)	2.38	3.71	6587	0.49	nd
89.9/5/5/0.1	2.28	3.87	13066	0.92	0.922
89.7/5/5/0.3	2.26	3.9	11980	0.92	0.919

*The test results are an average of 3 specimens, **nd = not determine

The effect of aryl amide nucleator on the dispersion of organoclay in the PP/PP-g-MA/ organoclay/aryl amide composites was also observed via XRD and TEM techniques. As shown in Figure 4.2, the interlayer spacing of pristine organoclay is 3.65 nm ($2\theta = 2.42^\circ$) before compounding. For the compatibilized system of 90/5/5/0, the diffraction peaks in the 2θ range of $1-5^\circ$ disappeared markedly or shifted to lower angles with very low intensity, i.e., highly disordered and partially exfoliated organoclay. This implies that intercalation of PP chains into the intergalleries of the organoclay and some exfoliation of the organoclay layers had taken place. The addition of 0.05 wt% aryl amide nucleator to the 89.95/5/5/0.05 composite induced the beta nucleation of composites with the k_β value of 0.50 whereas the characteristic of X-ray diffraction pattern was not significantly different from that of 90/5/5/0 composite, indicating a very similar level of dispersion. At the levels of 0.10 and 0.30 wt% nucleator, the beta-form in the PP and PP composites increased to the same k_β value of 0.92, while the diffraction peaks in the 2θ range of $1-5^\circ$ were still observed with the rather high intensity but were shifted to the lower angles at 2.28° and 2.26° . This means that the interlayer spacings of the clay were extended to 3.87 and 3.90 nm, respectively. However, the dispersion of clay layers showed less disorder or higher peak intensity than that with 0.05 wt% or non-nucleated composites. This agrees with the results of TEM micrographs in Figures 4.15 and 4.16.

Table 4.3 also lists densities of the samples, and the data exhibit a slightly lower density of the beta-nucleated samples compared to the alpha-form which is in good agreement with literature [3, 9]. Because the density of 5% nanoclay composites was 1.9% higher compared to the neat PP, the beta-nucleation can partially compensate for this negative effect (the higher part weight) and the density of beta-nucleated PP composite increased only by about 1.6%. In other words, the filler induced increase in density is ca. 16% lower in case of beta-nucleation. For the sheaf-like lamellar structure (radial arrays of parallel stacked lamellae) of beta-nucleated PP [3, 9, 11] a rough fracture surface and big pores are observed from the fractured tensile specimens. On the other hand, the alpha-form of PP and PP composites presented a cross-hatched structure, smooth fractured surface and lower porosity. The

SEM micrographs in Figures 4.17 to 4.18 show the etched and non-etched fracture surfaces of the neat PP and composites.

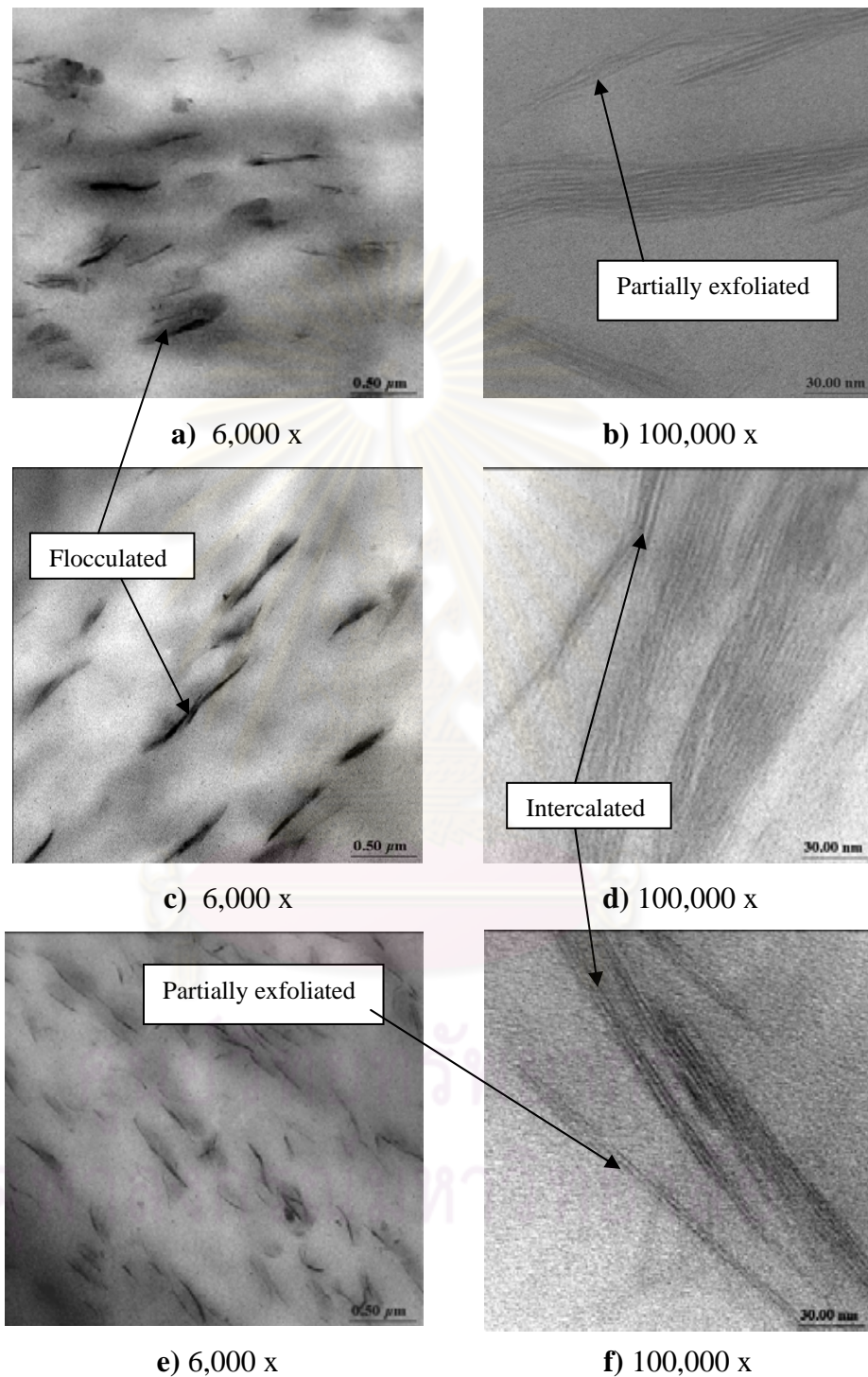


Figure 4.15 Transmission electron micrographs of the PP/PP-g-MA/OMMT composites:(**a-b**) 89.9/5/5/0.1, (**c-d**) 95/0/5/0, and (**e-f**) 70/25/5/0.

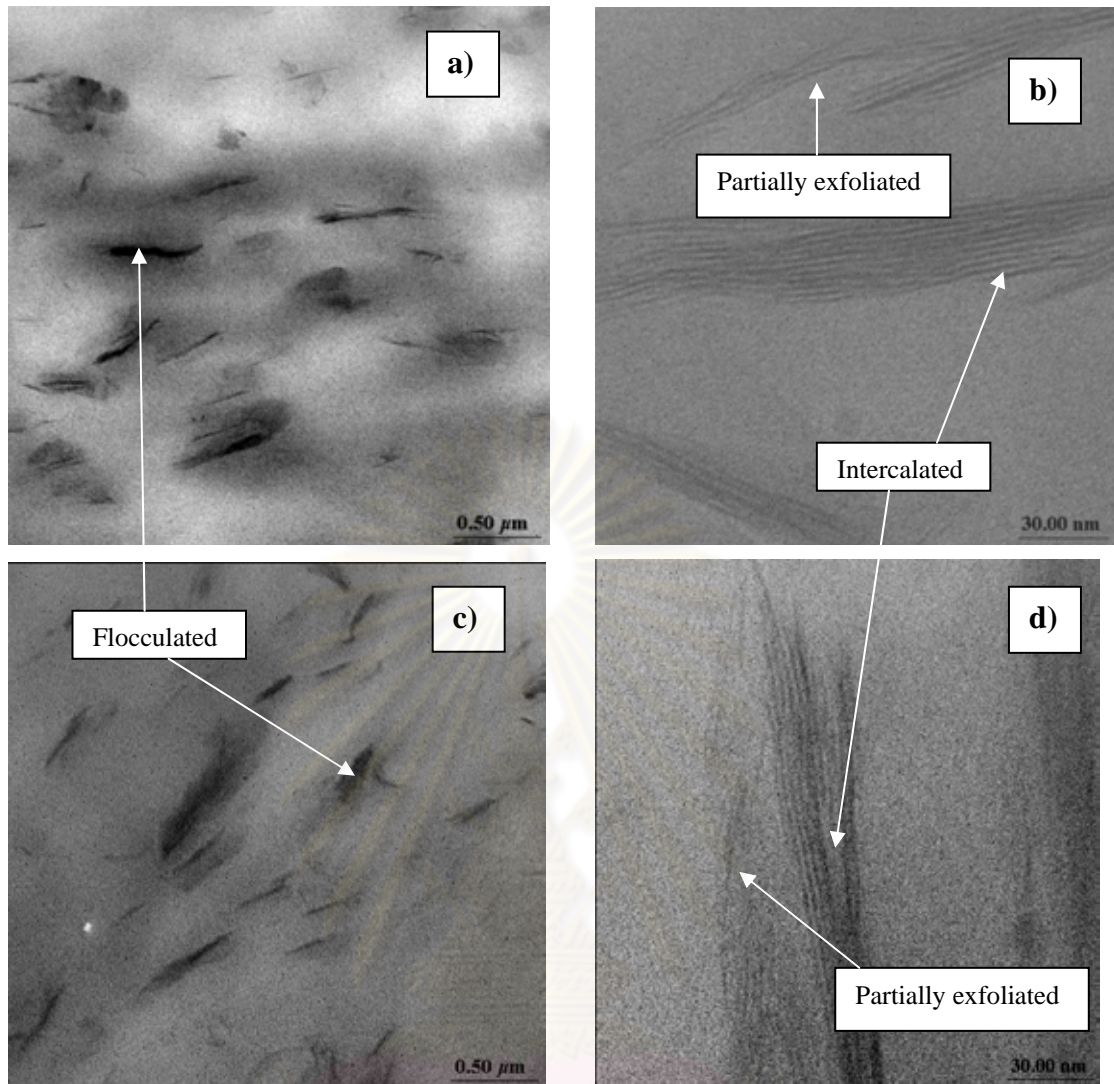


Figure 4.16 TEM micrographs of PP/PP-*g*-MA/OMMT composites showing flocculated, intercalated and exfoliated clay layers of **(a-b)**: 89.9/5/5/0.1 and **(c-d)**: 90/5/5/0 at 6,000x and 100,000x, respectively.

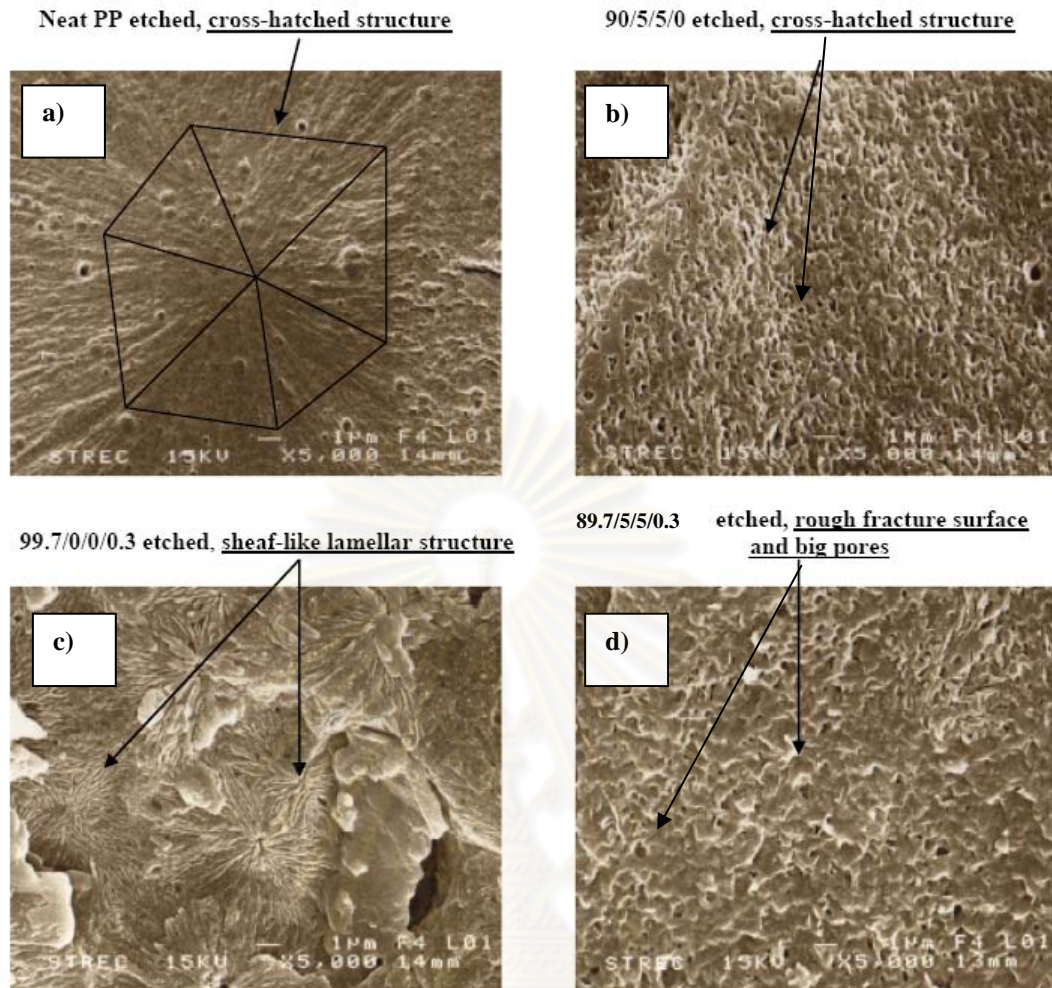


Figure 4.17 Scanning electron micrographs showing the etched impact fractured surface of PP and PP/PP-g-MA/organoclay composites (a-b): without and (c-d): with aryl amide nucleator.

ศูนย์วิทยทรัพยากร
จุฬาลงกรณ์มหาวิทยาลัย

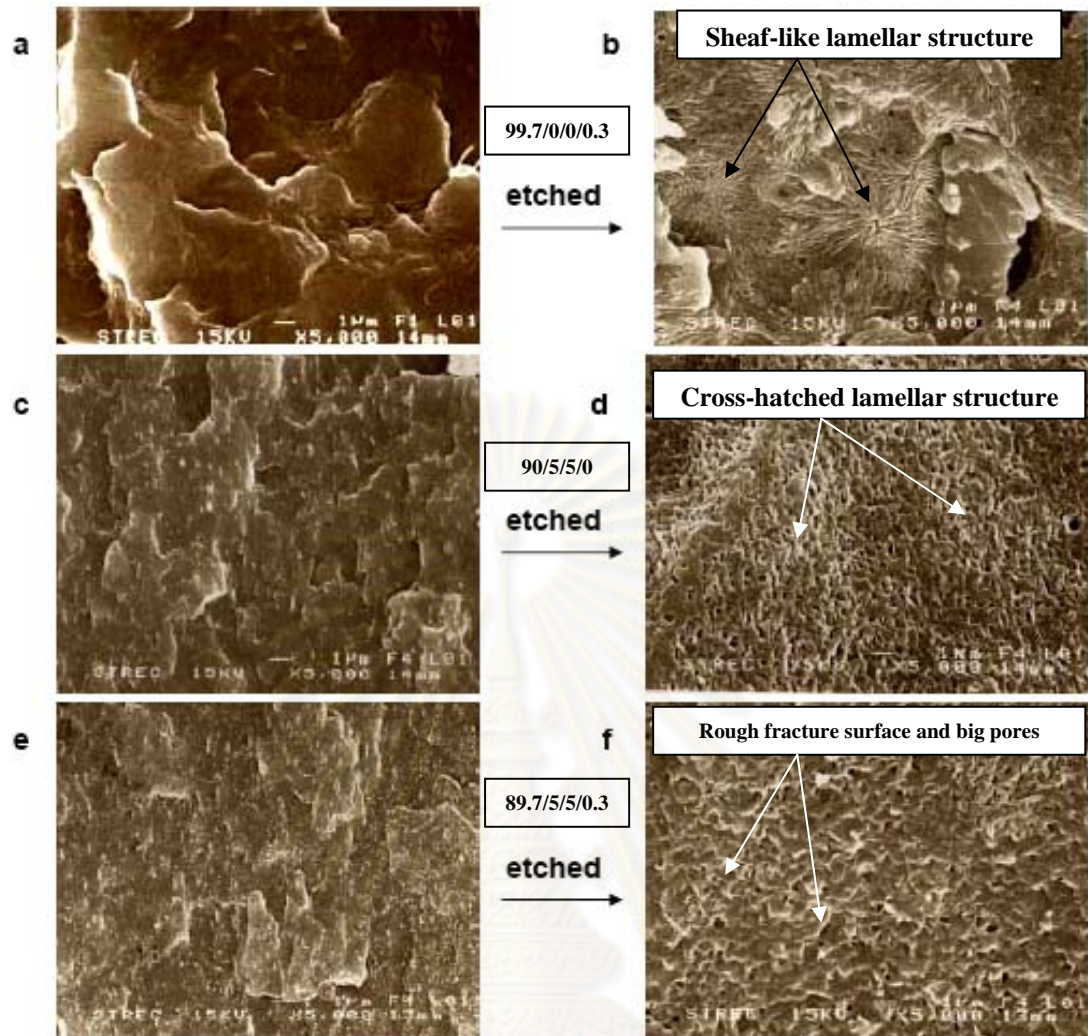


Figure 4.18 Scanning electron micrographs showing the unetched and etched impact fractured surfaces of PP and PP/PP-g-MA/OMMT (organoclay) composites with 0.30 wt% of aryl amide nucleator.

4.4.2 Thermal properties

The DSC measurements reveal the melting and crystallization characteristics of the nucleated and non-nucleated PP homopolymer and composites under non-isothermal conditions. The degree of alpha crystallinity and crystallization temperature (T_c) of PP/PP-g-MA/OMMT is significantly lower than that of neat PP. This result is in contrast to the literature [35] which reported that the organoclay acts as an alpha-nucleating agent in the uncompatibilized composites. This drastic difference is due to the domain effects of the compatibilizer (PB3200: PP-g-MA) that together with the hindered mobility of intercalated PP chains reduce the rate of PP

crystallization [29]. Even if the nucleation is promoted by the organoclay particles, crystal growth rate is seriously impaired. The PP and PP composites containing 0.05-0.30 wt% aryl amide nucleator crystallize essentially in the beta-modification as indicated by the beta-melting peak. In PP and PP composites, the peaks of alpha-melting and beta-melting are practically identical. There is a distinctive beta-fusion peak at 154 °C and alpha-fusion peak at 169 °C as shown in Figure 4.19(a). DSC thermograms can be used to evaluate the performance of aryl amide nucleator in both the PP and PP composites as shown in Table 4.4. The degrees of crystallinity and the percentage of alpha- and beta-fractions were determined from the respective fusion peaks of the DSC thermogram according to Equations (3.1) and (3.2) [23, 24] which is summarized in Table 4.4. Addition of 0.10-0.30 wt% beta-nucleator induces very high beta-modification levels in the PP and PP composites, up to 92% ($k_{\beta} = 0.92$) of the total crystallinity, and significantly increases the crystallization temperature of both the neat PP and PP composites. Figure 4.19(b) shows the crystallization thermograms of PP, PP/PP-g-MA/OMMT and beta-nucleated PP/PP-g-MA/OMMT composites at a cooling rate of 10 °C/min. From these thermograms, the crystallization onset temperature (T_{co}) and crystallization peak temperature (T_{cp}) can be determined. Also, the heat evolved during crystallization (ΔH_c) can be obtained as summarized in Table 4.4. Table 4.4 and Figure 4.20 show the relationship between the crystallization-peak temperature (T_{cp}) and cooling rate for PP/PP-g-MA/OMMT composites. It is observed that both the T_{co} and T_{cp} decrease with increasing cooling rate. At a lower cooling rate, more time is available to overcome the nucleation energy barrier and crystallization starts at the higher temperatures leading to higher crystallinity. At a higher cooling rate, the nuclei become active at lower temperatures [36]. The presence of beta-nucleator leads to a significant increase in T_{cp} at any cooling rate and T_{co} increases with increasing beta-nucleator content. For example, at a cooling rate of 10 °C/min, the crystallization peak temperature for PP/PB3200/organoclay composite is 116 °C, while for the 0.10 and 0.30 wt% beta-nucleated composites, T_{cp} increases to 123 °C and 128 °C, respectively. Aryl amide is a very effective nucleating agent to increase the number of beta-crystals and the rate of crystallization in PP/PP-g-MA/OMMT composites causing more and smaller spherulites in a heterogeneous nucleation process. For PP/PP-g-MA/OMMT composites without the nucleation, the crystallization temperatures are 7 °C lower

than that of the neat PP (at a rate of 10 °C/min) and increase the cycle time of injection and blow molding processes. However, when using an efficient beta-nucleator, crystallization temperature increases by up to 12 °C and so cycle times and energy consumption of industrial PP composite processing will substantially benefit.

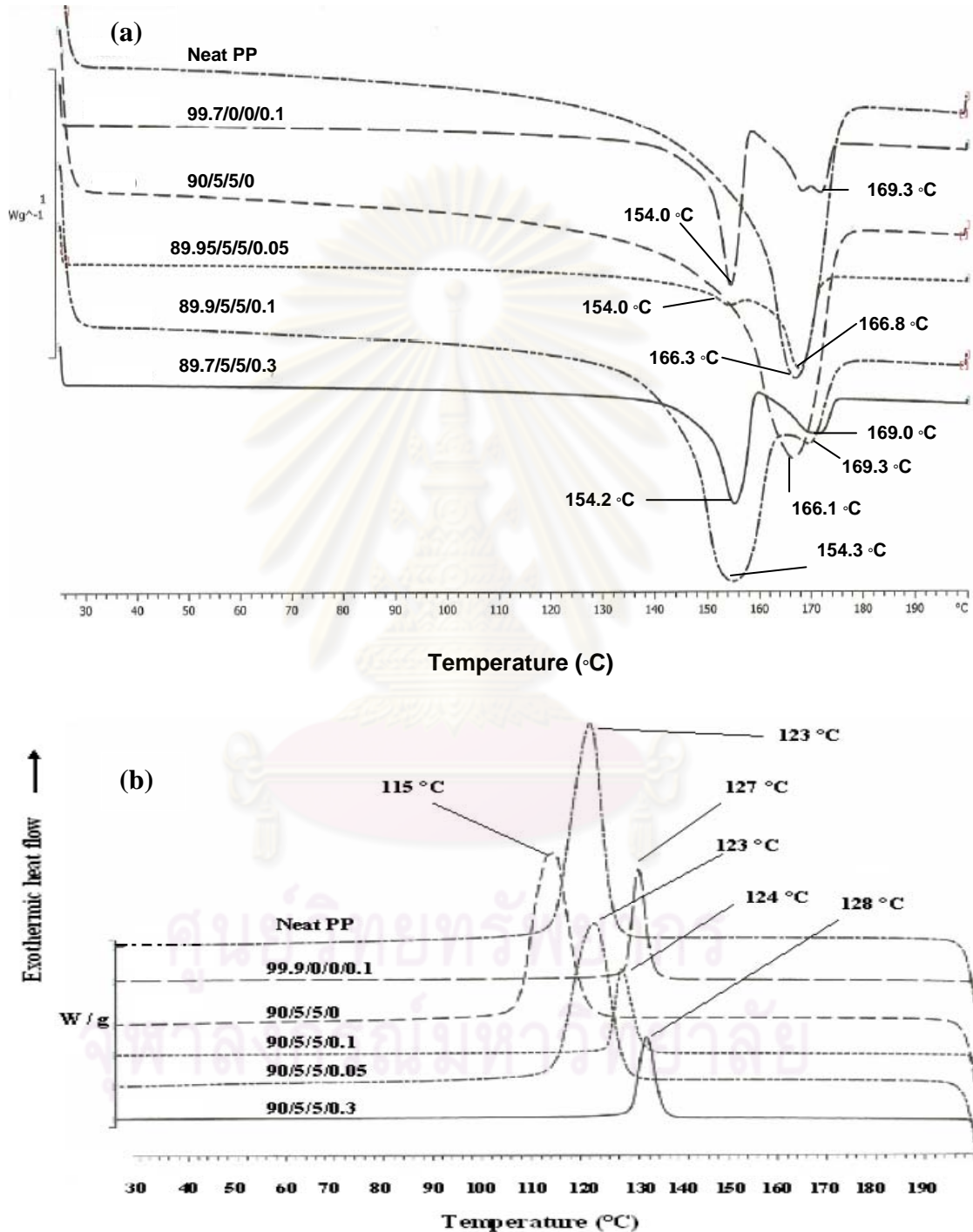


Figure 4.19 DSC thermograms (a) melting temperature, (b) crystallization temperature of PP and PP/PP-g-MA/OMMT composites with various amounts of aryl amide nucleator (The results are based on DSC curves recorded at the cooling and heating rate of 10 °C/min from 25-200 °C by Mettler Toledo instrument)

Table 4.4 Thermal properties of PP and PP/PP-*g*-MA/organoclay composites with various amounts of aryl amide nucleator at various heating and cooling rates based on DSC curves recorded at the cooling and heating rates from 2.5–20 °C/min

Formulation	Scan Rate (°C/min)	$\Delta H\alpha$ (J/g)	X_α	Tm- α (°C)	$\Delta H\beta$ (J/g)	X_β	Tm- β (°C)	ΔHc (J/g)	Tcp (°C)	** Total crystallinity	Φ_β (%)
Neat PP	2.5	106.66	0.60	167.0	0.00	0.00	none	114.44	129.5	0.60	0
	5.0	103.04	0.58	166.8	0.00	0.00	none	113.00	126.5	0.58	0
	10.0	95.53	0.54	166.3	0.00	0.00	none	104.21	122.9	0.54	0
	20.0	94.17	0.53	166.6	0.00	0.00	none	104.24	119.2	0.53	0
90/5/5/0	2.5	79.80	0.45	166.3	0.00	0.00	none	97.45	121.9	0.45	0
	5.0	85.25	0.48	165.9	0.00	0.00	none	94.65	118.7	0.48	0
	10.0	83.65	0.47	166.1	0.00	0.00	none	94.47	115.5	0.47	0
	20.0	84.75	0.48	164.4	0.00	0.00	none	93.76	111.9	0.48	0
99.9/0/0/0.1	2.5	41.68	0.23	168.3	94.74	0.56	154.3	111.05	132.3	0.79	70
	5.0	11.67	0.07	170.4	69.65	0.41	154.6	90.29	131.2	0.48	86
	10.0	9.83	0.06	169.3	79.30	0.47	154.0	97.59	126.7	0.52	89
	20.0	none	*nd	None	96.42	0.57	156.0	93.91	123.3	nd	nd
89.95/5/5/0.05	2.5	89.41	0.50	167.4	30.82	0.18	154.3	99.77	128.8	0.68	27
	5.0	63.07	0.35	167.2	29.78	0.18	154.2	100.11	125.7	0.53	33
	10.0	56.94	0.32	166.8	32.95	0.19	154.0	96.87	122.5	0.51	38
	20.0	86.13	0.48	167.1	none	nd	None	96.12	117.9	nd	nd
89.9/5/5/0.1	2.5	56.92	0.32	167.4	20.65	0.12	154.3	100.77	128.8	0.44	28
	5.0	18.53	0.10	170.6	60.37	0.36	153.3	98.03	127.3	0.46	77
	10.0	12.85	0.07	169.3	70.26	0.41	154.3	92.40	123.5	0.49	85
	20.0	none	nd	None	86.66	0.51	157.8	90.17	119.1	nd	nd
89.7/5/5/0.3	2.5	24.92	0.14	171.2	78.19	0.46	154.9	94.52	133.8	0.60	77
	5.0	17.16	0.10	170.9	73.33	0.43	154.2	105.57	129.7	0.53	82
	10.0	6.92	0.04	169.0	78.38	0.46	154.2	88.87	128.4	0.50	92
	20.0	none	nd	None	83.53	0.49	156.1	84.39	124.2	nd	nd

* nd = cannot determine, ** Total crystallinity = alpha crystallinity and beta crystallinity

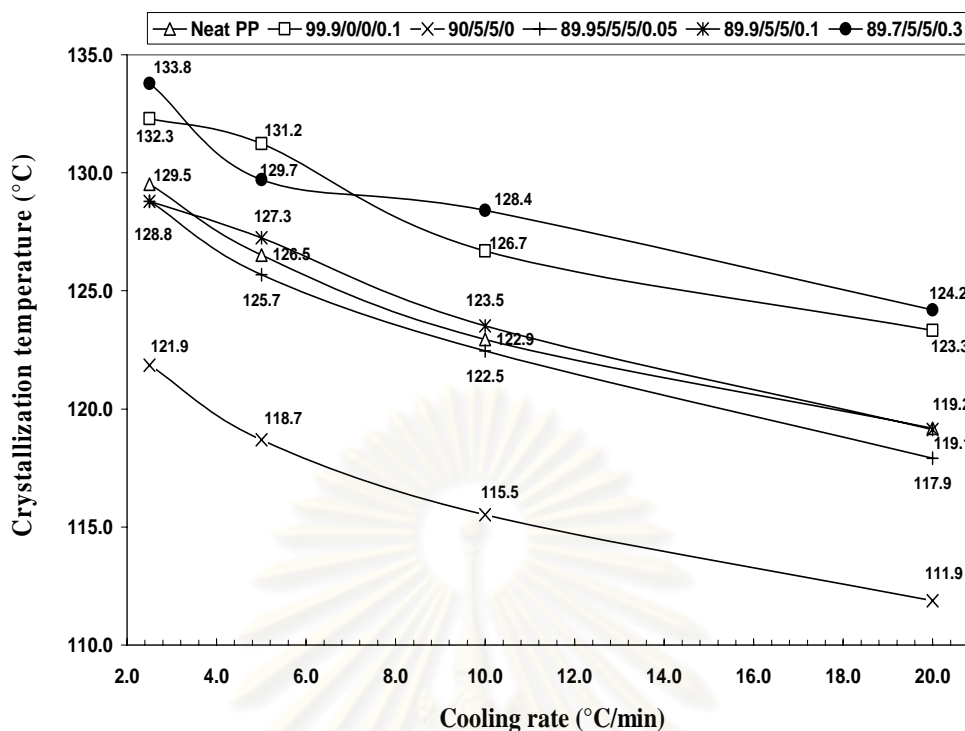


Figure 4.20 Crystallization temperatures of PP and PP/PP-g-MA/OMMT composites with various amounts of aryl amide nucleator at cooling rates of 2.5 °C/min, 5.0 °C/min, 10.0 °C/min and 20.0 °C/min.

4.4.3 Chemical interaction

To observe a chemical interaction in composites, Fourier Transform Infrared Spectroscopy (FTIR) was applied [31, 35]. In Figure 4.21, the FTIR spectra of clay, neat polymer, PP/PP-g-MA/OMMT and PP/PP-g-MA/OMMT/aryl amide composites are presented. The main infrared absorption bands assigned to molecular vibrations of neat components can be given as follows [37]. For OMMT, the IR peak at 1470 cm^{-1} is associated with CH_2 wagging deformation of alkyl ammonium clay modified surface, 1116 cm^{-1} for ν (Si-O) out-of-plane, 1050 cm^{-1} for ν (Si-O) in-plane, 1033 cm^{-1} for Si-O-Si stretching, 914 cm^{-1} for δ (Al-Al-OH), 797 cm^{-1} for δ (CH) out-of-plane from the surface modified. Absorption peaks at 530 and 466 cm^{-1} are for the Si-O and Si-O-Al stretching and Si-O and Si-O-Fe stretching, respectively.

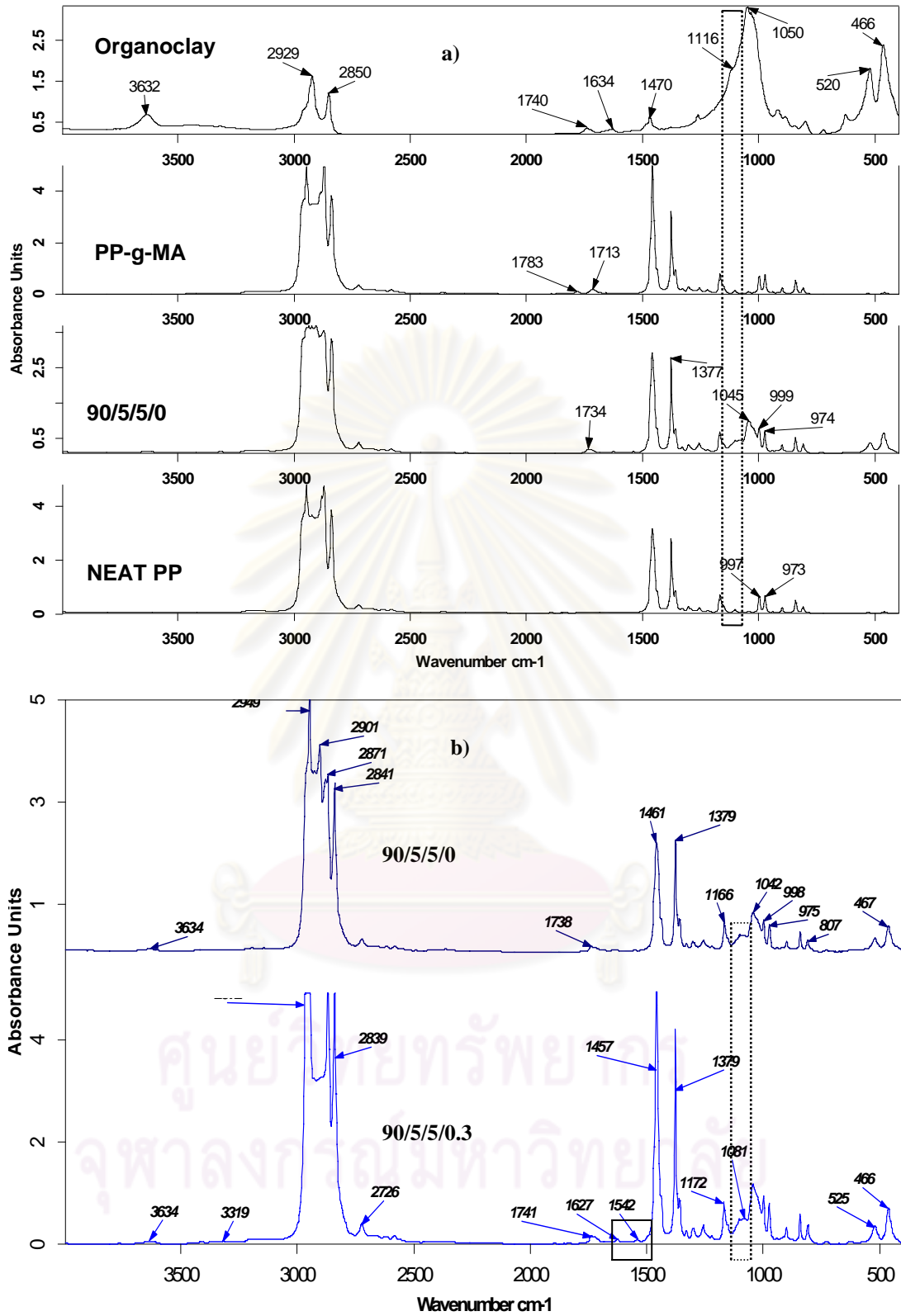


Figure 4.21 Fourier transform infrared spectroscopy spectra of a) OMMT (organoclay), PP, PP-g-MA, PP/PP-g-MA/OMMT composites, b) PP/PP-g-MA/OMMT composites without and with 0.30 wt% of aryl amide nucleator.

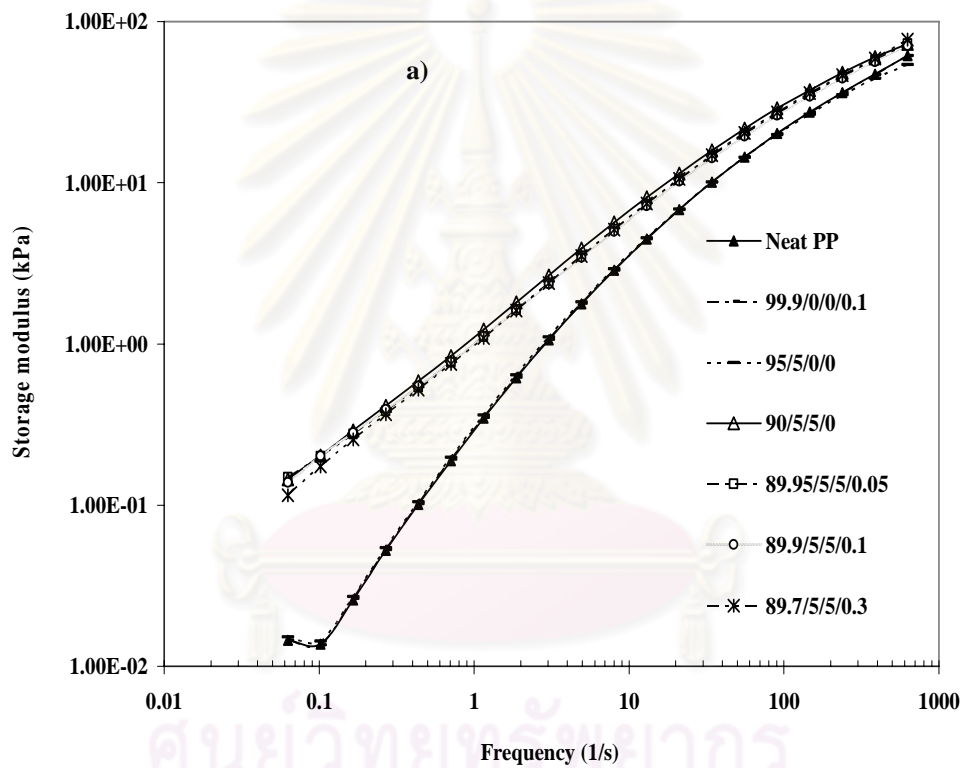
For the Neat PP, 1457 cm^{-1} for $\delta_{\text{as}}(\text{CH}_3)$; 1377 and 1358 cm^{-1} for $\delta_{\text{s}}(\text{CH}_3)$, 1327 cm^{-1} $\delta(\text{C-H})$; 1307 cm^{-1} CH_2 twisting; 1253 and 1219 cm^{-1} for CH_2 wagging; 1165 cm^{-1} for absorption perpendicular to stretch direction; 997 , 973 , 843 and 808 cm^{-1} for tertiary methyl stretch deformations. For the compatibilizer, PP-g-MA (PB3200) shows besides the neat PP spectra two weak absorption at 1783 and 1713 cm^{-1} and associated with $\nu(\text{C-OH})$ and $\nu(\text{C=O})$ stretching of maleic acid.

Addition of aryl amide nucleator creates the absorption peaks at 1627 and 1542 cm^{-1} as marked by a full line box in Figure 4.21(b). The FTIR spectra indicate that aryl amide nucleator does not affect the interaction between the PP matrix and organoclay. A close examination of Figure 4.21(a) and (b) suggests that reinforcement of the PP with organoclay alters the shape and position of the infrared absorption bands of PP. The absorption bands of PP between 998 and 975 cm^{-1} corresponding to the deformation of tertiary methyl skeletal and at about 1069 - 1104 cm^{-1} to the deformation of stretching of Si-O-Si bond in the tetrahedral silicate plane are highlighted by the dot boxes in Figure 4.21(a) and (b). This shift in the wavenumber and deformation of peak shape indicates a stronger chemical interaction between PP matrix and organoclay.

4.4.4 Rheological properties

The rheological properties of composites are sensitive to surface characteristics and level of dispersion. Therefore, melt rheology can be envisaged as a powerful tool for characterizing the state of dispersion, intercalation and exfoliation of clay composites [16, 25, 28, 30, 32-34]. Storage modulus, G' , loss modulus, G'' and complex viscosity, η^* , were measured as a function of oscillation frequency for the PP/PP-g-MA melt blend. No specific effect on G' , G'' and η^* is observed in Figure 4.22 between the the neat PP and 95/5/0/0 blend, indicating good miscibility between PP and PP-g-MA. The rheological behavior of the binary blend that corresponds to the weight ratios present in the PP/PP-g-MA/OMMT composites will be used as the reference matrix behavior. Figure 4.22(a-c) presents also G' , η^* , G'' as a function of oscillating frequency for the neat PP and the composites with different beta-nucleator loads. At low frequencies ($< 1\text{ rad/s}$) without the beta-nucleator, G' , G'' and η^* significantly increased when organoclay and compatibilizer (90/5/5/0) were added,

which was associated to high intercalation and partial polymer exfoliation. Referring to Solomon et al. [32], the increase in storage modulus at low frequency can be explained by the existence of a percolate network microstructure. By adding 0.05, 0.10 and 0.30 wt% of the beta-nucleator to these PP composites, G' , G'' , and η^* slightly decreased, which could be due to a kind of “gliding effect” of the very fine solid nucleator particles having melting points of greater than 300 °C between the clay layers and stacks.



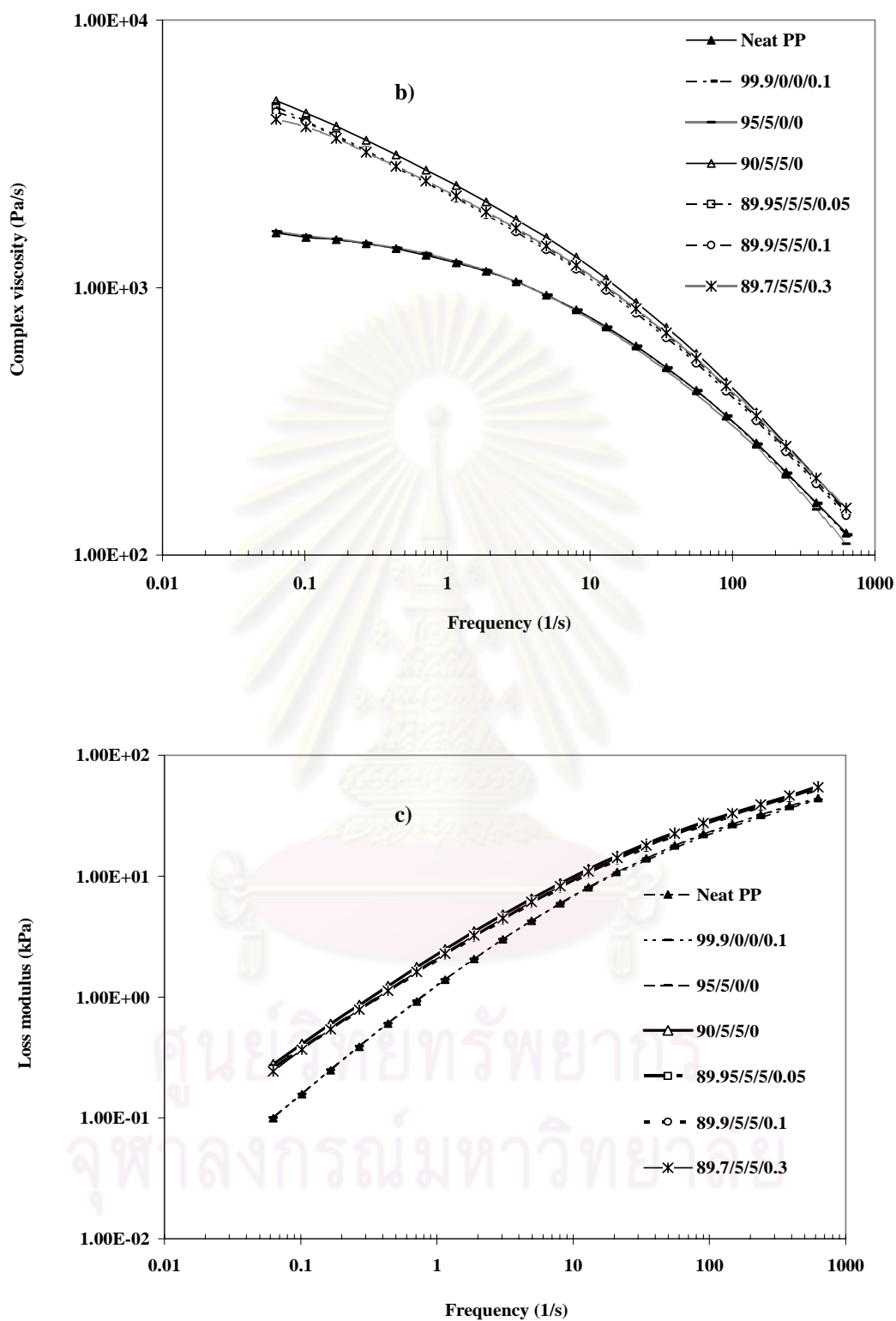


Figure 4.22 Rheological properties, a) storage modulus, b) complex viscosity and c) loss modulus of PP, PP/PP-g-MA and PP/PP-g-MA/organoclay composites with various loadings of aryl amide nucleator determined by cone and plate Rheometer.

4.4.5 Microscopic observations

Nucleation effect is also confirmed by polarized light microscopy as shown in Figure 4.23. There are some spherulite structures in the neat PP indicating of some degrees of its crystallinity. The size of spherulites decreased from 50-80 μm in PP/PP-g-MA/OMMT composites to 10-25 μm average in 92 wt% beta-nucleated composites (see Figure 4.23(b)). The latter shows two size ranges of beta-spherulites, i.e., 15 μm small spherulites at some areas, and 100 μm large spherulites with voids at the center at the other areas and differs from that of neat PP (alpha-phase).

The mechanical properties of the neat PP, beta-PP and PP/PP-g-MA/OMMT with various amounts of beta-nucleator are shown in Table 4.5. The flexural modulus of beta-nucleated PP (k_β value = 0.93) is slightly lower than that of the neat PP while elongation at break is similar. Izod impact strength is drastically improved by 125%. Flexural modulus and Izod impact strength of the PP/PP-g-MA/OMMT composites (90/5/5/0) are also much higher than for the neat PP by 30% and 40%, respectively. These improvements indicate good compatibilization and interaction between the OMMT and PP. However, the elongation at break of the reinforced composites is very low as expected. Addition 0.05 wt% of the beta-nucleator to PP/PP-g-MA/OMMT composites induces the beta-form at k_β value as 0.50, the elongation at break is greatly improved by 70% while Izod impact strength is slightly higher and flexural modulus is slightly lower. Above 90% beta-form in the composites (k_β value > 0.90), elongation at break is significantly improved by up to 200% whereas the flexural modulus and Izod impact strength are somewhat lower while tensile properties are not significantly different. Besides, the heat deflection temperature (HDT) of the beta-nucleated of the neat PP is significantly higher than that of the alpha-PP. However, the beta-nucleation of composites did not affect HDT.

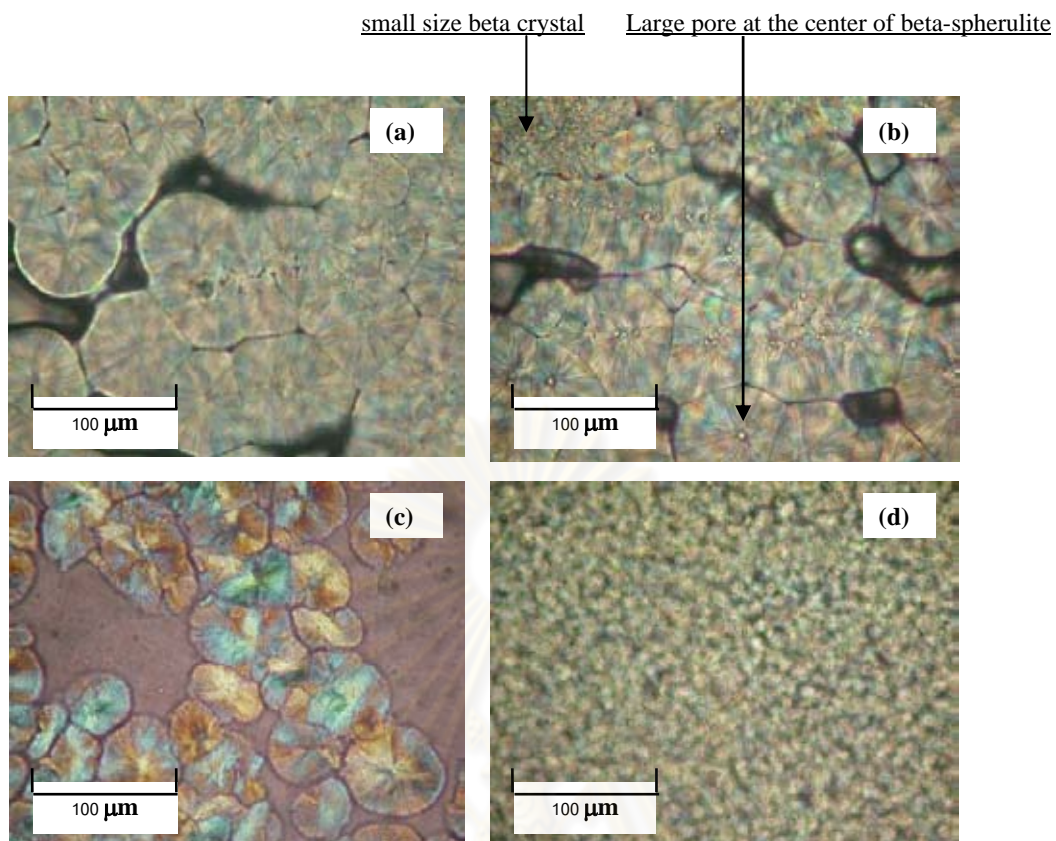


Figure 4.23 Optical micrographs of the neat PP, PP/PP-g-MA/OMMT with and without the beta-nucleating agent under isothermal condition at 135 °C: **(a)** Neat PP (>95% alpha-form) after 20 min, spherulite size, 70-100 μm; **(b)** 99.9/0/0/0.1 (92% beta-form), 20 min, 10 μm and 100 μm; **(c)** 90/5/5/0, 20 min, 50-80 μm; **(d)** 89.9/5/5/0.1, 10 min, 10-25 μm.

Table 4.5 Mechanical properties of PP/PP-g-MA/OMMT composites with various amounts of beta-nucleating and the control of the neat PP by the reverse screw configuration.*

Formulation	k_{β}	** Flexural Modulus (MPa)	** Izod impact Strength at 23 °C (J/M)	** Elongation at break (%)	***Heat deflection Temperature (°C)
100/0/0/0 (Neat PP)	0.00	1413 ± 17	28.6 ± 0.2	1087 ± 23	105 ± 1
99.9/0/0/0.1	0.93	1332 ± 20	67.6 ± 2.0	1063 ± 103	120 ± 1
90/5/5/0	0.00	1825 ± 6	43.0 ± 1.8	54 ± 5	127 ± 1
89.95/5/5/0.05	0.50	1777 ± 14	45.8 ± 1.7	91 ± 4	126 ± 1
89.9/5/5/0.1	0.92	1821 ± 22	40.3 ± 2.0	50 ± 7	126 ± 0
89.7/5/5/0.3	0.92	1747 ± 9	35.3 ± 1.0	166 ± 31	128 ± 1

* see pages 34 in Chapter 3, ** The test results are an average of 5 specimens, *** The test results are an average of 3 specimens.

ศูนย์วิทยทรัพยากร
จุฬาลงกรณ์มหาวิทยาลัย

CHAPTER V

CONCLUSIONS AND SUGGESTION FOR FURTHER WORK

5.1 Conclusions

Aryl amide beta-nucleating agent was found to improve impact property of the neat PP by 125% with only little loss in flexural modulus; Izod impact strength of PP/PP-g-MA/OMMT (organoclay) composite was not further increased by the nucleator addition. However, the organoclay composite system of this study gave 40% higher impact and 30% higher modulus compared to the neat PP. The most striking result is the effect of beta-nucleator on crystallization temperature of the composite. The crystallization of the un-nucleated PP/PP-g-MA/organoclay is highly retarded with a T_{cp} at 116 °C; the beta-nucleation increased the temperature to 128 °C which is expected to offer big advantages for mold processing of the composite, such as, lower cycle times. Other positive effects of the beta-nucleation of PP composites are a slight reduction of the composite density (the lower weight of the molding part) and the partial recovery of the very low elongation at break for the composite tensile property which can be improved by 200%.

5.2 Suggestion for further work

A better understanding of interfacial adhesion between PP matrix and montmorillonite should be investigated via spectroscopic techniques. Block copolymer of polypropylene series are the topical research to search for novel products. Further investigations of effects of aryl amide on PP block copolymers can be the good candidates for this type of research.

Based on the research results, it is interesting to apply this formulation to produce industrial products that require high flexural modulus and impact strength. Applications in automotive parts, electrical parts and consumer products are worthwhile investigating.

REFERENCES

- [1] Michael J. B. Handbook of Polypropylene and Polypropylene composites. Amsterdam: Elsevier, 1999.
- [2] Nicholas P.C. Handbook of Polymer Science and Technology. London: Chapman & Hall, 1989.
- [3] Moore E. P. Polypropylene Handbook. Ohio: Hanser Publishers, 1996.
- [4] Padden F. J., Keith H. D., Spherulitic Crystallization in Polypropylene. Journal of Apply Polymer Science. 30(1959): 1479-1484.
- [5] Turner-Jones A., Aizlewood J. M., and Beckett D.R. Crystallization forms of isotactic polypropylene. Makromolekular Chemie. 75(1964): 134-154.
- [6] Trongtosak K., Supapol P., Tantayanon S. Effect of calcium stearate and pimelic acid addition on mechanical properties of heterophasic isotactic polypropylene/ethylene-propylene rubber blend. Polymer Testing. 23(2004): 533-539.
- [7] Cho, K., Seheb, D. N., Choi, J. and Yang H. Real time in situ X-ray diffraction studies on the melting memory Effect on the crystallization of beta-isotactic polypropylene. Polymer. 43(2001): 1407-1416.
- [8] Karger-Kocsis J. Polypropylene Structure Blend and Composite. London: Chapman&Hall, 1995.
- [9] Michler G. H., Balta-Calleja F. J. Mechanical Properties of Polymers Based on Nanostructure and Morphology. Madrid: CRC Press Taylor & Francis Group, 2005.
- [10] Varga J., Beta-modification of isotactic polypropylene: preparation, structure, processing, properties, and application. Journal of Macromolekular Science Physics. 41(2002): 1121-1171.
- [11] Lotz B. α and β phases of isotactic polypropylene: a case of growth kinetic 'phase reentrancy' in polymer crystallization. Polymer. 39(19)(1998): 4561-4567.
- [12] Ray S. S., Okamoto M. Polymer/layered silicate nanocomposites: a review from preparation to processing. Progress in polymer science. 28(2003): 1539-1641.
- [13] Harutun G. K. Handbook of polypropylene and polypropylene composites. Second edition, revised and expanded. Michigan: Marcel Dekker, 2003

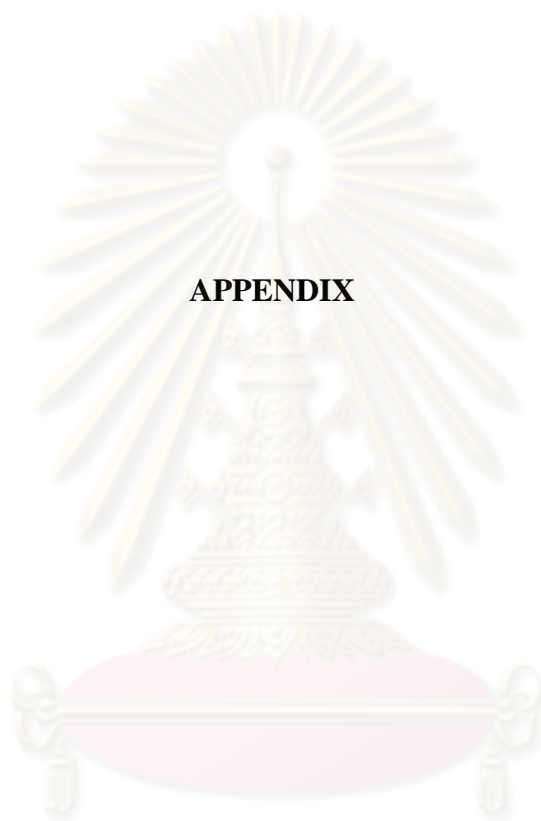
- [14] Sperling L. H. Introduction to physical polymer science. Fourth edition, New Jersey: John Wiley & Sons, 2006.
- [15] Reichert P., Nitz H., Klink S., Brandasch R., Thomann R., Mulhaupt R. Polypropylene/organoclay nanocomposite formation: influence of compatibilizer functionality and organoclay modification. Macromolecular Material and Engineering. 275(2000): 8-17.
- [16] Wang Y., Chen F. B., Li Y. C., Wu K. C. Melt processing of polypropylene/clay nanocomposites modified with maleated polypropylene compatibilizers. Composites: Part B. 35(2004): 111-124.
- [17] Nam P. H., Maiti P., Okamoto M., Kotaka T., Hasekawa N., Usaki A. A hierarchical structure and properties of intercalated polypropylene/clay nanocomposites. Polymer. 42(2001): 9633-9640.
- [18] Zhang P., Liu X., Li Y. Influence of β -nucleating agent on mechanics and crystallization characteristics of polypropylene. Materials Science & Engineering A. 434(2006): 310-313.
- [19] Tedjeman P., Robert C., Marin G., Gerard P. The effect of alpha, beta-crystalline structure on the mechanical properties of polypropylene. European Physic Journal. 4(2001): 459-465.
- [20] Olley R., Bassett D. C., Hine P. J., Ward I.M. Morphology of compacted polyethylene fiber. Journal of Material Science. 28(1993): 1107-1112.
- [21] Dealy J. M., Wissbrun K. F. Melt Rheology and its Role in Plastics Processing. New York: Van Nostrand Reinhold, 1990.
- [22] Stephen L. R. Fundamental Principles of Polymeric Materials. New York: John Wiley & Sons, 1993.
- [23] Li J.X., Cheung W. L., Jia D. A study on heat of fusion of beta-polypropylene. Polymer. 40(1999): 1219-1222.
- [24] Li J.X., Cheung W. L. Conversion of growth and crystallization of beta-phase in doped iPP. Polymer. 40(1998): 2085-2088.
- [25] Wang K., Liang S., Deng J., Yang H., Zhang Q., Fu Q., Dong X., Wang D., Han C. C. The role of clay network on macromolecular chain mobility and relaxation in isotactic polypropylene/organoclay nanocomposites. Polymer. 47(2006): 7131-7144.

- [26] Gianelli W., Ferrara G., Camino G., Pellegatti G., Rosenthal J., Trombini R.C. Effect of matrix features on polypropylene layered silicate nanocomposites. Polymer. 46(2005): 7037-7046.
- [27] Liu X., Wu Q. PP/clay nanocomposites prepared by grafting-melt intercalation. Polymer. 42(2001): 10013-10019.
- [28] Kim D. H., Fasulo P. D., Rodgers W. R., Donald, R. P. Structure and properties of polypropylene-based nanocomposites: Effect of PP-g-MA to organoclay ratio. Polymer. 48(2007): 5308-5323.
- [29] Jayaraman K., Kumar S. Polypropylene layered silicate nanocomposites. Michigan State University, U.S.A: Woodhead, 2006.
- [30] Lertwimolnun W., Vergnes B. Influence of compatibilizer and processing conditions on the dispersion of nanoclay in a polypropylene matrix. Polymer. 46(2005): 3462-3471.
- [31] Lew C. Y., Murphy W.R., McNally G. M., Abe K. and Yanai S. Synthesis and characterization of polypropylene nanocomposite fibers. ANTEC. 2005: 1449-1455.
- [32] Solomon M. J., Almusallam A. S., Seefeldt K. F., Somwangthanaroj A., Varadan P. Rheology of polypropylene/clay hybrid materials. Macromolecules. 34(2001): 1864-1872.
- [33] Rohlmann C.O., Failla M.D., Quinzani L.M. Linear viscoelasticity and structure of polypropylene montmorillonite nanocomposites. Polymer. 47(2006): 7795-7804.
- [34] Wang K., Liang S., Zhao P., Cheng Q., Tan H., Du R., Zhang Q., Fu Q. Correlation of rheology-orientation-tensile property in isotactic polypropylene/organoclay nanocomposites. Acta Material. 55(2007): 3143-3154.
- [35] Deshmane C., Yuan Q., Perkins R. S., Misra R. D. K. On striking variation in impact toughness of polyethylene-clay and polypropylene-clay nanocomposite systems: The effect of clay-polymer interaction. Materials Science and Engineering A. 458(2007): 150-157.
- [36] Yuan Q., Awate S., Misra R. D. K. Nonisothermal crystallization behavior of polypropylene-clay nanocomposites. European Polymer Journal. 42(2006): 1994-2003.

- [37] Nayak P. S, Singh B. K. Instrumental characterization of clay by XRF, XRD and FTIR. Bull Material Science. 30(2007): 235-238.



ศูนย์วิทยทรัพยากร
จุฬาลงกรณ์มหาวิทยาลัย



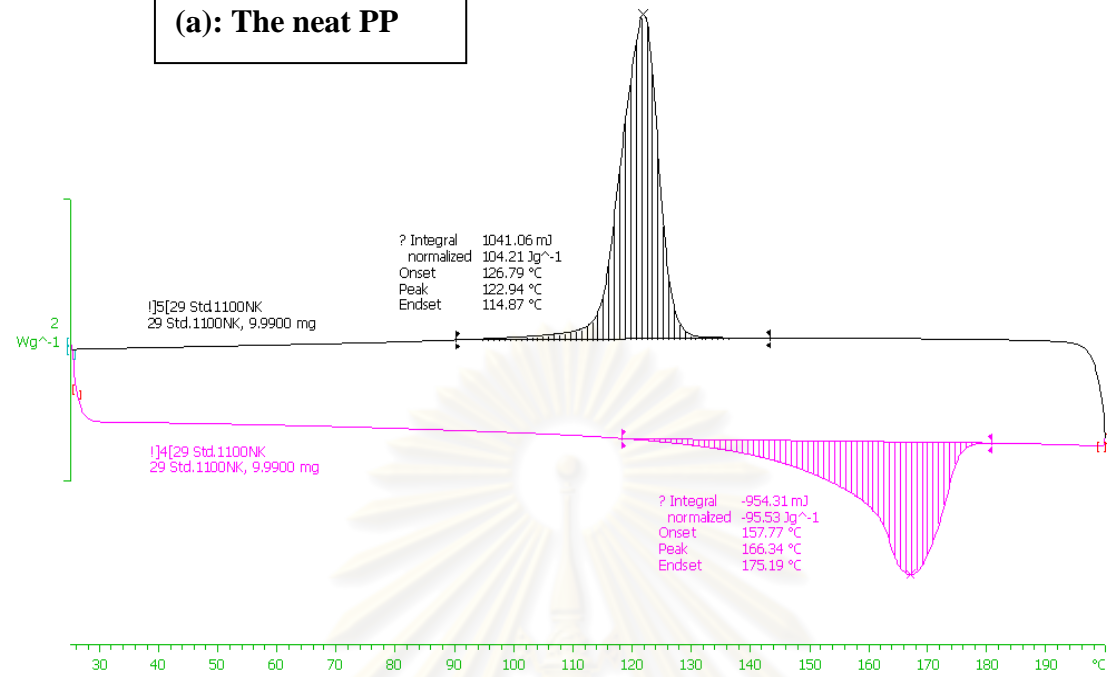
APPENDIX

ศูนย์วิทยทรัพยากร
จุฬาลงกรณ์มหาวิทยาลัย

^exo

20.06.2008 18:04:47

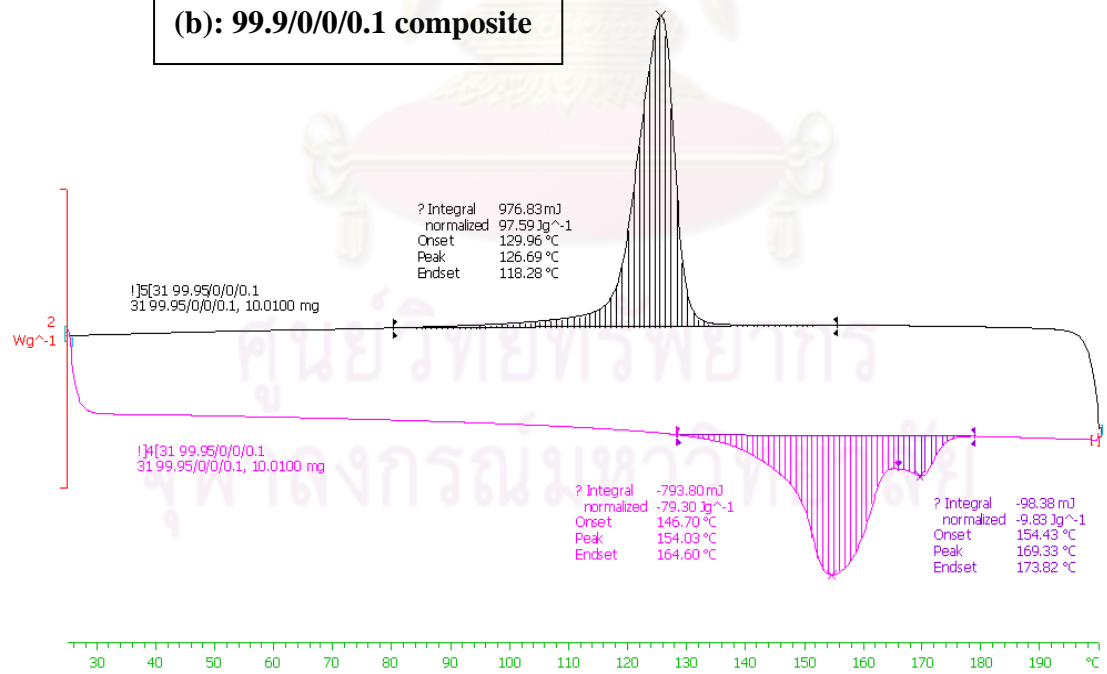
(a): The neat PP



^exo

20.06.2008 18:45:38

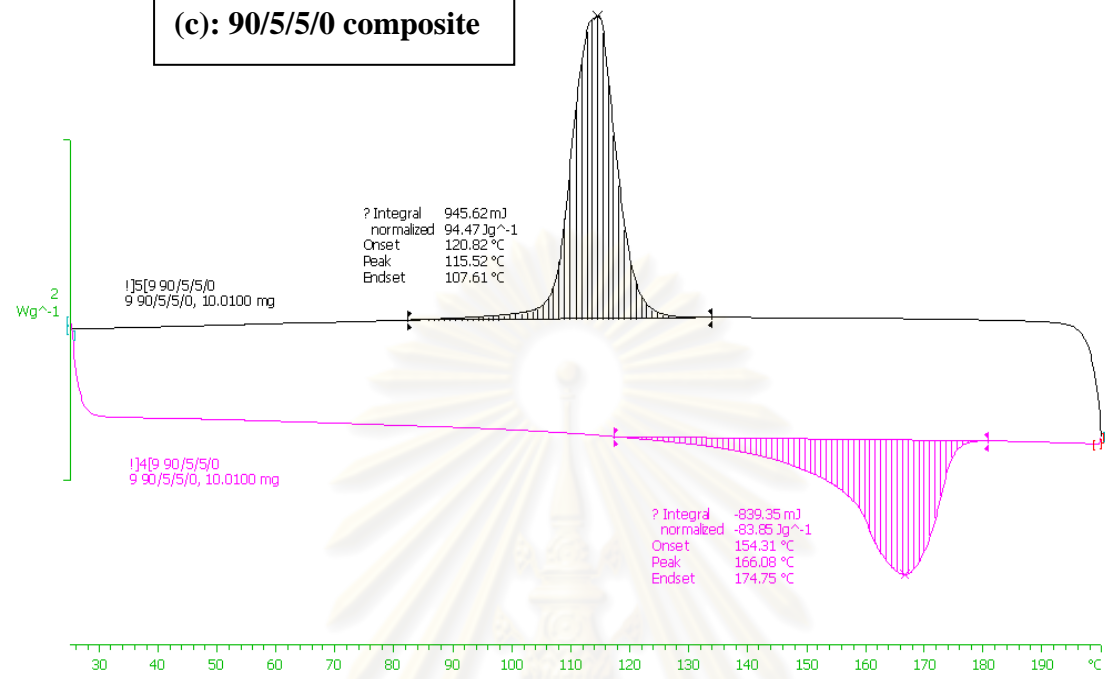
(b): 99.9/0/0/0.1 composite



^exo

20.06.2008 18:08:39

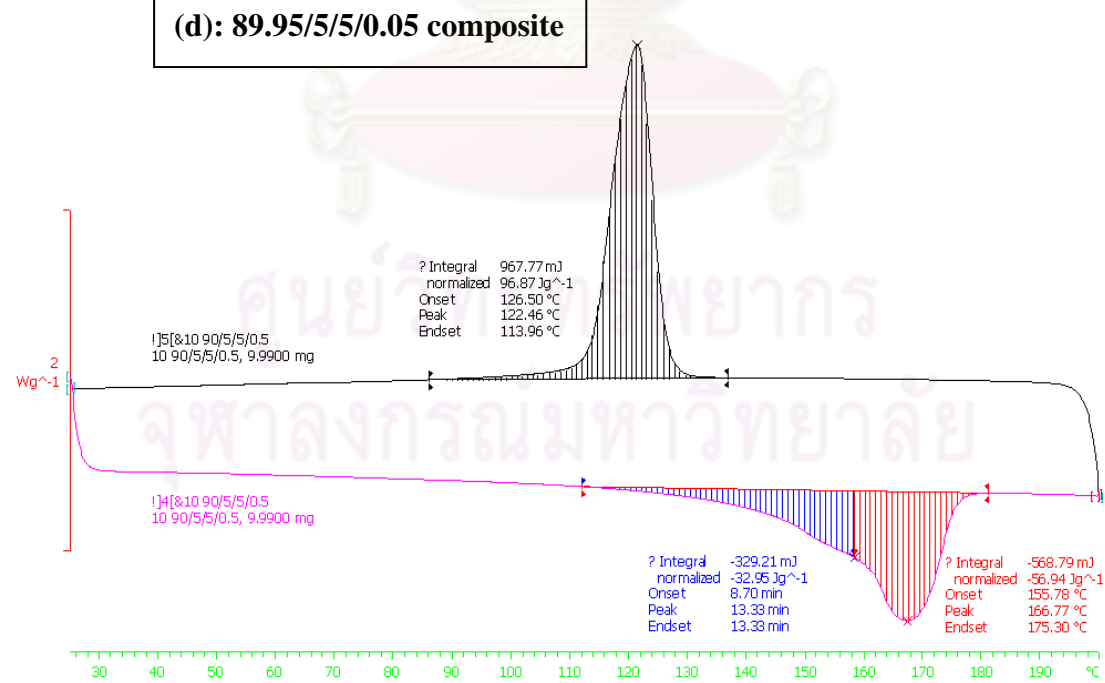
(c): 90/5/5/0 composite



^exo

20.06.2008 18:50:22

(d): 89.95/5/5/0.05 composite



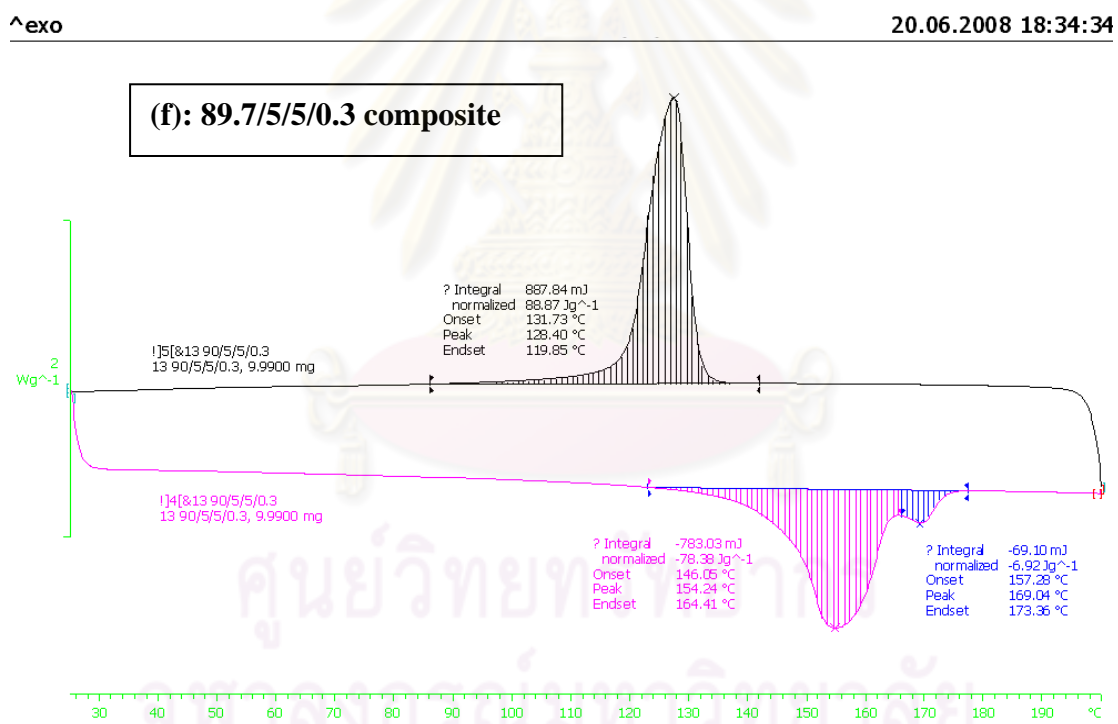
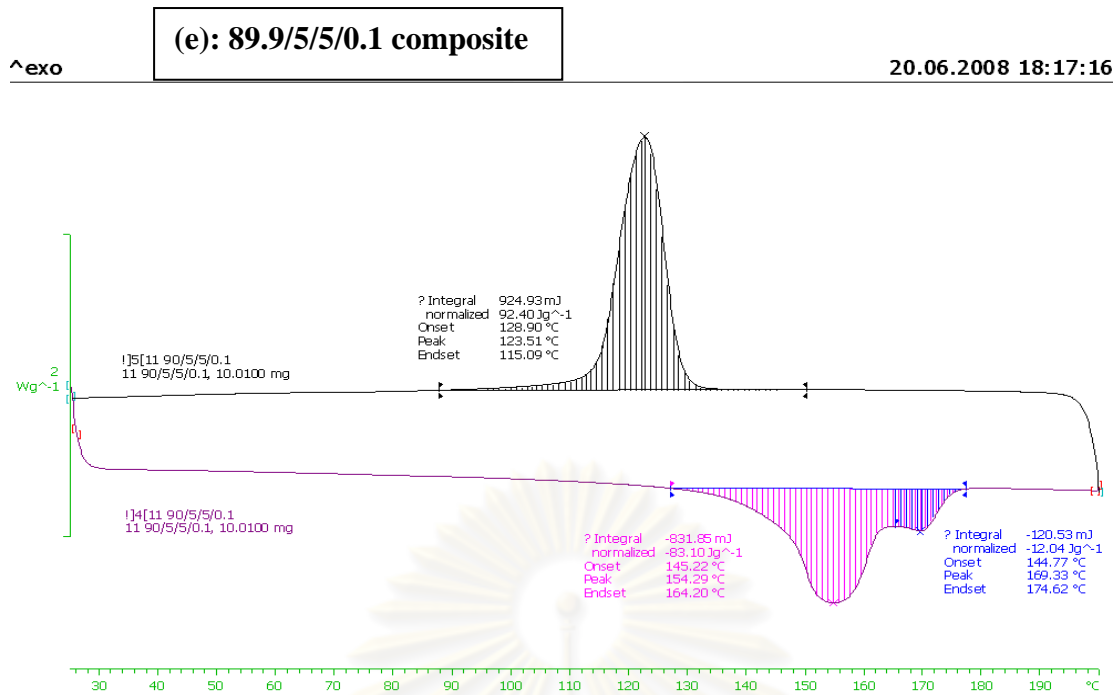


Figure A.1 DSC thermograms of melting temperature, crystallization temperature of the PP and PP/PP-g-MA/organoclay nanocomposites with various amounts of aryl amide nucleator. The results are based on DSC curves recorded at the cooling and heating rates of 10 °C/min from 25-200 °C by Mettler Toledo instrument. (a): The neat PP; (b): 99.9/0/0/0.1 composite; (c): 90/5/5/0 composite; (d): 89.95/5/5/0.05 composite; (e): 89.9/5/5/0.1 composite; (f): 89.7/5/5/0.3 composite.

VITA

Mr. Yongyut Prachum was born on August 21, 1974 in Nakornratchasima. He graduated with a Bachelor's degree of Science in Chemistry from Srinakharinwirot University in 1996. Since then he has joined the Research and Development Group at IRPC (Public) Co., Ltd. In 2006, he was accepted as a graduate student in the M.Sc. course program in Petrochemistry and Polymer Science, Faculty of Science, Chulalongkorn University. He received a Master's degree of Science in Polymer Science, in November 2008.



ศูนย์วิทยทรัพยากร
จุฬาลงกรณ์มหาวิทยาลัย